DISCOVERY OF A CARDIOPROTECTIVE MECHANISM REGULATED BY HSPB7

A Dissertation

Presented to the Faculty of the Weill Cornell Graduate School

of Medical Sciences

in Partial Fulfillment of the Requirements for the Degree of

Doctor of Philosophy

by

Emily Joel Mercer

May 2017

Discovery of a cardioprotective mechanism regulated by HSPB7

Emily Joel Mercer, Ph.D.

Cornell University 2017

Small heat shock proteins are chaperones with variable mechanisms of action. The function of cardiac family member Hspb7 is unknown, despite being identified through GWAS as a potential cardiomyopathy risk gene. I discovered that zebrafish *hspb7* mutants develop cardiomegaly with mild focal cardiac fibrosis and sarcomeric abnormalities. Strikingly, significant mortality was observed in *hspb7* mutants subjected to exercise stress, demonstrating a genetic and environmental interaction that determines disease outcome. I identified large sarcomeric proteins FilaminC and Titin as Hspb7 binding partners. In the absence of Hspb7, FilaminC was prone to aggregate formation, which arises following protein damage and is detrimental to cardiac function. Damaged FilaminC undergoes autophagic processing to maintain sarcomeric homeostasis. I discovered that loss of Hspb7 in zebrafish or human cardiomyocytes stimulated autophagic pathways and expression of the sister gene encoding Hspb5. Finally, inhibiting autophagy caused FilaminC aggregation in *HSPB7* mutant human cardiomyocytes and developmental cardiomyopathy in *hspb7* mutant zebrafish embryos, demonstrating enhanced reliance on autophagy in the absence of Hspb7. These studies highlight the importance of damage-processing networks in cardiomyocytes, and a previously unrecognized role in this context for Hspb7. Additionally, *hspb7* mutant zebrafish are a model system of cardiomyopathy in which additional insults precipitate a severe phenotype, mimicking human cardiac disease. Thus, it provides a novel tool for finding modifier genes or pathways that impact severity of cardiomyopathy.

Previous work suggested that *hspb7* is regulated by the Gata4 transcription factor. In a separate but complementary project, I generated novel zebrafish lines with mutations in *gata4*, *gata5*, and *gata6*. I characterized defects in cardiac development that arise in embryos null for *gata6*, including a previously undiscovered alteration in ventricular myocyte identity. Additionally, I observed failure in pancreas and liver development. Surprisingly, I discovered that *gata4* is dispensable for zebrafish development. However, *gata4* mutants have a developmental delay, suggesting a role for Gata4 in regulating early epiboly. Finally, I documented compensation between *gata4* and *gata6* in the developing zebrafish, including a novel role in the establishment of left-right asymmetry. This work provides tools for further elucidation of the unique and overlapping roles of GATA factors during zebrafish development.

BIOGRAPHICAL SKETCH

Emily Joel Mercer was born in Aldershot, U.K. to Liam and Amanda Mercer in the late 1980s. Her early life was spent terrorizing her younger brother, Ben, and instructing assemblies of other small children in the correct strategies for enjoyable play. During her childhood, Emily picked up an interest in fossils and evolution from her paternal Grandmother, Mary, an amateur geologist and all-around accomplished matriarch; and from her Uncle Dom, then a gold prospector whom she imagined to be Indiana Jones. This interest grew into an affinity for the biological sciences as Emily learned about inherited genetic traits and diseases within her own family. A particular interest in Hox genes and stem cells culminated in her pursuing a Bachelors degree in Biochemistry (Pharmacology) at the University of Surrey, which she elected to attend on the basis of their sandwich year Professional Training program, and the microscopic possibility of obtaining a placement in New York City. Having spent a year's undergraduate internship working under the supervision of Dr. Steven Gross at Weill Cornell Graduate School, Emily was inspired to return to Weill for her doctoral studies. She followed her early interests in stem cells and development to join the laboratory of Dr. Todd Evans, a decision for which she has been thankful every day of her graduate school tenure. When she is away from the bench, Emily likes to say she is the ultimate New York tour guide, entertaining visitors from the U.K. with the hidden gems of the city. She has an especial depth of knowledge in the field of cuisine appreciation. Upon completion of her PhD, Emily intends to indulge in some outrageously decadent meals, travel to at least 3 new countries, finally let her younger (much cooler) brother give her a tattoo, and generally put off being an adult for as long as possible.

In memory of my Grandmother, Mary,

whose love of learning inspired those who knew her.

ACKNOWLEDGEMENTS

It would be utterly unthinkable to begin these acknowledgements with anyone other than my mentor, Dr. Todd Evans, who has been an unwavering source of support, empathy and inspiration over the past 5 years. Todd always makes time to commiserate or celebrate my latest data and had an abiding faith that I could, and would, succeed, even when I doubted myself. I defended this thesis in a blizzard that shut down the northeast, and it is down to Todd's drive and determination that it went ahead at all. Todd, thank you for everything. I am incredibly lucky to have conducted my graduate research under your mentorship, and am grateful every day for my good fortune.

The hurdles and hazards of my scientific journey have been navigated with the help of Dr. Lorraine Gudas and Dr. David Christini, who served on my Thesis Committee. Lorraine, the Pharmacology family you have built within Weill has always made me feel at home. Thank you. My gratitude goes to Dr. Richard Kitsis, who brought his expertise to serve on my Final Examining Committee. I especially wish to thank Dr. Steven Gross, who took me into his lab when I could barely hold a pipette and has always been my advocate, and my friend. I would also like to acknowledge the mentorship of Dr. Tal Nuriel and Dr. Pam Wille, who answered more questions than at all reasonable, and are always there for me.

Science is not a solo endeavor, and in the Evans Lab, Todd has created a community of scholars, scientists and friends on whom I lean every day. Dr. Ritu Kumar, Dr. Miriam Gordillo and Dr. Bran Cook, I hope I soaked up some of your wisdom. To Dr. Gabe Rosenfeld, thank you for taking me under your wing, and for introducing me to zebrafish and to HSPB7. To Suveg, Kelly and Jin, my comrades, thank you for the high fives, the sympathy, the hugs and the laughter. To Arielle and to Ingrid,

thank you for your considerable help, your conversation and, most of all, your friendship. I also wish to extend my everlasting gratitude to Sarah Kendall, who tackled this project alongside me for a whole year and is now well on her way to being a superstar scientist in her own right.

I offer my deepest gratitude to my family, who support me from afar with phone calls, letters, care packages and love. To my parents, Mandy and Lee, who always encouraged me to be independent and to follow my dreams, little knowing that they would carry me across an ocean. Your love and support has made me who I am. To Dom and Liz, who are my cheerleaders in times of joy and in times of struggle, thank you. To Becky, Dave, Dan and Joe, thank you for the continuous supply of chocolate and smiles.

Finally, to the friends who ran, walked, and crawled this grad school journey by my side, I do not think I would have made it without you. Thank you for being my source of strength, solace and laughter through every turn of this rollercoaster. Here's to the future!

TABLE OF CONTENTS

LIST OF FIGURES

LIST OF TABLES

CHAPTER 1: INTRODUCTION

Cardiac development, function and disease.

Introduction to cardiac disease

Cardiovascular disease (CVD) accounts for 1 in 3 deaths in the United States[1] and 1 in 4 in the United Kingdom[2]. Heart pathologies can be broadly subdivided into diseases of cardiac morphogenesis, which affect around 8 in 1000 live births[1], and cardiomyopathies of the adult cardiovascular system. Adult cardiomyopathies can either be attributed to inheritance of a particular gene variant, or can be a complex disease with various smaller genetic or environmental influences presumed to have a combinatorial deleterious effect. Despite causing problems to a common organ, the mechanisms by which these separate pathologies arise are remarkably diverse.

The leading cause of CVD in the Western world is ischemic heart disease (also known as coronary artery disease, CAD), although the margin between mortality caused by CAD and that caused by other forms of CVD is narrowing[3]. CAD is a complication of atherosclerosis, a disease caused by the buildup of fatty deposits, known as plaque, in the blood vessels. The presence of plaque leads to progressive dysfunction and remodeling of the walls of the blood vessels as well as pathological activation of inflammatory signaling pathways. Narrowing of the blood vessels supplying the heart to the extent that the supply of oxygen to the heart is compromised leads to chest paid known as angina. However, the most severe consequence of CAD is a heart attack, where a blood clot occurs following rupturing of an atherosclerotic plaque and blocks the cardiac oxygen supply. The original plaque rupture may occur anywhere in the body. CAD has been a focus of

many studies that have linked its increased prevalence to unhealthy lifestyle choices; plaque buildup is increased with high-fat, high-sugar diet, lack of regular exercise and smoking. Lifetime risk of CAD is increased 10- to 20-fold with the addition of these environmental risk factors*. There are known genetic contributors, and even causal mutations, for CHD, and it is important to note that CAD and its associated risk factors will likely have an impact on the progression and outcome of any adult cardiac pathology. However, this thesis will now focus exclusively on congenital and complex genetic-based cardiomyopathies.

Inherited cardiomyopathies can manifest during development in the form of congenital heart defects. These defects in cardiac development are a result of errors in the migration, patterning or morphogenesis of cardiac precursors as they mature into adult cardiomyocytes and can often be mapped to mutations in key regulators of cardiogenesis, including transcription factors. Alternatively, inherited cardiomyopathies may only become apparent later in life. Such adult-onset pathologies are often attributable to mutations in structural components of the sarcomere, the contractile unit of the cardiomyocyte, including myosin, actin and myosin binding proteins[4,5], cardiac troponins[6] and filamin C[7,8].

Often, the development of cardiovascular disease in adults is not associated with a mutation in one particular risk gene. Instead, a number of factors are presumed to contribute *en masse* to the prevention or promotion of 'complex' heart disease. These can include external contributions from the lifestyle and environmental influences discussed above. Over the past decades, large genome-wide association

* Lifetime risk with an optimal risk factor profile is <1%(females), 3.6%(males) but rises to 18.3%(females), 37.3%(males) with 2 or more major risk factors[3]. Risk factors include smoking, high chlolesterol, low HDL, high blood pressure and diabetes.

studies (GWAS) have sought to identify genetic contributors to complex heart disease. To date, candidate genes from the structural sarcomeric components as well as regulators of calcium signaling, contraction and growth have all been implicated[4]. One problem in this field is the lack of reproducibility of candidate genes, highlighting the importance of delineating the role and mechanism of action of such candidates in the heart.

Inherited and complex cardiomyopathies can lead to different types of cardiomyopathy: hypertrophic, dilated and restrictive. Hypertrophic cardiomyopathy (HCM) is characterized by the thickening and stiffening of the cardiac walls. Conversely, in dilated cardiomyopathy (DCM) the cardiac walls become thinner and weaker, leading to enlargement of the ventricles. Restrictive cardiomyopathy is the least common of the three types and is characterized by wall stiffening without the thickening found in typical HCM. Unlike other cardiomyopathies, HCM is often asymptomatic in patients until sudden cardiac arrest.

Heart failure is the final common outcome of CAD, DCM and restrictive cardiomyopathies and occurs when the heart is no longer strong enough to pump sufficient blood around the body, leading to fatigue, generalized and pulmonary edema and shortness of breath. The pathways that lead to the development of heart failure are complex, for as the heart becomes progressively more dysfunctional, the increased load on the myocytes activates various compensatory systems are activated which lead to remodeling of the cardiac tissue. Although these pathways are intended to offset initial dysfunction, they are ultimately damaging and lead to pathological alteration in heart structure and function.

The stepwise progression to heart failure is incompletely elucidated, but is thought to arise following dysregulation of adrenergic activation and calcium signaling following alteration in cardiac load. This could be chronic, following slow progression of a congenital cardiomyopathy, or acute in response to a heart attack[4].

The prevention and treatment of controllable risk factors for cardiac disease, e.g. recognition of the influence of diet on heart health, and the treatment of high blood pressure with statins, has gone a considerable way to improve heart health in many individuals predisposed to heart disease[9]. However, the treatment for the end-stage of these diseases, heart failure, remains either palliative care or heart transplant. Mortality rates for heart failure are documented to be falling, but the 5-year survival rate remains around 50%[1]. This high mortality rate for patients suffering from end-stage heart disease is indicative of a bottleneck in our progress in the development of effective therapeutics. Additionally, studies indicate that the overall population with heart failure will grow in the coming years as a result of a growing and aging population[1].

The huge threat and enormous complexity of cardiovascular disease necessitate considerable further investigation in order to better understand both the pathogenic processes, and how best to treat these patients. One strategy to better understand cardiac disease is to study cardiac development**.** In this manner, we can gain a fundamental understanding of the physiological roles of genes and pathways that are important for the genesis and maintenance of a functioning heart, and learn more about what can go wrong when these genes and pathways are compromised. Ultimately, we might hope to be able to take these discoveries

and translate them into treatments or tools to prevent, correct or ameliorate the human pathologies.

An Overview of Cardiac Development

The early stages of cardiogenesis are relatively well conserved, and, given the focus of much of the studies detailed in this thesis, the zebrafish is here used as an example system.

The embryo starts out as a single fertilized egg, which undergoes a series of divisions to form a multicellular blastocyst (Figure 1-1A). Prior to the specification of particular organs, the cells of the developing embryo first become one of three primitive germ layers: endoderm, ectoderm, or mesoderm, from which the heart is derived (Figure 1-1B).

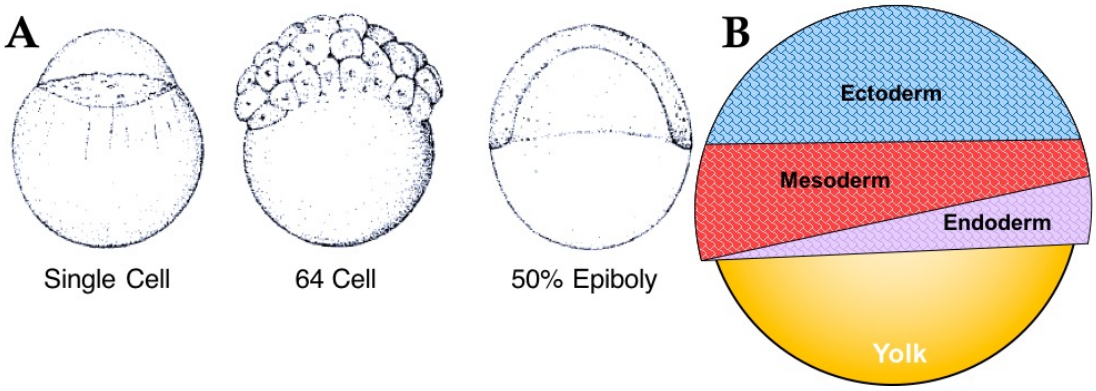

Figure 1-1: Initial embryogenesis leads to the formation of germ layers.
(A) Progression of zebrafish egg from fertilized single cell through numerous cell divisions until the cells begin to envelop the yolk. Adapted from Kimmel et al (1995)[10]*.*
(B) Schematic detailing the germ layers in the developing zebrafish at 50% epiboly.

At 50% epiboly, the earliest stages of zebrafish cardiac development occur, including the specification of progenitors (Figure 1-2A). The myocardium is the product of two waves of cellular influx from distinct progenitor populations, referred to as the first and second heart field (FHF/SHF). Early specification stages

are controlled by morphogen signaling gradients that relate positional information to cells in the developing embryo.

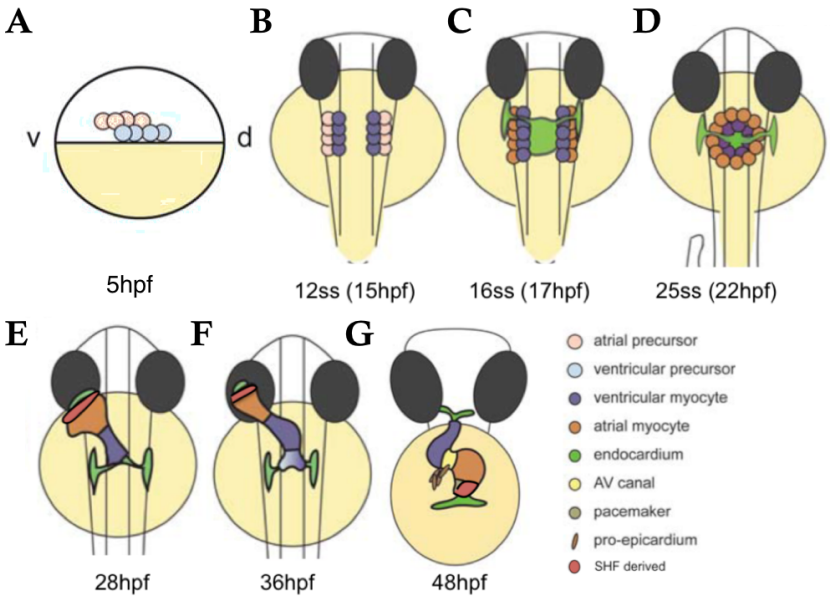

Figure 1-2 Stages of zebrafish cardiogenesis.
Schematic detailing the stages of zebrafish cardiac specification and morphogenesis, occurring in the first 48 hours post fertilization. For more details see text. Adapted from Bakkers (2011)[11].

At the 15 somite stage (Figure 1-2B), the FHF myocardial progenitors are situated in the anterior lateral plate mesoderm (ALPM) of the developing embryo and begin to undergo instructional interactions with the developing endoderm (Figure 1-2C). The importance of this interaction is highlighted by the phenotype of incomplete migration and resultant cardia bifida in animals with defects in genes important for endoderm specification[12,13], as well as in endoderm-derived signaling molecules such as sphingosine-1-phosphate[14]. Reciprocally, the cardiac mesoderm is known to modulate the migration of endocardial precursors.

FHF cells migrate to the midline of the embryo (Figure 1-2B,C) and form a circular population called the cardiac cone (Figure 1-2D). Following the specification and migration of cardiac progenitors, the developing heart begins a complex morphogenetic process. The cardiac cone periscopes to form a linear heart tube (Figure 1-2E), which begins to beat in a peristaltic motion. The heart tube extends out and jogs to the left (Figure 1-2F). During the extension process, the cardiomyocytes of the developing heart tube have very low levels of proliferation, and instead growth is mediated by the migration of SHF-derived cells that add to the poles of the heart[15].

The heart tube subsequently undergoes a process known as 'looping' to bring presumptive atrial and ventricular sections of the heart tube to a side-by-side position (Figure 1-2G,Figure 1-3). The genetic regulators and signaling pathways that control the looping process are poorly understood. Intriguingly, the processes of looping and jogging appear to be linked, since the low percentage of hearts that jog to the right usually ultimately form a 'D-loop' mirror image of the normal morphology.

During looping, the cardiac chambers also become visually distinct through a process known as 'ballooning', in which both the presumptive atrial and ventricular portions of the heart tube take on separate curvatures, which are separated by a constricting region, the atrio-ventricular (AV) canal (Figure 1-3A, see below). Changes in overall cardiac morphology are also associated with chamber-specific changes in the cytoskeletal structure of individual myocytes. Work from the Stainier lab has capitalized on the zebrafish's visual accessibility during development to observe actin rearrangements in developing atrial and

ventricular myocytes[16]. The cytoskeletal structure of myocytes is essential for their function, and in turn myocyte function drives changes in cardiac morphology.

Mutants in sarcomeric genes such as *myh6*[17] and *vmhc*[18], which alter sarcomeric development in the atrium or ventricle respectively, have defective cardiomorphogenesis, secondary to alteration in signaling pathways stimulated by blood flow and myocardial stretch. Likewise, loss of or abnormalities in the cardiac conduction system lead to alterations in the size and shape of both the individual myocytes and the overall chambers[19].

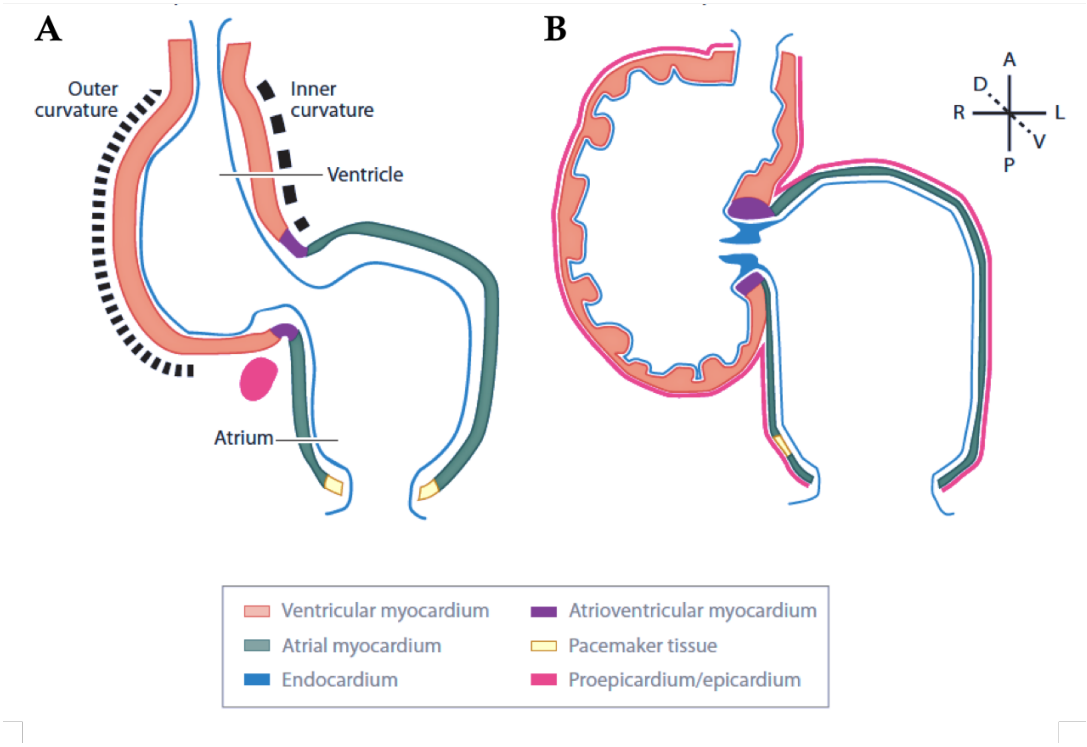

Figure 1-3 Structure of the developing zebrafish heart.
Cross-section through the developing zebrafish heart at (A) 48hpf and (B)120hpf, detailing the endo-, myo- and epicardial layers. Taken from Staudt and Stainier (2012)[19].

As the chambers specify, there is concurrent specialization of the endocardium that lines them. Endocardial cells in the AV canal region thicken into endocardial cushions which will ultimately become the AV valve, important for ensuring unidirectional blood flow. Key developmental signals BMP, Notch and Wnt become restricted to the AV region between 36 and 48hpf. The AV endocardium undergoes progressive changes in cell shape over the following 3 days which result in two valve leaflets through invagination†. The process of endocardial cushion formation and subsequent division of the heart into separate chambers is recapitulated during the process of septation in the four-chambered mammalian heart[20]. As seen for chamber morphogenesis, valve formation is affected by fluid forces, and mutations that affect myocyte contraction lead indirectly to errors in valvulogenesis[21].

The cardiomyocytes that form the two chambers must also specialize to become either an atrial or a ventricular myocyte. The restriction of the expression of some genes to either the atria or the ventricle has been long established, however the external cues and transcription factor programs that result in these differences are less well elucidated. Recent studies have identified *nkx2-5* and *2-7* as essential for the repression of atrial genes in zebrafish ventricular myocytes[22], and the Tbx family of transcription factors are known to be differentially expressed in human cardiac chambers[20]. Studies from our own laboratory are making progress in understanding how the GATA transcription factor family (see page 24) are involved in myocyte identity (Unpublished data E.J.M. see Chapter 6, and Tang and Evans). The utilization of novel sequencing techniques to understand the

† In amniotes this process occurs via endothelial-mesenchymal transition and subsequent delamination rather than invagination.

transcriptomes of specific cell types in development[23], and in the adult[24] and regenerating[25] heart, will certainly lead to discoveries in this field.

The period between 48hpf and 6dpf is also characterized by marked cardiomyocyte proliferation leading to overall growth of the heart and thickening of the myocyte wall. The Tgfβ, Igf and Hedgehog pathways have been identified as regulators of cardiomyocyte proliferation during development[26‡]. Fibroblasts and endocardial tissues are known to be the originators of these signals, and thus crucial drivers of myocardial proliferation. In the absence of adequate proliferation, hearts become pathologically enlarged and thin-walled, a phenotype reminiscent of dilated cardiomyopathy. Proliferating ventricular myocytes may also undergo an identity change and delaminate from the ventricular wall, migrating inwards to form the network of internal muscle called trabeculae.

For a more detailed review of cardiogenesis in the zebrafish, see Bakkers (2011)[11] or Staudt and Stainier (2012)[19].

A network of evolutionarily conserved core transcription factors, some of which have already been mentioned above, coordinates these complex cardiac specification and morphogenetic events[27–29] (Figure 1-4). These factors include *NKX2-5*, *TBX5* and *GATA4*. Our lab has focused considerable effort toward understanding the roles of the *GATA* factors, including *GATA4*, in development. The GATA proteins and their roles in embryogenesis are explored further on page 24.

‡ And were subsequently shown to also be important for the proliferation of cardiomyocytes in the regenerating zebrafish heart[26].

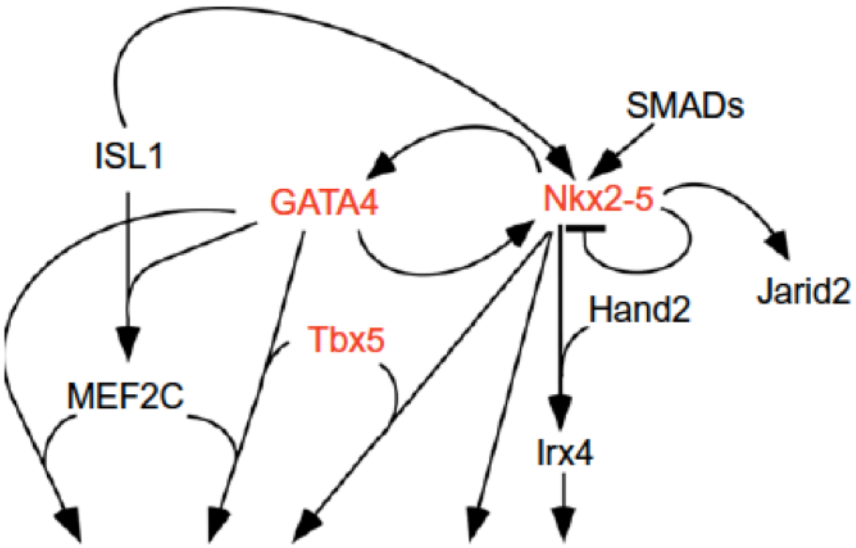

Figure 1-4: Core network of key transcription factors for cardiac development. *The transcription factor GATA4 works in cooperation with other cardiac transcription factors including Nkx2-5 and Tbx5 to regulate cardiac specification and morphogenesis. Figure from McCulley and Black (2012)*[30]

An introduction to the functioning cardiomyocyte

The heart is the earliest organ to form and function. As discussed above, myocytes initiate a lifelong contractile routine as soon as the initial heart tube is formed, and continue to beat as morphogenesis occurs.

Contractile Units of the heart

The minimal force-generating unit in a muscle cell is the subunit of the myofibril; the sarcomere (Figure 1-5). Sarcomeric structure is based around thin-filament chains of polymerized actin, which overlap with thick filaments composed of myosin. By hydrolyzing ATP, myosin heads are able to move along the thin actin filaments and pull the surrounding structure together to contract. The thick and thin filaments are framed by larger, structural proteins that form scaffolds around them.

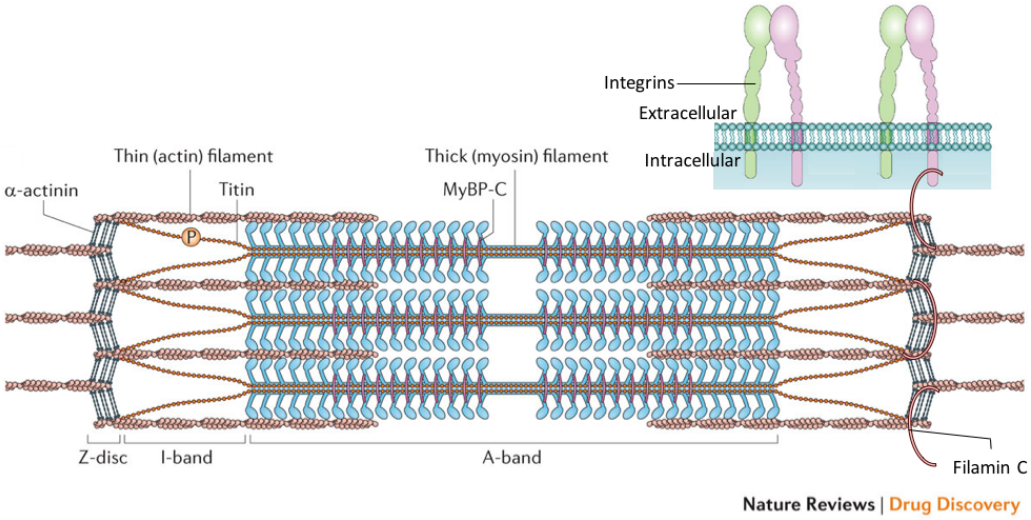

Figure 1-5: Structure of a sarcomere.
Basic schematic detailing the components of a sarcomere. Myosin makes up the thick filament (A band), which slides along the thin filament (I band, predominantly actin) during contraction. The Z-disc is composed of structural proteins, including Filamin C, and is also attached to the sarcolemma. Integrins and other signaling proteins localized on the sarcolemma facilitate transduction of external signals, including changes in the tension on the cell or the force of surrounding contraction. Adapted from Hwang and Sykes (2015)[31].

These scaffolding proteins include titin, which acts as a molecular spring, and runs half the length of a sarcomere. Titin limits the amount of stretch that can occur to the sarcomere, helping maintain tension in a muscle. Filamin-C (FLNC) is another of the scaffolding proteins that help to structure the sarcomere. The filamin family are known to be involved in the cross-linking of actin in all cell types, and FLNC is the isoform specifically expressed in striated muscle. FLNC is usually localized to Z-discs; multiprotein complexes involved in sensing and communicating biomechanical stress. Sarcomeric structures are coupled to the plasma membrane at various foci, which facilitate signal transduction, and FLNC has been hypothesized to have a conduit role, allowing communication from the extracellular space to the sarcomere. This signal transduction allows the

contraction of the sarcomere to be coupled to external stimuli including mechanical stressors, adrenergic signals and surrounding myocyte contraction.

Multiple overlapping models exist of myofibrillogenesis (the assembly of initial sarcomeres and their subsequent coalescence into myofibrils). Recent advances in imaging technologies have facilitated more detailed studies of cardiac myofibrillogenesis in the zebrafish. Huang *et al.* describe a multistep process in which an initial non-striated network of actin stress fiber-like structure develops in developing cardiomyocytes[32](Figure 1-6A). This network is similar to that found in many cell types.

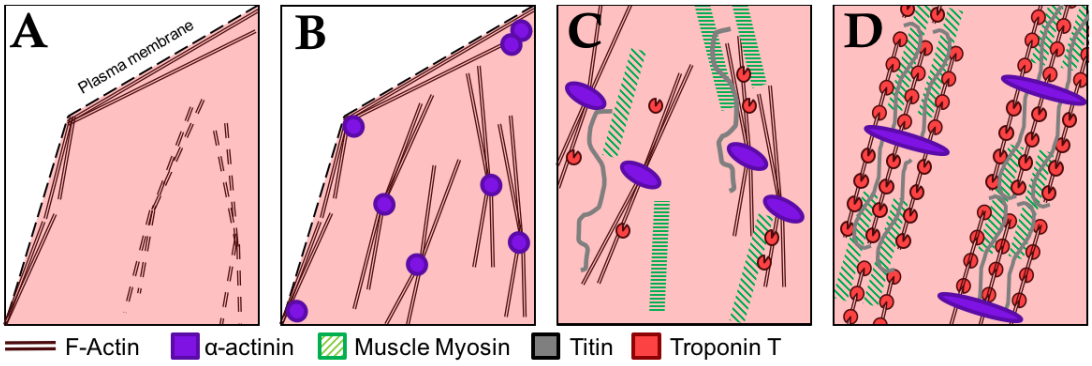

Figure 1-6: Stages of myofibril assembly.
Diagram detailing the basic stages of myofibril assembly. For details see text.

Z-bodies composed of α-actinin assemble along the actin stress fibers (Figure 1-6B). Subsequently, sarcomeric protein expression is upregulated and muscle myosin and troponin t begin to assemble into thick and thin 'rodlet' pre-myofibrils respectively (Figure 1-6C). As α-actinin begins to localize in regular nuclei along the stress fiber-like actin structure, the pre-myofibrils begin to assemble in striations along with it (Figure 1-6D). Finally, the overall distance between adjacent striations increases, and the heart begins to beat. Sarcomeric maturation

after this point includes increases in size, positional alignment and synchronous contraction.

The importance of the sarcomeric proteins is highlighted by what happens when they do not function correctly. Mutations in sarcomeric component proteins including titin, FLNC, γ-sarcoglycan and α-actinin are among those most commonly identified in cardiac disease. Sarcomeric dysfunction is central to the pathologies of hypertrophic and dilated cardiomyopathies.

Whilst the sarcomere appears a stable mechanical structure, it has become increasingly apparent that it is highly dynamic. Studies have shown turnover of even large sarcomeric proteins, including actin[33], titin[34] and FLNC[35], which occur even while the sarcomere continues to contract. A recent study has also suggested that FLNC actually plays a functional role in sarcomeric turnover, facilitating repair of damaged myofibrils[35]. Following removal from the sarcomere, damaged proteins must then be degraded to prevent their forming into pathological aggregates. Though somewhat unexpected, it is evident that the processes that allow for removal of damaged proteins from the sarcomere are extremely important for continued cardiac function because mutations in many genes involved in this process lead to cardiac disease. This is striking because in some cases, such as for mutations of cardiac Troponin T[6] and FilaminC[7], the protein in question is broadly expressed in striated muscle, but disease can be localized to the heart[5].

Proteostasis in the heart.

Protein turnover is very important in the heart.

The cardiomyocyte represents a relatively unique cell type for a number of reasons. First, it has to continuously contract and relax in order to maintain blood

flow, exposing the cytoskeletal components to continuous mechanical strain. Second, the mammalian cardiomyocyte has been shown to be post-mitotic, with low levels of cytokinesis following the first few days of life[36–38]. It is generally believed that following the loss of proliferative ability, growth in the overall size of the mammalian heart is achieved through hypertrophy of the cardiomyocyte rather than division[§]. Dilution of protein aggregates through cytokinesis is thus a response mechanism that is not available in this instance.

Although the post-mitotic state of mammalian cardiomyocytes is well accepted, it is not true in all organisms. For example, the zebrafish retains a significant amount of plasticity in its heart and cardiomyocytes are able to partially dedifferentiate and proliferate following traumatic damage or cardiomyocyte death[26,39], resulting in complete healing of the damaged portion of the heart with minimal scarring. Additionally, recent studies have suggested that there may be transient periods during the life of an organism in which the cardiomyocytes re-enter the cell cycle. Work from the Husain and Graham labs recently identified a pre-adolescent cardiomyocyte proliferative burst in mice[40] that interestingly falls in a similar period of development to the juvenile expansion stage of the cardiac wall in zebrafish, a process that is known to be reliant on Gata4[41].

[§]Newer studies suggest that some cytokinesis is retained in young human hearts[38], but this falls to below 1 in 10,000 after the first decade of life. Therefore, this is unlikely to be a relevant source of cardiac growth, or a useful strategy to deal with protein aggregates.

General mechanisms of protein turnover.

The lack of cell division and requirement for continuous movement in a cardiomyocyte put it at particular risk for the formation of aggregates, and so a functional adult cardiomyocyte employs a number of strategies for the removal of damaged proteins. One of the most comprehensively applicable of these is the process of autophagy, outlined in Figure 1-7.

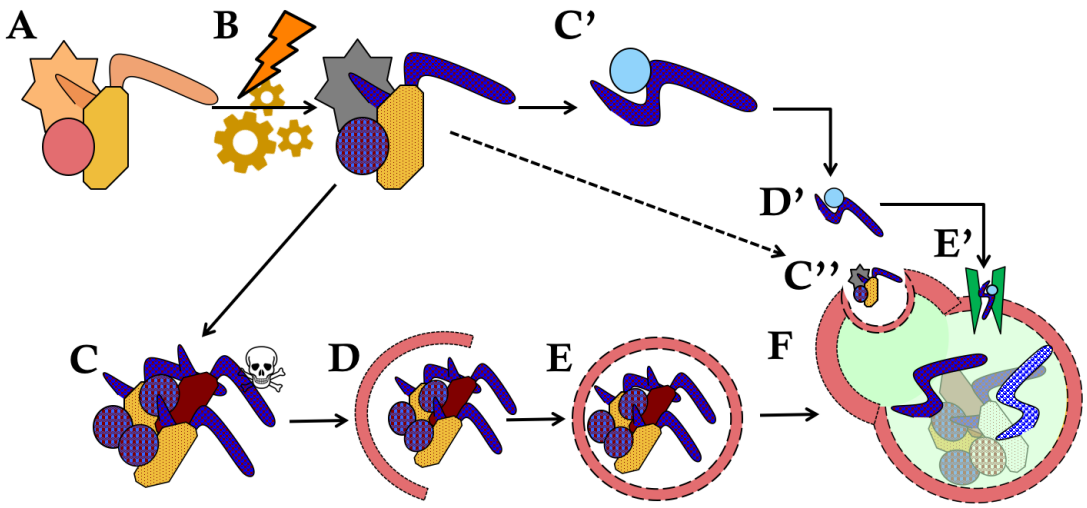

Figure 1-7: Autophagy is a mechanism for degrading damaged proteins
Schematic: (A-B) Damage can occur to normal proteins or protein complexes that may then be processed by (C-F) macroautophagy, (C'-D') chaperone-assisted autophagy or (C'') microautophagy. For more details see text.

Depletion of energy or nutrients activates autophagic genes (Atg family) and inhibits negative regulators of autophagy. Initially, an isolation membrane is formed. It subsequently elongates, a process that requires sequential activation of various Atg family members including Atg8/LC3, which is processed from a soluble precursor (LC3-I) to an autophagic-membrane associated form (LC3-II). The growing membrane sequesters proteins and organelles targeted for autophagic degradation. Following completion of the autophagosome, it fuses with

a lysosome; lysosomal proteases catabolize the contents, making their component parts available for reuse. Finally, the autophagolysosome is degraded[42].

It is increasingly recognized that the process of macroautophagy, described above, is a simplified view of the situation. In addition to macroautophagic generalized degradation of cellular materials, two additional pathways have been detailed: microautophagy (Figure 1-7C'') and chaperone-assisted autophagy (Figure 1-7C'-F').

Non-canonical forms of autophagy

Like macroautophagy, the process of microautophagy can mediate the engulfment and degradation of larger structures such as entire organelles, or of protein aggregates. In contrast to macroautophagy, microautophagy involves the direct invagination of the lysosomal membrane (Figure 1-7C'') to engulf the nearby cytoplasm. The regulation of microautophagy is not well understood, but it is increased by nutrient-low conditions[43].

Chaperone-assisted autophagy can mediate the degradation only of soluble proteins, and is thus inherently more limited than macro- or microautophagy in terms of its targets. However, an important consideration is that indiscriminate self-eating may ultimately be detrimental to the cell. Chaperone-mediated autophagy is able to specifically select proteins for recycling through the protein-protein interactions of the chaperone proteins. Therefore, for particularly aggregate-prone proteins or those that need to be closely regulated, chaperone-mediated autophagy is a targeted strategy. The process can actually be further divided into two pathways: chaperone-mediated autophagy (CMA) and chaperone-assisted selective autophagy (CASA).

Proteins targeted for the CMA pathway contain a characteristic pentapeptide motif that can be recognized by the chaperone protein Hsc70 (Figure 1-7C'), which binds the substrate protein and translocates to the lysosomal membrane (Figure 1-7D'). The hsc70:substrate complex interacts with LAMP2-A protein on the target of the lysosome, whereby the substrate is unfolded and, assisted by LAMP2-A, crosses the lysosomal membrane (Figure 1-7E'). Within the lysosome, the substrate protein is degraded. As is evident, the key determinant of CMA degradation is the pentapeptide motif, which is composed of a sequence of amino acids carrying specific charges[**]. Around 30% of proteins carry such a motif[44], and so it has been proposed that these proteins can avoid degradation through burying the pentapeptide motif in hydrophobic domains, or through post-translational modifications that mask or alter the charge sequence. Conversely, proteins that do not naturally have a pentapeptide motif can acquire one through post-translational modifications that add charge. A key example protein of therapeutic interest that is regulated in this manner is huntingtin, acetylation of which has been shown to target it for CMA-mediated degradation[45].

An alternate form of autophagy in which chaperones play a pivotal role, CASA, was recently described in a series of papers from the Höhfeld laboratory[46–48]. In this paradigm, the substrate protein is bound by a complex of chaperone proteins including Hsc70, BAG3 and HSPB8. In contrast with the direct delivery to lysosomal LAMP2 seen in CMA, CASA substrates and their associated chaperone protein BAG3 are subsequently ubiquitylated. Ubiquitin is a regulatory protein

[**] The canonical hsc70 recognition sequence is KFERQ, which carries positive charges on lysine and arginine, a central hydrophobic phenylalanine and a negatively charged glutamatic acid followed by a glutamine. Studies have shown that the overall pattern of charges and hydrophobicity is more important than the specific amino acids, although a glutamine is always found at the beginning or end of the motif.

that is ligated onto proteins that are usually targeted for degradation by the proteasomal system. In the case of CASA, ubiquitylated substrate and its associated chaperone complex recruit a ubiquitin-autophagy adaptor which subsequently induces the formation of the autophagosome to engulf the complex. The CASA pathway has been shown to be active in muscles, where it is integrated with tension sensing and upregulation of substrate proteins[48], ensuring the stoichiometric ratios of myoskeletal components is maintained.

Further complicating the overall picture, the forms of autophagy presented above are not mutually exclusive and can interact with each other to form combination pathways under certain circumstances. In addition, other auxillary pathways exist that mediate degradation of specific cellular components, including direct degradation of phagocytosed material. These pathways, their regulation, targets and interactions are currently a field of active research with many unknowns and controversies. As such, they are not discussed further herein, but the reader is referred to recent reviews on the topic[43,49–51].

Autophagy in the heart

Autophagy occurs constitutively in cardiac tissue, and genetic or pharmacologic inhibition of autophagy can induce heart failure[52]. In addition, upregulation of autophagy in response to cardiomyopathy is long established[53], and has been illustrated following various insults, including ischemia-reperfusion, anthracycline-mediated cardiotoxicity and heart failure. In some situations induction of autophagy exacerbates pathology[54]; however, upregulation of autophagy has been shown to be protective in some models of heart failure[55–58]. Thus, physiological function requires autophagic processes to be carefully regulated and operating at appropriate levels.

Model systems for studying cardiac development and function

In order to study the development of organ systems, including the heart, a number of different model systems are routinely employed. These include, but are not limited to, the zebrafish, and human embryonic stem cell-derived cardiomyocytes (hESC-CMs). Whilst hESC-CMs may seem the logical choice for the study of pathways and genes relevant to human disease, current research techniques cannot generate fully differentiated, adult cardiomyocytes or entire functioning hearts. Conversely, in the zebrafish one can rapidly gain a mature, complete organ but are compromised by differences from the human system and limitations in available biochemical tools. Thus, the use of a combination of model systems confers complimentary benefits.

The Zebrafish Model System

The zebrafish has a number of distinct characteristics that recommend it for the study of development. Zebrafish embryos develop externally and can be easily maintained in a transparent state for the entirety of embryogenesis, either through the use of small molecules or of pigment-free Casper line[59]. The process of zebrafish embryogenesis is substantially progressed by 72 hours post fertilization (hpf), commencing with the laying of several hundred eggs by a single adult female. An important consideration here is that in the zebrafish we can easily observe stages of the developmental process that occur post-implantation in the mouse, and are thus near impossible to track in mammals with any accuracy. A beautiful depiction of the stages and accurate timing has been in existence for decades[10], allowing consistent comparison of zebrafish mutants between strains, research groups and generations.

Importantly, genetics of the zebrafish are well conserved with that of the human and mutagenesis screens in zebrafish have resulted in the identification of a number of key genes that control developmental pathways in higher vertebrates. The study of genetic pathways in the zebrafish has been aided by the technique of microinjection, in which macromolecules including DNA, RNA, proteins and modified oligonucleotides such as morpholinos can be injected directly into the 1-2 cell stage embryo. This allows researchers to easily modulate levels and locations of gene expression during early embryogenesis. Additionally, the aquatic abode of the zebrafish enables easy exposure to soluble small molecules. Most recently, the advent of genome editing technologies such as TALEN and CRISPR has enabled targeted, rapid and specified mutation of genes of interest in the zebrafish system for the first time[60–62].

Embryonic Stem Cell Model System

ESCs are derived from the inner cell mass of developing blastocysts[63]. These cells maintain a pluripotent state; they are able to both renew themselves indefinitely and to differentiate to form any of the tissue types that are found in the adult body. This system is complemented by induced pluripotent stem cells (iPSCs), which are derived by the transfection of adult somatic cells with factors that drive them to dedifferentiate back to pluripotency[64]. iPSCs offer the advantage of the production of stem cell lines with disease-associated genotypes, facilitating identification of abnormalities in the development and function of specified cell types, and are now routinely used in laboratories all over the world.

Many groups have contributed to the development of robust protocols for the derivation of various tissues, including the heart, from these stem cells, often

recapitulating the signaling events that are known to play key roles in *in vivo* organogenesis.

Human embryonic stem cell-derived cardiomyocytes.

Human ESC-derived cardiomyocytes (hESC-CMs) arise spontaneously, if sporadically, when ESCs are allowed to differentiate into aggregated clusters, known as embryoid bodies[65]. Following initial observations of spontaneous myogenesis, decades of work have defined and refined protocols for cardiomyocyte derivation from ESCs[66].

ESC/iPSC-CMs represent a desirable system for the study of cardiac genes and processes for several key reasons. First, they provide a model in which we can directly study the differentiation and function of human cardiomyocytes, rather than representatives from other animals. This is particularly useful for the exploration of the effects of specific genetic inconsistencies that have been associated with disease, by making iPSCs from patients who exhibit particular symptoms. Second, the hope remains that one day we may be able to derive enough numbers of functionally mature iPSC-CMs to use in the treatment of human heart disease – through the replacement of damaged heart tissue or valves, or even by growing entire functioning hearts in the lab for organ transplant.

The excitement of being able to generate hESC-CMs is tempered by important caveats. First, the cardiomyocytes generated by this method are functionally immature: displaying morphology, cytoskeletal arrangements and electrophysiological profiles more closely matched to human fetal cardiomyocytes than to adult cells. Although these phenotypes can be partially mitigated through engineered maturation methods, including extended culture periods, enforced

synchronization of contraction, mechanical loading and tissue engineering, the discrepancies between the model system and the real human heart remain[67].

HL-1 cells as a model system

Finally, the murine atrial cell line, HL-1, has been routinely used in the study of cardiac proteins and functions. This cell line was developed by the Claycomb lab through optimization of conditions for cell culture passage of the AT-1 differentiated cardiomyocyte tumor, a line derived through targeting the Simian Virus 40 large T antigen under the atrial natriuretic factor promoter[68]. It is the only spontaneously beating, passageable cardiac cell line to date and has been a huge asset for research in this field, providing adequate numbers of manipulatable cells for biochemical experimentation and imaging. However, in contrast with early reports, research using this model system has been compromised by heterogeneity in phenotype and proteome within the population of HL-1 cells ([69] and E.J.M. observations).

Summary: Cardiac Development, Function and Disease

There is a large literature exploring the heart and its physiological and pathological development and function. In this section, the basic stages of cardiac development have been explored. In addition, various model systems used to study heart development and function were outlined and their relative merits discussed. Of particular note, recent advancements in the field of human embryonic stem cell research are the cause of excitement as they enable the examination of human cardiac differentiation *in vitro*. In addition, such protocols facilitate the comparison of differentiation and function in lines derived from patients with various genetic alterations that lead to cardiac disease. When combined with novel genome editing technologies, the true contribution of single mutations in isogenic backgrounds

can be elucidated, raising hopes that more intricate mechanisms of action and possible treatment avenues for these diseases may be revealed.

However, despite centuries of research, there is still much to be uncovered. As discussed above, the numerous contributors to adult-onset cardiomyopathy are more difficult to unravel. There is an ongoing requirement for model systems that more closely resemble human disease and its complex nature, and for a better understanding of the various contributors to and stages of cardiomyopathy.

Particular attention has been paid to discussing the process(es) of autophagy, and its role in the heart. As a generally applicable strategy for disposing of problematic unfolded, faulty or excess proteins or aggregates, autophagy is uniquely poised to play a protective role in the cardiomyocyte. A better understanding of autophagic processes and their compensatory role in the heart might facilitate therapeutic interventions that can accurately titrate this pathway to optimal efficacy.

An introduction to GATA Transcription Factors

GATA proteins are transcription factors

The GATA proteins are a family of zinc finger transcription factors that recognize and bind to an WGATAR motif in genomic DNA[70]. The zinc finger domain is comprised of a C-X-X-C-X_{17}-C-X-X-C motif which coordinates zinc ions with the cysteine residues, and is required for DNA-binding activity[71].

The GATA family members have been shown to have roles as regulators of tissue-specific developmental programs. GATA proteins can be divided into GATA-1, -2 and -3, which have important roles in hematopoiesis, and GATA-4, -5 and -6 which are important in endoderm and mesoderm development, including in the heart, liver and gut (Figure 1-8).

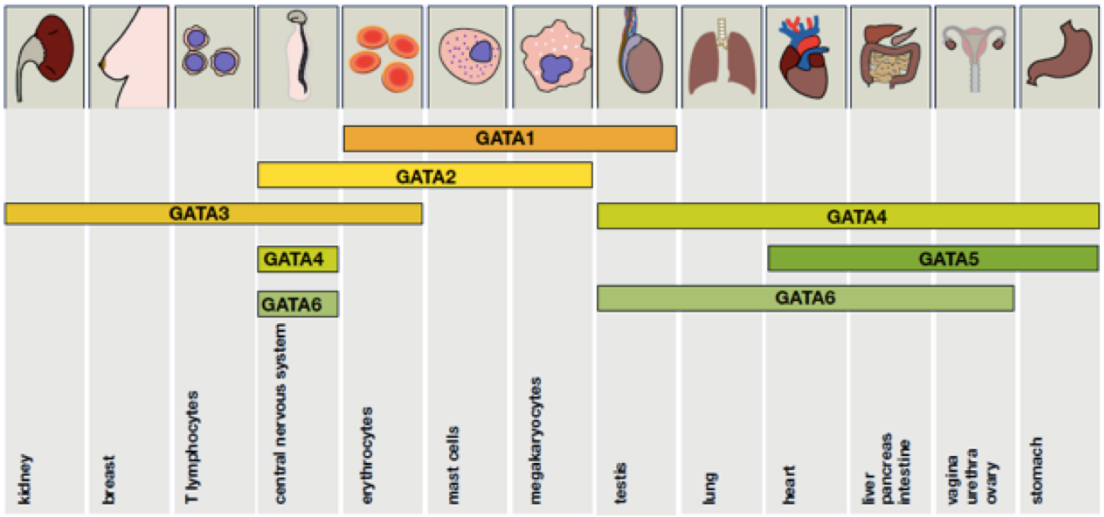

Figure 1-8: The GATA factors play roles in the development of many different organs.
Schematic depicting the relative expression patterns and roles of the GATA factor family members in each tissue type. Adapted from Lentjes et al. (2016)[72]

In contrast to the two zinc-finger DNA-binding domains detailed above, the roles of the remaining domains of the GATA proteins are not well described. A nuclear localization sequence has been identified in GATA4, -5 and -6 and presumably exists in the other family members, which are routinely localized to the nucleus. The N- and C- terminal regions of the proteins are more variable and are believed to play transactivation roles through interactions with other transcription factors, co-activators and co-repressors. The tissue specificity-based bisection of the GATA family is recapitulated by increased similarity between the proteins within each

subgroup (Figure 1-9). The GATA4, -5, -6 family are of particular interest to the research detailed herein.

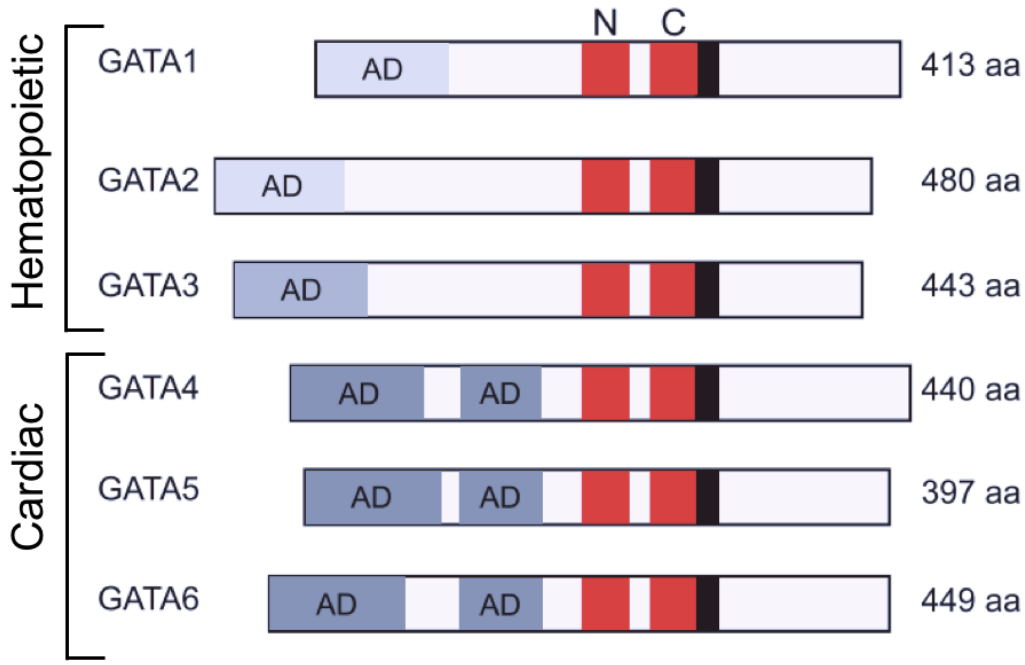

Figure 1-9: Structure and homology of the GATA factor proteins.
The GATA factors have high homology specifically in the DNA binding domain (dark blue) with relatively unconserved N and C terminals. They can be divided into two separate familes. Adapted from Chlon and Crispino (2012)[73]. Zinc finger domains in red (N and C terminal). Nuclear localization sequence in black.

An introduction to GATA4

One of the earliest roles of GATA factors is in the development of the extra-embryonic tissues. Mouse embryos null for GATA4 die around E8.5 due to defects in the extra-embryonic visceral endoderm that precipitate abnormalities in folding of the embryonic tissues[74,75]. When the early defects are rescued by tetraploid complementation, cardiac defects (discussed below) are lethal at E9.5, however subsequent studies have utilized tissue-specific and/or conditional knockout systems to determine later roles for GATA4 in various organs. Loss of GATA4 in the intestine leads to changes in the gut epithelial barrier, changing resorption of

bile acid and suggesting a role for GATA4 in gut repair following injury[76,77]. Conditional knockout in the osteoblasts leads to perinatal death secondary to defects in bone formation[78], and loss of GATA4 in the hepatic endoderm or septum transversum mesenchyme (STM††) promotes liver fibrosis[79]. GATA4 has also been shown to play a role in gonadal development[80,81].

These studies are complemented by work from our laboratory conducted in the zebrafish[82]. Knockdown of *gata4* with a morpholino leads to defects in the development of the heart, gut, pancreas, liver and swim bladder. The overlap of organ systems affected by depletion of GATA4 in the zebrafish and in the mouse suggests that its role is conserved through evolution. In humans, mutations in GATA4 are predominantly associated with a spectrum of congenital heart malformations, with some concomitant testicular abnormalities[83].

GATA4 in cardiac development and function

Gata4 is expressed in the early cardiac progenitor populations on either side of the midline in the developing embryo, and expression is retained in the differentiating cardiomyocyte. In contrast with the drosophila *pannier* mutant, cardiomyocytes are still specified following loss (mouse) or knockdown (zebrafish) of GATA4. Following rescue of early embryogenesis by tetraploid complementation, GATA4 null embryos have subsequent problems in cardiac morphogenesis, namely disruption to the looping process, septation defects and hypoplastic ventricular myocardium[84]. The pro-epicardium is missing in GATA4 null embryos[84].

†† The STM is a transient structure in the developing embryo that gives rise to the diaphragm, and is an important source of signals that conduct liver development.

GATA4 has been shown to be required following initial heart tube formation, with zebrafish *gata4* morphants and *Gata4* null mice both exhibiting failure of jogging of the presumptive atrial portion of the tube and failure of the chambers to expand[82,84,85]. Deletion of *Gata4* later in mouse embryonic development leads to decreased myocardial wall thickness and decrease in cardiomyocyte proliferation, illustrating that Gata4 has a continued role following initial morphogenesis[85]. In humans, mutation of *GATA4* leading to hemizygosity is associated with a variety of congenital heart defects, demonstrating that its function during cardiomorphogenesis is conserved. However, there is considerable variation even between family members carrying the same *GATA4* mutation. Thus, loss of one allele of *GATA4* is in itself insufficient to determine disease phenotype. Haploinsufficiency of *Gata4* has been further investigated in mice. Mice heterozygous for a GATA4 mutation that truncates the protein express half the wildtype protein level. In mice of mixed genetic background, cardiac development is normal. However, in inbred C57 mice the same genotype leads to defects in cardiac development, including septal and endocardial cushion defects similar to those seem in human disease[86]. These studies lead to the insight that *GATA4* haploinsufficiency is paradigmatic of haploinsufficiency in a developmental regulator and highlights the importance of modifier genes for determining the ultimate outcome of such heterozygous mutations for congenital birth defects.

GATA4 in the adult heart.

Genes that are important during the development of the heart often have a continued role in the adult cardiomyocyte in physiological or pathological states.

In the adult zebrafish cardiomyocyte, *gata4* expression is normally very low or absent, but is upregulated upon injury, and required for successful repair of

ventricular injury[87]. Inducible knockout of *Gata4* from the hearts of adult mice leads to progressive cardiac enlargement and dysfunction, which appears to occur downstream of dysregulation of a network of genes required for cardiomyocyte survival[88]. In humans, null mutations in GATA4 have not been identified in patients with late-onset cardiomyopathies, however it seems likely that severe phenotypes occurring early in the GATA4-deficient heart obscure the later requirement.

Conditional knockout of *Gata4* from mouse cardiomyocytes (CM) demonstrated an ongoing role for GATA4 in developing myocardium, with these mice exhibiting myocardial thinning, abnormal ventricular morphogenesis and CM proliferation defects[85]. Although re-expression of GATA4-regulated fetal genes in an adult has been considered to be pathological[89–91], other groups have shown that GATA4 is required to maintain normal homeostatic heart function throughout life[88]. Mice heterozygous for *Gata4* exhibit mild cardiac dysfunction with decreased CM number, and are hypersensitive to pressure overload[92]. Moreover, it is well established that GATA4 expression is cardioprotective in a variety of stress conditions including hyperglycemia[93], anthracyclin-induced cardiotoxicity[94,95] and ischemia-reperfusion[96].

Thus, GATA4 is essential for cardiac morphogenesis, is required for the maintenance of post-natal cardiac function, and is of particular importance under conditions of increased cardiac stress. Some progress has been made to identify targets of GATA4 that might facilitate its cardioprotective activity. These include anti-apoptotic BCL2 family members[94,97], as well as less predictable targets. For example, the muscle transcription factor CARP is regulated by GATA4, and CARP depletion mimics a doxorubicin (dox)-mediated sarcomeric disarray phenotype[98]. However, CARP overexpression is insufficient to rescue CM treated with dox,

consistent with multiple mechanisms acting downstream of GATA4 to mediate cardioprotection. This example highlights a major gap in our knowledge concerning the molecular mechanisms contributing to both physiological and pathological response to stress in the heart.

In summary, although many previous studies have carefully outlined a role for GATA4 throughout the life of the heart, and in particular during stress response, the mechanistic basis of GATA4 function is incompletely understood. A better understanding of cardioprotective pathways is key for the development of effective therapies. Mutations in cardiac stress response genes have been associated with cardiomyopathy[99–101], suggesting that loss of protective mechanisms that counteract cardiac stress contributes to the enormous burden of heart failure.

As a master regulator transcription factor, GATA4 has myriad targets within the genome and controls the expression of hundreds of genes[28,102]. It is therefore a strong hypothesis that multiple mechanisms downstream of GATA4 coordinate to control tissue migration, differentiation and identity.

An introduction to GATA6

Similar to GATA4, embryos in which *GATA6* has been knocked out die around E5.5 due to defects in the extra-embryonic endoderm. This early lethality was recently demonstrated to be due to a requirement for GATA6 in the specification of primitive endoderm through inhibition of Nanog signaling[103]. Following rescue by tetraploid complementation, GATA6 null embryos can develop to E10.5, although they are smaller than sibling controls[104]. Analyses of the embryos at E10.5 indicated that up until this point GATA6 is dispensable for formation of the heart, vasculature and STM, but that there are defects in liver formation. The hepatic bud

specifies but fails to expand in GATA6 null embryos, indicating that GATA6 is required for hepatic outgrowth. The cause of death in GATA6 null embryos remains unknown.

The exploration of conditional GATA6 knockout in various tissue types has been less thorough than for GATA4. Knockout of GATA6 in the neural crest-derived vascular smooth muscle cells (SMCs) led to malformations of the cardiac outflow tract and aortic arch[105]. The neural crest-derived SMCs are known to be a source of patterning cues for the developing heart, but appeared to have developed normally in these animals, suggesting that the role of GATA6 is specifically to regulate expression of SMC-derived signaling molecules. Mice with conditional deletion of GATA6 in endothelial cells still develop normally but develop spontaneous hypertension, suggesting that GATA6 plays a role in blood vessel tone or function[106].

Zebrafish embryos with *gata6* knockdown develop early defects in cardiac development, with abnormalities in cardiac precursor migration. These defects are earlier than those observed in the mouse, suggesting a species-specific requirement for GATA6 at different stages of heart development. In humans, mutation in GATA6 is associated with congenital cardiac malformations[107]. In addition, some patients present with pancreatic agenesis, suggesting a role for GATA6 in pancreatic development that is not revealed by *Gata6* gene knockout studies in the mouse.

Redundancy between GATA factors during cardiac development.

Although the single knockout and single conditional knockout studies have been informative, combination knockout/down studies by our lab and others has demonstrated that GATA factors are able to compensate for each other during

development. Xin *et al.* (2006) showed that whilst mice heterozygous for Gata4 or Gata6 can develop normally, compound heterozygosity resulted in a range of defects in cardiogenesis with early embryonic lethality, illustrating that GATA dosage is an important factor in cardiogenesis[108]. Work from our own lab has demonstrated that Gata5 and Gata6 are redundant for cardiac development[109]. Redundancy between GATA factors appears to vary according to species and to tissue type.

In mouse, compound heterozygosity of GATA4 and GATA6 leads to defects in cardiovascular development including thinning of the myocardium[108]. Strikingly, a similar phenotype is observed in GATA4/GATA5 compound heterozygotes[110], suggesting that overall GATA load is potentially more important in heart development than the contributions of specific GATA factors. In zebrafish, work from our laboratory has demonstrated that *gata5* and *gata6* are redundant for the specification of cardiomyocytes but that cardiomyocytes are lost following the knockdown by morpholino of both genes[109]. Combined knockdown of *gata4* and *gata5* or *gata6* did not lead to the same phenotype, suggesting that in the zebrafish *gata4* is less important than the other family members for cardiac specification.

Combinatorial conditional deletion of murine GATA4 and GATA6 has also revealed that they play a role in pancreatic development[111]. Here, again, overall GATA load appears to play a role, since deletion of one *GATA6* allele in a GATA4 null background led to a substantial loss of pancreatic mass. The same was not true for loss of one GATA4 allele in a GATA6 null background, suggesting that GATA6 is better able to compensate for GATA4 than *vice versa,* at least in the pancreas.

Questioning whether the differential expression pattern or inherent differences in the protein prevented complete redundancy, a recent study replaced the murine

GATA4 gene with the *GATA6* cDNA and demonstrated that GATA6 is able to recapitulate the role of GATA4 in extraembryonic tissues, but not in the developing heart[112]. Such replacement studies will be of particular use to help deconvolute the various contributions of each GATA family member to developmental processes.

Regulation and modification of GATA activity

When considering different model systems, there are some differences in the roles of and redundancies between GATA-4, -5 and -6. The factors that control binding of GATA4 rather than GATA5 or GATA6 are not well understood, although there is evidence that they do not have entirely overlapping binding sites. Potential explanations for the differences in target genes include the contribution of cofactors to binding location and activity upon binding, as well as post-translational modifications.

Key candidate cofactors for mediating some of these redundancies and differences are the friend of GATA (FOG) proteins. These proteins contain a series of zinc finger domains, as well as domains known to recruit corepressors[73]. In humans there are two FOG proteins, FOG1 and FOG2, which can be generally associated with the hematopoietic and cardiac GATA factor families, respectively. This is based on expression pattern during development. FOG2 has predominantly been studied in terms of its relationship with GATA4. Although knockout of FOG2 in mice leads to lethal cardiac defects during embryogenesis, they arise later than those seen in GATA4 null embryos[113], indicating that GATA4 has FOG2-independent roles. FOG2 has also been shown to cooperate with GATA4 in other tissues, including the liver[114] and lung[73]. Interestingly, there is evidence that FOG1 cooperates with

GATA4 in the small intestine[115], highlighting how co-factors can regulate the specificity and activity of GATA factors.

In addition to dedicated co-factors, improvements in ChIP and chromatin mapping technologies have allowed researchers to identify complexes of transcription factors within which the GATA factors reside. A recent study of differences in the expression patterns of cardiomyocytes harboring a mutation in another cardiac transcription factor, TBX5, demonstrated that the relationship between GATA4 and TBX5 was altered, driving a loss of identity for the cardiomyocyte through a genome-wide alteration in the binding sites of transcription factor complexes[116]. Studies such as this highlight how master transcription factors can work in concert to conduct genome-wide alterations in transcription to define cell identity, and serve as a reminder that the activity of each GATA factor is highly regulated by a plethora of binding partners.

The relationship between the GATA factor and its binding partners, as well as with DNA, can be regulated by post-translational modifications. A conserved stretch of basic amino acid residues is known to be an important site of post-translational modifications that control DNA binding and the ability of the GATA factor to initiate transcription. Phosphorylation and acetylation sites have been identified within and surrounding the zinc finger domains, and such post-translational modifications have been demonstrated to be important for the activity of GATA4[117,118], illustrating how signaling pathways can act on kinases or acetyl transferases to rapidly act to alter GATA function.

GATA factors are also thought to heterodimerize[119], which may contribute to redundancy, particularly in mutants in which the protein is partially truncated rather than completely deleted.

In summary, the mechanisms by which GATA activity can be modulated and regulated are myriad, and are still under investigation. By appreciating the abilities of GATA factors to compensate for each other under defined circumstances, and what those circumstances are, we will be better able to understand their roles in development and disease.

Gata4 regulates expression of *hspb7*

With a view to identifying cardioprotective targets of GATA4, a previous graduate student in our laboratory performed an RNA-sequencing experiment. Using injected morpholinos (MOs), he depleted Gata4 in zebrafish embryos from the *tg(myl7:gfp)* strain, which expresses GFP in CMs. GFP^+ CMs were purified by FACS from stage-matched morphants and controls, and RNA was deep-sequenced using the Illumina Hi-Seq platform. Using this platform, he discovered that Gata4 regulates the expression of small heat shock protein beta 7 (Hspb7)[120]. ChIP-seq data from murine HL-1 cells indicates that Hspb7 is a conserved and direct target gene of Gata4 in mammalian CMs[102,120].

The small heat shock proteins

Introduction to the small heat shock proteins.

The small heat shock proteins (sHSPs) are a family of 15-30kDa chaperone proteins that, unlike their higher-molecular-weight counterparts, do not depend on ATP for their cytoprotective actions. The family is conserved down to invertebrates, with demonstrated roles for sHSP family members in the development of *Drosophila*[121]. sHSPs are characterized by a C-terminal alpha-crystallin domain composed of eight β-strands that interact to form a β-sheet, and has been demonstrated to play a role in homo- and hetero-oligomerization of various sHSP family members. The human sHSP family is composed of 10 core members and one associated protein[122], whereas the zebrafish has 14 predicted sHSPs[123] (Table 1-1).

Gene	Alternate Name	Conservation	Expression	Human Mutations
hspb1	HSP27	H, M, Z	Ubiquitous	Syndromes with peripheral nerve pathologies or neuromuscular defects
hspb2	MKBP	H, M, Z	Heart and muscle	
hspb3	HSPL27	H, M, Z	Heart and muscle	Adult-onset motor neuropathy
hspb4	CRYAA	H, M, Z	Eye lens	Microphthalmia, cataracts
hspb5	CRYAB	H, M, Za, Zb	Ubiquitous	Myofibrillar myopathy, cataracts, cardiomyopathy, multiple sclerosis
hspb6	HSP20	H, M, Z	Ubiquitous	
hspb7	cvHSP	H, M, Z	Heart and muscle	
hspb8	HSP22, H11	H, M, Z	Ubiquitous	Syndromes with peripheral nerve pathologies or neuromuscular defects
hspb9	CT51	H, M, Z	Testis	
hspb10	ODF1	H, M	Testis	
hspb11	HSP30, IFT25	H*, M*, Z	Placenta	
hspb12		Z	Heart	
hspb15		Z†	Unknown	

Table 1-1: Summary of the small heat shock protein family
*Detailing the members of the small heat shock protein family and their alternate names. Conservation in human (H), mouse (M) and zebrafish (Z) is indicated. Human disease in which specific mutations in an HSPB family member has been identified are detailed in the right-hand column. *Considered to be 'HSPB-like' based on sequence similarity. †Expression identified by blast query and confirmed at mRNA level only.*

Alignment of the HSPB familes from human, mouse and zebrafish demonstrates that most members are more closely related between species than to each other (Figure 1-10).

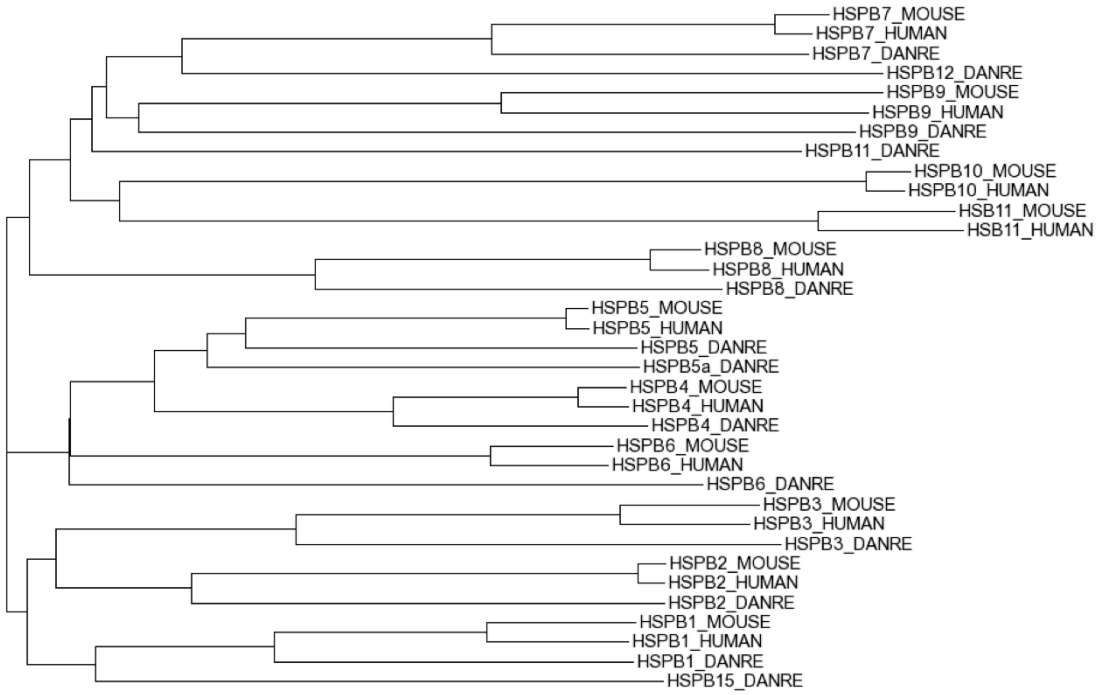

Figure 1-10: Phylogenetic tree of the HSPB family.
Phylogenetic tree of the human, mouse and zebrafish (danre) small heat shock proteins generated with ClustalX. Zebrafish small heat shock proteins cluster more closely with their human or mouse orthologs than with other zebrafish paralogs.

sHSP have varied expression patterns during development[124] and in the adult (Table 1-1), and the molecular mechanisms of action of the sHSP, where they are known, are heterogeneous. For these reasons, it is difficult to extrapolate the function of one sHSP from another, and for several family members the physiological role and mechanism of action is as-yet unknown. Indeed, a number of studies evaluating the activity of each of the human sHSP proteins in specific stress scenarios clearly demonstrate variety in both their function and mechanism of action[125–128].

Small heat shock proteins and protein aggregation

There are an increasing number of discoveries linking the sHSP to protein aggregation. Sequencing data from patients with protein aggregate disorders has unearthed mutations in HSPB5 (also known as CRYAB). These mutations are associated with myofibrillar myopathies, in which electrical or clinical cardiomyopathy is also a symptom[129].

The presumed role of sHSPs in preventing protein aggregation has been explored by various groups through testing the ability of overexpression of a specific sHSP to prevent aggregation of an overexpressed aggregate-prone protein or protein fragment. Experimental aggregate proteins include polyglutamate-containing polypeptides such as mutated huntingtin and mutated ataxin-3[127], as well as non-polyglutamate pre-aggregates such as mutated amyloid-beta protein. In most studies, the full panel of sHSPs were screened for their ability to prevent aggregation of the mutant protein in question.

Small heat shock proteins in the heart

A subset of the sHSP, HSPB1-3 and HSPB5-8, are expressed in the human heart. Interestingly, there is not complete agreement across all species regarding the expression pattern of particular sHSP family members, suggesting that their relative contributions to cardiac function may vary between species. Knockout of HSPB1, a highly expressed cardiac sHSP, did not result in any cardiac abnormalities[130], however high levels of over-expression of HSPB1 appeared to result in a decrease in reductive stress. This is attributed to contributions of HSPB1 (and also HSPB8) to the modulation of the redox state of glutathione[131].

Small heat shock protein beta 7

HSPB7 is among the least characterized sHSPs, except that its expression is known to be highly restricted to the developing and adult heart[124,132], and at lower levels in skeletal muscle. The structural and functional diversity of the sHSP family precludes inference of HSPB7 function from findings concerning other sHSP family members, and so much was left to uncover when I started this project.

Early work characterizing HSPB7 identified an interaction partner in the human heart, α-filamin (FLNA)[132], which crosslinks actin filaments and links actin with membrane glycoproteins. FLNA is involved in remodeling the cytoskeleton to facilitate changes in cellular morphology, migration and mechanosensory transduction[133,134]. However, a functional relationship between HSPB7 and FLNA was never characterized. HSPB7 has also been shown to prevent aggregation of poly-glutamate tract-containing proteins, albeit in an ectopic overexpression system[127]. The authors conducted a series experiments which eliminated activation of the general cell stress response; active refolding of unfolded proteins; targeting of aggregates to the proteasome; and upregulation of other small heat shock proteins as the molecular mechanism underlying this activity. However, the authors did demonstrate that the anti-aggregate activity of HPSB7 was attenuated by loss of a key autophagic protein, Atg5. Interestingly, this study also demonstrated that, unlike other HSPB family members, HPSB7 does not form large oligomers.

Work from the Brundel lab reported that HSPB7 co-localizes with tachypacing-induced F-actin stress fibers, and is protective against both their formation and tachypacing-induced calcium transient reductions in cultured murine CM (HL-1) cells[126]. In keeping with the preceding studies, the anti-aggregate activity of HSPB7

has been shown to operate exclusively by preventing aggregate formation rather than through promoting clearance of pre-formed aggregates[135].

A recent conditional knockout study in mice demonstrated that skeletal muscles undergo progressive myopathy in the absence of HSPB7[136]. This study also identified dimerized FLNC as a binding partner of HSPB7 in skeletal muscle, and showed that FLNC aggregates form in *HSPB7*$^{-/-}$ myofibers.

Thesis objectives

Having identified HSPB7 as a GATA4 target gene in the developing heart, we were interested in uncovering its physiological role in the cardiomyocyte. Taken together, the literature suggests that HSPB7 does have an important role in the heart. Restriction of HSPB7 expression to striated muscle suggests that this role may be muscle specific.

I hypothesized that HSPB7 binds to potentially problematic cardiac proteins and prevents their unfolding and/or aggregation. I hypothesized that in the absence of HSPB7, cardiomyocytes would develop pathological aggregates that interfered with their function, potentially to the point of causing cardiomyopathies in HSPB7 null animals. My thesis studies were designed to test these hypotheses.

CHAPTER 2: MATERIALS AND METHODS

Basic Zebrafish Methodologies

Zebrafish Husbandry

All zebrafish strains were maintained at 28.5°C in our zebrafish facility, and all procedures carried out as approved by the WCMC IACUC. Embryos were staged as described[137].

Zebrafish Lines

The *tg(myl7:gfp)* strain was originally obtained from H.J. Tsai (Taiwan) and has expression of GFP in the myocardium. The *tg(lfabf:dsRed;elaA:EGFP)*(LiPan) strain[138] was originally obtained from Z. Gong (Singapore) and expresses GFP in the pancreas and dsRed in the liver. The *tg(fli:gfp)* line was obtained from the Zebrafish International Research Center (ZIRC) and expresses GFP in the endothelium. The *tg(gata1:rfp)* line was a kind gift of Leonard Zon (Harvard Medical School) and expresses RFP in the erythrocytes. The *tg(fli:gfp)* and *tg(gata1:rfp)* lines were crossed in our laboratory to generate the double transgenic *tg(fli:gfp; gata1:rfp)* line.

Preparation of fertilized embryos

The day before injection, adult animals were set up in individual breeding tanks males and females separated by a divided to prevent premature egg release and allow accurate embryo staging. Up to two males and two females were housed in one individual breeding tank. The following morning, the fish were transferred to fresh system water. The divider was removed to allow breeding to commence. A perforated screen separated adult fish from the fertilized eggs, which sank through

the screen to the bottom of the tank and were collected around 20 minutes after adult release.

Microinjection

Needles for microinjection are made as needed from 3.5" capillary tubes (VWR) that have been prepared with a Model-97 micropipette puller (Sutter). Needles are cut with a razor blade to a tip diameter of 0.14-0.18 μm.

Exercise of adult zebrafish

Equal numbers of *hspb7* mutant zebrafish and wildtype sibling controls were placed in a swim tunnel (Loligo Systems, Denmark) and subjected to water flow of 50 cms^{-1} for 30 minutes, once a day. Zebrafish mortality was tracked by physical daily count, and fish locations tracked with an iPhone camera. Zebrafish location during swim challenge was tracked with MTrackJ for ImageJ[139].

Monitoring oxygen consumption of adult zebrafish during exercise

Following placement of equal numbers (10 each) of *hspb7* mutant zebrafish and wildtype controls in a swim tunnel, the apparatus was sealed. The respirator, which measures oxygen concentration (Witrox4, Loligo Systems, Denmark) was calibrated to minimum and maximum levels by bubbling nitrogen or air, respectively, through breeding tanks of system water for 10 minutes before taking measurements. Oxygen concentration in the water was recorded every 1 second throughout the period of exercise using the Witrox CTRL software (Loligo Systems). Oxygen saturation (%) was calculated using the Witrox CTRL software. Overall change in oxygen saturation from the beginning to the end of the swim was used to determine oxygen consumption during the swim. Oxygen levels in the swim tunnel were restored to maximum by replacement of water and aeration before a new school of fish was exercised.

Small molecule treatment of embryonic zebrafish

Zebrafish embryos were manually dechorionated with forceps at 24 hpf and exposed to increasing concentrations of bafilomycin A1, chloroquine diphosphate or 3-methyladenine (all from Sigma) in a solution of E3 medium (5.0mM NaCl, 0.17mM KCl, 0.33mM CaCl, 0.33mM $MgSO_4$) with 1% DMSO (all Sigma). Small molecule compounds were refreshed every 24 hours.

Microdissection of complete hearts from embryonic zebrafish

Hearts were dissected from 3-5dpf zebrafish larvae as described[140]. This protocol is suitable for the isolation of larval zebrafish hearts for immunostaining or generation of RNA:

- Zebrafish larvae were anesthetized in 1X Tricaine in E3 until touch response was lost.
- Transfer one larva and a pool of E3 with 1X Tricaine to the well of a concave microscope slide, positioned under a light microscope.
- Taking two X-gauge needles, use one to spear the zebrafish larva dorsal to the heart, trying to avoid piercing the yolk. Insert the second needle immediately ventral to the first needle and pull forward swiftly. The heart will detach from the embryo at the inflow and outflow tracts and float into the liquid surrounding the fish.
- Use a cut-off 20µl pipette set to 2µl to capture the dissected heart. Transfer to buffer of your choice for further processing

Dissection of hearts from adult zebrafish

Hearts were dissected from adult zebrafish as described[141].

- Aesthetize adult (3-18 month) zebrafish on ice for 20 minutes.

- Immobilized fish by inserting one half of a pair of forceps into the mouth and pinching the head.
- Bisected the fish with a clean razor blade immediately posterior to the pectoral fins.
- Use forceps to cut the ventral attachment of the operculum to the body, exposing the dorsal aorta. Use forceps to bisect the dorsal aorta.
- Hold the fish head in place with one set of forceps, and use a second set of forceps to grasp the pectoral fins and attached body cartilage, and lift them away from the main torso.
- The heart will either have come away with the pectoral fins, or remains in the torso, but is easily visible. In many cases the heart will still be beating slowly.
- Release the fish head and use both pairs of forceps to tease the heart away from the torso and remove the pericardium.
- Grip the heart by the remainder of the dorsal aorta and place onto a clean microscope slide for imaging, or transfer to a buffer of your choice for extraction of nucleic acids or protein.

Measuring zebrafish heart size.

Following dissection, adult zebrafish hearts were placed on a microscope slide and imaged on a dissection microscope (Nikon) with top-lighting. Hearts were rotated to present maximal ventricular area and images were captured with Spot Imaging Software. Ventricular area was calculated with FIJI software, as described[56].

Prior to dissection, anesthetized zebrafish were partially dried with paper towels and weighed. Zebrafish mass was used as a normalizing factor for heart size index (VA/BW) since it is a greater variable than body length in adult fish[56].

Generation of mutant zebrafish lines

Sequences of TALEN and CRISPRs used in this thesis are provided in Table 2-2.

Generation of TALENs and TALEN-derived mutant lines

TALENs were designed using the Cornell TAL Effector Nucleotide Targeter 2.0 website[142] and plasmids encoding specific TALENs were generated with the TALEN Golden Gate 2.0 kit (Addgene) as previously described[143]. Generation of correct sequences was confirmed through digestion with BspEI, which generates a characteristic fingerprint. Resultant vectors were linearized with SmaI and mRNA encoding TALENs was synthesized with the mMessage mMachine kit (Thermo Fisher). mRNA was quantified with a Nanodrop machine and run out on a 1% agarose gel with ethidium bromide in order to verify that there was no degradation. 100-400 pg of mRNA was injected into zebrafish embryos at the 1-2 cell stage.

Generation of CRISPRs and CRISPR-derived mutant lines

Guide RNAs (gRNAs) for CRISPR-Cas9 mediated mutagenesis were designed with the CHOPCHOP website[144] and ordered as double stranded oligo cassettes with a T7 promoter at the 5' end from IDT. The gRNA was generated with the MEGAshortscript kit (Thermo Fisher) and purified through ammonium acetate precipitation as per the manufacturers instructions. mRNA was quantified with a Nanodrop machine and run out on a 1% agarose gel with ethidium bromide in order to verify that there was no degradation. 250 ng/µl gRNA was combined with 500 ng/µl recombinant Cas9 protein (PNA BIO) and 0.2M KCl, and incubated at room temperature for 15 minutes to allow RNA-protein complexes to form. 1nl of the gRNA-Cas9 complexes was injected into embryos at the 1-2 cell stage. Cell injections were performed in this case but it is worth noting that yolk injections

have subsequently been shown to lead to equivalent mutation rates by members of the community and may be more efficient for future experiments.

Identification of mutant lines by genotyping of pools of embryos

DNA was generated from 2-3 pools of 5-10 individuals from clutches of F0-injected embryos using the DNEasy kit (Qiagen). DNA was quantified by nanodrop and stored at 4°C. For HSPB7, carriers of mutations were identified through PCR across the target locus followed by RFLP analysis with HpyCH4V (NEB). Primers for each target locus are listed in Table 2-3. For all other genes targeted, carriers of mutations were identified through re-naturation of PCR products followed by digestion with T7 endonuclease I (NEB) as described[145]. PCR products were cloned into a TOPO vector (Invitrogen) and sequenced to identify mutant alleles. Clutches of embryos containing mutations were raised to adulthood and outcrossed to wildtype animals. Pools of F1 embryos were screened for mutations as described above, and clutches of embryos from F0 fish that were transmitting mutations were raised to adulthood.

gDNA collection from larval zebrafish by tail biopsy

DNA was extracted from 3dpf embryos for genotyping as previously described[146]:

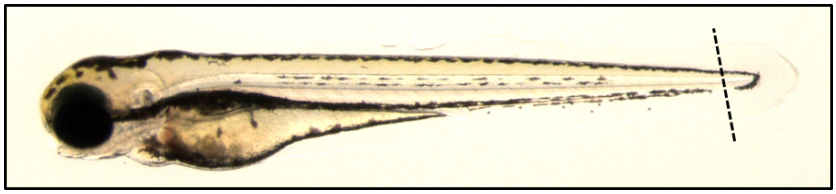

Figure 2-1: Detailing the desired dissection for tail biopsy of 3dpf zebrafish
Brightfield image of 3dpf zebrafish embryo, showing pigment gap in the tail. Desired cut for tail biopsy (dashed line) is immediately posterior to the looping caudal vein.

- Before commencing, dechorionate all zebrafish and remove discarded chorions.
- To a 24 well plate, add 1ml E3/well.

- To a 96 well plate, add 35µl 50mM NaOH/well.
- To a petri dish, add 15µl 20% Tween in 1X Tricaine in E3. Move embryos to be genotyped to 1X Tricaine in E3+Tween in batches of ~4.
- Transfer single embryos to the upturned lid of a petri dish. Minimize the amount of liquid transferred.
- Under a microscope, use a microscalpel to dissect off tail fin in pigment gap posterior to blood stream (Figure 2-1)
- Use 20µl tip to suck up dissected tail and add to 1 well of 96 well plate.
- Move embryo to numbered well of 24 well plate in 1ml E3 medium.
- Following dissection of tails for all embryos to be genotypes, transfer 24 well plate to incubator at 28°C.
- Seal 96 well plate with foil.
- Heat to 98°C for 2-5 minutes and spin down for 10 seconds at 500*g*.
- Add 10% (3µl) 1M Tris-HCL, pH8 and spin down for 10 seconds at 500*g*.
- Use 2µl of gDNA immediately in PCR reaction. gDNA generated in this manner is prone to degradation and should be used within 48 hours.

gDNA extraction from adult zebrafish

DNA was extracted from adult animals for genotyping as follows:

- Anesthetize adult fish in 0.16mg/ml Tricaine in system water for 5 minutes.
- Use a clean razor blade to slice off a small section of the anal or the ventral caudal fin.
- Return the animal to system water in a labeled isolation tank
- Place fin in 50µl gDNA extraction buffer (10mM Tris-HCl pH8.4, 50mM KCl, 1.5mM $MgCl_2$, 0.3% Tween-20, 0.3% NP-40) in a PCR tube
- Heat at 95°C for 15 minutes then cool to 55°C

- Add 3µl Proteinase K (20mg/ml stock, Roche), incubate at 55°C for 1 hour
- Heat at 95°C for 20 minutes
- Use 2µl of gDNA in PCR reaction and store the remainder at 4°C

Identification of F1 animals carrying mutations was performed by RFLP analysis or T7 assay as described below. PCR products from heterozygous mutant animals were cloned into the pCR-BluntII-TOPO vector (Thermo) according to the manufacturer's instructions. Vectors were sequenced from the M13Reverse primer at the Cornell Institute of Biotechnology Resource Center, or by GeneWiz, New Jersey. Primers for genotyping of zebrafish are provided in Table 2-3. Primers for sequencing of mutant alleles are provided in Table 2-5.

T7Endonuclease 1 (T7E1) assay:

The T7E1 assay allows identification of mutants within pools of embryos or of heterozygosity within a particular region. The T7E1 enzyme will cleave at mismatched base pairs, generating digestion products.

- To 10µl PCR product add 1.5µl NEB Buffer 2 and 3.5µl ddH2O
- Hybridize PCR products on the thermocycler (95°C 5 min, 95-85°C at -2C/sec, 85-25°C at -0.1C/sec, hold at 4°C).
- Remove from thermocycler. To each reaction add 0.5µl NEB Buffer 2, 4.3µl ddH2O and 0.2µl T7E1.
- Incubate the 20µl reaction at 37°C for 20 minutes. Run on gel or freeze immediately to prevent star activity of T7E1.

A novel PCR-based strategy for screening for known mutations

For identification of some mutations the published RFLP analysis and T7E1 assay strategies are insufficient. The T7E1 assay is not useful for distinguishing between homozygous mutants and wildtype individuals, since neither of these animals will

have mismatched base pairs following PCR and hybridization. RFLP analysis requires the convenient gain or loss of a relatively uncommon restriction site. As an alternative screening tool, I devised a PCR-based strategy in which two forward primers are combined with one reverse primer in the same PCR reaction. The outside forward primer (F) binds to a section of gDNA unaltered in the mutant animal. The internal forward primer (F') is designed so that the 3' terminus falls directly onto the base(s) that are altered in the mutant allele (Figure 2-2A). In a heterozygous genome, both primer pairs (F-R and F'-R) are equally able to bind and amplify, resulting in a long amplicon (derived from F-R) and a short amplicon (derived from F'-R). In the mutant genome, F' is totally unable to bind, resulting in the production of only the long amplicon. In the wildtype genome, both primer pairs are theoretically able to bind and one might initially anticipate the production of both the long and short amplicon from wildtype. However, we observe near-exclusive generation of the short amplicon (derived from F'-R). Since F' is able to bind to both amplicons, but F only to the long amplicon, we find that F'-R pairing outcompetes F-R pairing, resulting in visible production of the short amplicon only from wildtype genomes (Figure 2-2B,C).

Sequences of genotyping primers are provided in Table 2-3.

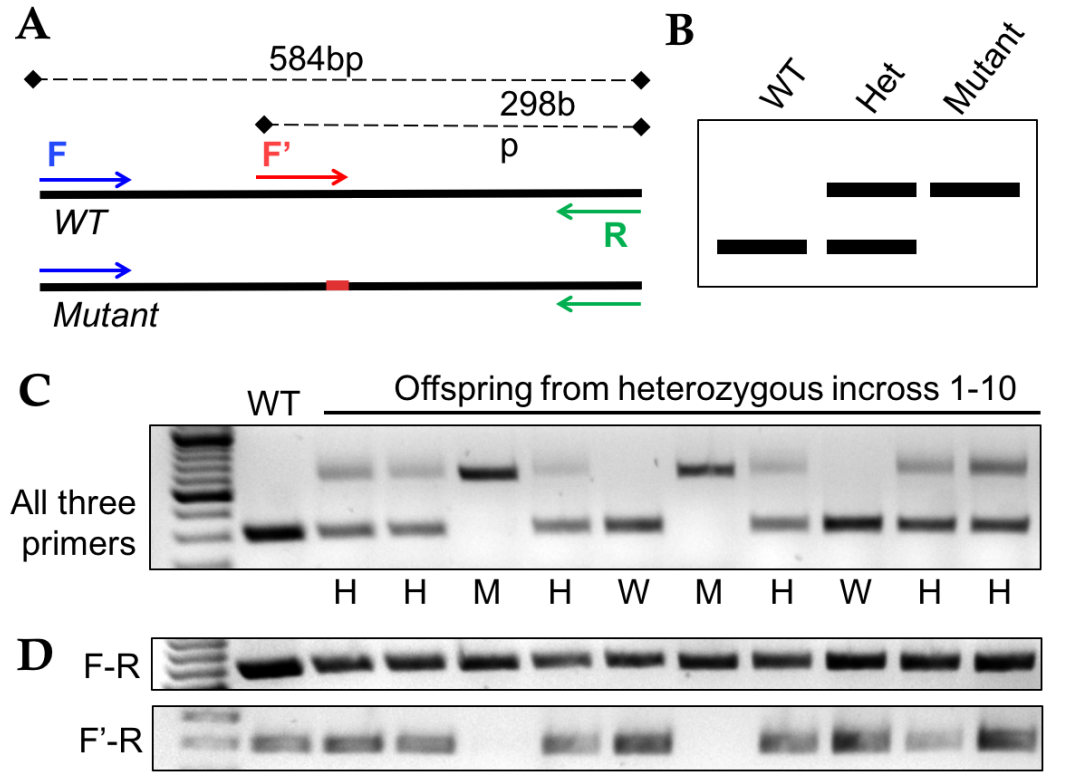

Figure 2-2: A novel PCR-based screening method for known mutations.
(A) Schematic to show locations of primers F, F' and R on wildtype (WT) and Mutant alleles. (B) Schematic illustrating predicted PCR readout of wildtype, heterozygous and mutant genomes using a combination of primers F, F' and R. (C) Genotyping of offspring from a heterozygous incross using a combination of primers F, F' and R. Derived genotypes wildtype (W), heterozygote (H) or homozygous mutant (M) are written below each lane. (D) Confirmation of identification of mutants using individual primer pairs F-R and F'-R, in which F'-R is unable to amplify the mutant genome.

Generation of inducible cardiac CRISPR mutant line

The *tg(myl7:Cas9;U6:hspb5b-gRNA)* (EM02) line was generated as follows. gRNAs against *hspb5b* were designed as described above and cloned into a tissue specific expression system adapted from Ablain *et al*[147]. Briefly, complimentary single stranded DNA oligos with 3' –GT overhangs were ordered from IDT and hybridized together by heating a 1:1 ratio to 95°C and lowering the temperature down to 4°C over the course of 20 minutes. The resultant double stranded oligonucleotide was

ligated into the pDest Tol2pA2 U6:gRNA (a kind gift from J. Ablain, Zon laboratory, Harvard) vector which had been digested with BseRI. The Gateway LR II Clonase enzyme was incubated overnight at room temperature with 150ng of the resultant pDest Tol2pA2 U6:hspb5b-gRNA, 100ng pME-Cas9T2AGFP (also from J. Ablain), 100ng p5'cmlc2 and 100ng p3'polyA. 1-2 cell stage embryos were injected with 25 pg of the final vector (pEM02) combined with 25pg Tol2 mRNA. F0 embryos were screened for GFP signal in the hearts. Successful generation of mutations in *hspb5b* were identified in pools of F1 embryos as described above. Since mutations are isolated to the heart, fin clip genotyping was not performed.

Cell Culture Methodologies

Formulations of media described below are described in Table 2-1.

Culture of HL-1 cells.

HL-1 cells (a kind gift from Dr. W. Claycomb, LSU) were maintained in Supplemented Claycomb medium (Sigma) according to manufacturer's instructions.

Coating Plates

- Coat tissue culture flasks with 5μg/ml fibronectin in 0.02% gelatin. Incubate at 37°C for one hour.
- Remove excess gelatin/fibronectin by aspiration just before adding cells.

Thawing Cells

- Transfer 10ml Wash Media into 15ml tube and put in 37°C water bath.
- Thaw cells in water bath at 37°C (~2min)

- Transfer cells to 15ml tube containing wash medium and centrifuge for 5 minutes at 500*g.*
- Aspirate wash medium and resuspend pellet in 6ml Supplemented Claycomb. Add to 3 wells of 6-well plate (2ml/well).
- Replace the medium with fresh Supplemented Claycomb Media after 4 hours and every 24-48 hours thereafter.

Splitting Cells

Note that HL-1 cells are happiest at high confluency (>60%).

- Aspirate spent medium.
- Rinse with sterile PBS warmed to 37°C. Aspirate PBS.
- Add 1ml trypsin/EDTA (Gibco) and incubate at 37°C for ~3 minutes until cells are detached.
- Add 1ml wash medium, pipette to capture all detached cells. Transfer trypsinized cells to 15ml tube in 5ml wash medium.
- Centrifuge at 500*g* for 5 minutes.
- Aspirate wash medium from 15ml tube and resuspend cells in 2ml Supplemented Claycomb.
- Plate 2E5 cells per well of 6-well plate for around 50% confluence.

Freezing Cells

- Label cryovials. Make 5% DMSO in FBS. Place at -20°C.
- Aspirate spent media. Rinse with pre-warmed PBS and add 1ml Trypsin/EDTA.
- Incubate at 37°C for 3 minutes or until cells dislodge.
- Add 1ml wash medium, pipette to capture all detached cells. Transfer trypsinized cells to 15ml tube in 5ml Wash Medium.

- Centrifuge at 500*g* for 5 minutes
- Remove Wash Medium by aspiration and resuspend pellet in 1.5ml of 5% DMSO in FBS.
- Pipette 1ml of freezing media into each cryovial. Place cryovials in polystyrene at -80°C.
- Transfer after 12 hours to liquid nitrogen.

Culture of hESCs

Human embryonic stem cells (hESCs) containing inducible Cas9[148] (generously provided by Dr. Danwei Huangfu, MSKCC) were maintained as described[145] in hESC Media, or in mTESR media or TESR-E8 media (both from STEMCELL technologies) on Matrigel (VWR).

Generation of *HSPB7* and *HSPB5* mutant lines

The hESC clonal lines carrying mutations in *HSPB7* were generated as described[145]. Briefly, gRNAs targeting *HSPB7* and *HSPB5* (Table 2-2) were designed with the CHOPCHOP website[144]. Guide sequences were flanked with the T7 promoter and the constant chimeric sgRNA sequence, and ordered as gBlocks from IDT (Figure 2-3).

CTCGCGTAATACGACTCACTATAGGG***NNNNNNNNNNNNNNNNNNN***GT
TTTAGAGCTAGAAATAGCAAGTTAAAATAAGGCTAGTCCGTTATCAAC
TTGAAAAAGTGGCACCGAGTCGGTGCTTTT

Figure 2-3: Standard sequence for gRNA gBlock.
gBlocks for the synthesis of gRNAs are ordered as shown. Black nucleotides are a spacer region to facilitate T7 binding and achieve the minimum sequence length. Blue nucleotides are the T7 promoter. Green nucleotides denote the location of the gene-specific gRNA targeting sequence (20bp). Red nucleotides are the constant chimeric sgRNA sequence.

gBlocks were diluted to 5ng/µl in RNAse-free water and 10-20ng was used as the template for short RNA synthesis with the MegaShortScript T7 kit (Thermo Fisher). Resultant sgRNA was purified with the MegaClear kit (Thermo Fisher) or diluted to 150µl in 0.5M Ammonium Acetate, 10mM EDTA and then precipitated with 2 volumes ethanol at -20°C for 60 minutes. sgRNA was eluted or resuspended in RNAse-free water.

- Day 0: When hESCs are 60% confluent, pretreat cells with doxycycline (2ug/ml) for 24 hours before transfection.
- Day 1: Dissociate cells with TrypLE and replate with 0.2, 0.4 and 1E6 cells/ml in hESC Media with 5µM Rock inhibitor and 2µg/ml doxycycline.
- Plate 0.5ml/well into a 24-well plate. Plate in duplicate for transfection plus one well for each dilution to serve as a non-transfected control for T7 assays.
- For each well prepare:
    - Mix 1: 25µl Opti-MEM + 0.5µg sgRNA (160ng total).
    - Mix 2: 25µl Opti-MEM + 1.5µl RNAiMAX
- Combine Mix 1 and Mix 2, incubate for 5 minutes at room temperature, then add 50µl/well dropwise to dissociated hPSCs.
- Day 2: Refresh hPSC medium with 2µg/ml doxycycline and repeat transfection with sgRNA as above.
- Day 3: Aspirate media and replace with Supplemented DMEM/F12 without doxycycline.
- Day 4: Take one well from each pair, and extract gDNA from transfected and nontransfected control cells with DNeasy columns. Adjust final concentration to 50ng/µl.

Mutation efficiency was assessed by PCR across the CRISPR target locus followed by analysis with the T7E1 assay, as described above. Indel percentage was determined by the formula $100 \bullet (1-(1-(b+c)/(a+b+c))^{1/2})$ where *a* is the intensity of the undigested PCR product and *b* and *c* are the intensities of each cleavage product. Transfected cells with an indel percentage >20% were replated 3 days after final gRNA transfection.

Isolation of clonal hESC lines.

- The day before replating, seed irradiated mouse embryonic fibroblasts (MEFs) in Feeder Media into a 10cm dish precoated with gelatin.
- Dissociate to single cells with TrypLE Express followed by passing through a 40μm cell strainer.
- Plate 2000 cells into 10cm dish on MEFs in hESC Mediawith 5μM Rocki.
- Change media 3 days after plating and remove Rocki. Change every 2-3 days.
- 10 days after replating single cells, manually pick around 48 colonies and pipette into an uncoated 96 well plate in 100μl hESC Media with 5μM Rocki.
- Clone is mechanically disaggregated by pipetting up and down five times and immediately re-plated: twice 50μl into duplicate wells of 2 96 well plates, on MEFs in hESC Media with 5μM Rocki.

3 days after replating into duplicate 96 well plates, gDNA was extracted:

- To each well of one 96 well plate add 50μl gDNA extraction buffer (10mM Tris-HCl pH8.4, 50mM KCl, 1.5mM $MgCl_2$, 0.3% Tween-20, 0.3% NP-40).
- Heat at 95°C for 15 minutes then cool to 55°C
- Add 3μl Proteinase K (20mg/ml stock, Roche), incubate at 55°C for 1 hour
- Heat at 95°C for 20 minutes

- Use 2µl of gDNA in PCR reaction and store the remainder at 4°C

Clones carrying mutant alleles were identified by PCR across the CRISPR target locus followed by TOPO cloning and Sanger sequencing of 5 clones.

Differentiation of hESC-CMs

The following protocol (Figure 2-4) was modified from the method described by Lian *et al.*[149], and used to generate beating cardiomyocytes from hESC lines.

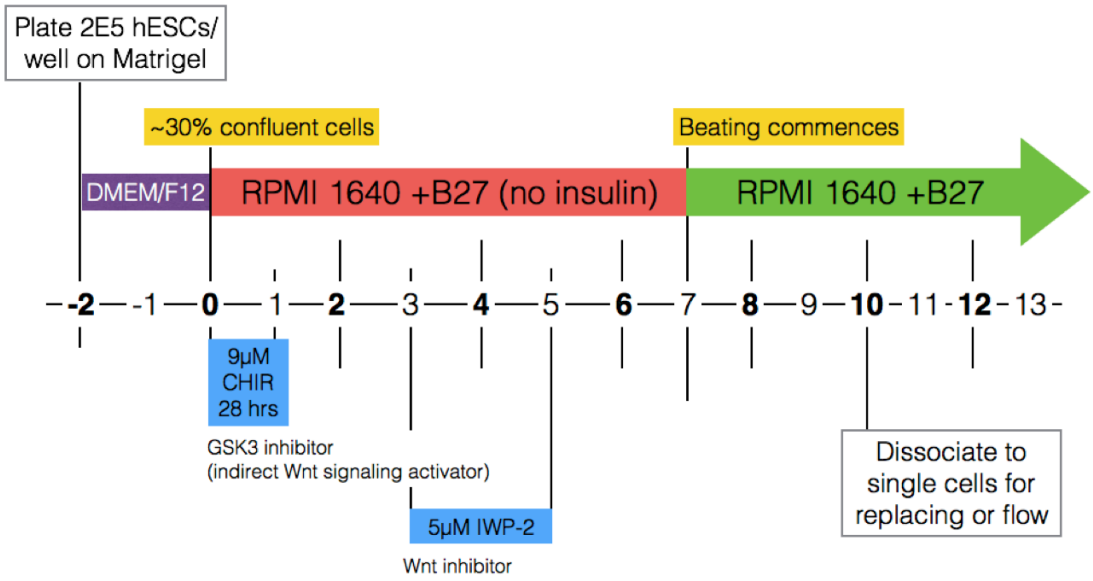

Figure 2-4: Protocol for differentiation of cardiomyocytes from hESCs.
Schematic of protocol for derivation of cardiomyocytes. Alterations from the referenced method[149] are number of hESCs initially plated and length and concentration of CHIR99021 treatment. DMEM/F12 media is supplemented (see Table 2-1) and we routinely include 1X Pen/Strep in RPMI 1640 to prevent growth of contaminants.

Dissociation of hESC-CMs for replating or flow cytometry.

At day 10, cells were processed for further analysis as described[150].

- Wash well 3X with sterile PBS to remove extracellular calcium and inhibit beating.
- Add 0.5ml/well TrypLE Express and incubate for 5 minutes at 37°C. Pipette up and down to disaggregate cells and repeat incubation and pipetting.
- Transfer cells to a 15ml Falcon tube in Cardiomyocyte Media and centrifuge at 400*g* for 5 minutes.
- Resuspend in 2ml Cardiomyocyte Media and pass through 100μm cell strainer to ensure single cells.
- Dilute to 1e6 cells/ml. To replate for IF staining, plate 5e5 cells/well onto 4 well microscope slide on Matrigel or 5μg/ml fibronectin in 0.02% gelatin. Alternatively, process single cells for flow cytometry.

Flow cytometry of cardiomyocytes.

Day 10 or higher hESC-CMs were dissociated into single cells as described above.

- Transfer 1.5e6 cells for each required sample at 400*g* for 5 minutes. Resuspend in 100μl feeder media. Note that additional samples are required for unstained and single stained controls.
- Add 100μl 4% PFA to give a final concentration of 2% PFA. Incubate at room temperature for 30 minutes.
- Transfer cells to a U-bottom 96 well plate. Spin down at 950*g* for 2 minutes. Resuspend in 200μl FACs buffer (10% FBS in PBS). Incubate for 5 minutes at room temperature. Repeat this step once.
- Spin down at 950*g* for 2 minutes. Resuspend in 200μl FACs buffer + 0.5% Saponin with desired primary antibodies. Incubate for 1 hour at room temp.

    - Mouse anti-cardiac troponin (13-11, 1:500, Thermo)
    - Rabbit anti-HSPB7 (ab150390, 1:250, Abcam)
- Spin down at 950*g* for 2 minutes. Resuspend in 200µl FACs buffer. Incubate for 5 minutes at room temperature. Repeat this step once.
- Spin down at 950*g* for 2 minutes. Resuspend in 200µl FACs buffer + 0.5% Saponin with desired secondary antibodies. Incubate for 1 hour at room temp.
    - AlexaFluor 647 goat anti-mouse IgG (Thermo) at 1:400
    - AlexaFluor 488 goat anti-rabbit IgG (Thermo) at 1:400
- Spin down at 950*g* for 2 minutes. Resuspend in 200µl FACs buffer. Incubate for 5 minutes at room temperature. Repeat this step once.
- Resuspend in 200µl FACs buffer and pipette through mesh-top flow cytometry tubes. Add 800µl additional FACs buffer/tube.
- Run samples on Accuri CFlow.

Table 2-1: Cell Culture Media Composition

Supplemented Claycomb Media (500ml)	
Claycomb Media (Sigma)	435ml (87%)
Fetal Bovine Serum (Sigma, F2442, Batch 11A568)	50ml (10%)
Penicillin/Streptomycin (VWR)	5ml (100µg/ml)
Norepinephrine (Sigma, 10mM stock in 30mM Ascorbic Acid, filter sterilized)	5ml (0.1mM)
L-Glutamine (VWR)	5ml (2mM)
Wash Media (100ml)	
DMEM Media (VWR)	90ml (90%)
Fetal Bovine Serum (Sigma)	10ml (10%)
Feeder Media (500ml)	
DMEM Media (VWR)	440ml (88%)
Fetal Bovine Serum (Sigma)	50ml (10%)
Penicillin/Streptomycin (VWR)	5ml (100µg/ml)
L-Glutamine (VWR)	5ml (2mM)
Freezing Media (10ml)	
Base Media for Cell Type (Claycomb or hESC)	5ml (50%)
DMSO (Sigma)	1ml (10%)
Fetal Bovine Serum (Sigma)	4ml (40%)

Table 2-1: Cell Culture Media Composition continued

Supplemented DMEM/F12 (500ml)	
DMEM/F12 (VWR)	490ml (98%)
Penicillin/Streptomycin (VWR)	5ml (100µg/ml)
L-Glutamine (VWR)	5ml (2mM)
hESC Media (500ml) – Filter Sterilize after making	
Supplemented DMEM/F12	400ml (80%)
KnockOut Serum Replacement (Invitrogen)	100ml (20%)
Non-Essential Amino Acids (Invitrogen)	5ml (1X)
β-Mercaptoethanol (Sigma)	900µl (0.2%)
Recombinant Human FGF basic (R&D Systems, 10µg/ml stock)*	1ml (20ng/ml)
Cardiomyocyte Media (50ml)	
RPMI 1640 with L-Glutamine (VWR)	50ml (98%)
B27 Supplement (Gibco)	1ml (2%)
Penicillin/Streptomycin (VWR)	500µl (100µg/ml)

**Add FGFb to aliquots of hESC media (2µl/ml) as required.*

Microscopy and Imaging

Anatomical analysis of adult zebrafish

Adult male zebrafish were submitted for histopathological processing and blinded analysis by the pathology core at Memorial Sloan Kettering Cancer Center. The fish was fixed in Bouin's solution for 24 hours, cut parasagitally, processed via automated tissue processor, embedded in paraffin, and two 4 micron sections were taken 100 microns apart. Sections were then stained with hematoxylin and eosin and Masson's trichrome using standard methods.

Adult zebrafish hearts were dissected as described[151] and fixed in 2.5% glutaraldehyde, 4% paraformaldehyde, 0.02% picric acid (all Sigma). Samples were submitted to the imaging core at Weill Cornell Medicine. Following post-fixation processing, as described[152], samples were contrasted with lead citrate and viewed on a JEM 1400 electron microscope (JEOL, USA, Inc. Peabody, MA) operated at 100kV. Digital images were captured on a Veleta 2K x 2K CCD camera (Olympus-SIS, Germany).

Immunofluorescence techniques

Immunostaining on cultured cells was performed after fixing cells with 4% paraformaldehyde (VWR) and permeabilizing with 0.1% Triton X-100 (MP Biomedicals) at room temperature or 50 μg/ml digitonin (Sigma) in PBS at 37°C. Digitonin permeabilization was followed by quenching with 40mM NH_4Cl (Sigma). Cells were blocked with 2% IgG-free bovine serum albumin (Jackson), 5% lamb serum (Invitrogen) and incubated overnight at 4°C with the appropriate primary antibodies: anti-cardiac troponin T (13-11, 1:500, Thermo Fischer); anti-HSPB7 (ab150390, 1:250, Abcam); anti-LC3B (ab51520, 1:250, Abcam); anti-FLNC

(sc48496, 1:100, Santa Cruz). Cells were counterstained with DAPI (1:10000, Invitrogen) and imaged on an Axio Observer.Z1, or LSM 510/880 Confocal (Zeiss).

Quantification of puncta in immunofluorescence images

Number and size of puncta were quantified as described[153]. For easier visualization, the process is summarized in Figure 2-5. Some modifications were made to the parameters used for identification of puncta:

- Image was converted to RGB and despeckled in FIJI prior to further processing.
- Threshold was set to 0-150 to filter out additional background.
- An individual cell was outlined with a freeform shape in FIJI, and the area of the cell was measured for normalization of puncta.
- The selected cell was processed using a published macro for the counting of puncta in FIJI[153].
- Required particle size was set to 1-300μm^2 to filter out any large auto-fluorescent areas.
- Resultant data (individual particle sizes, shapes and overall counts) was exported into Microsoft Excel. Average particle number/10μm^2 and average particle size were calculated for each cell. An average of 3 cells were taken per image from an average of 7 images for each genotype of hESC-CM examined.

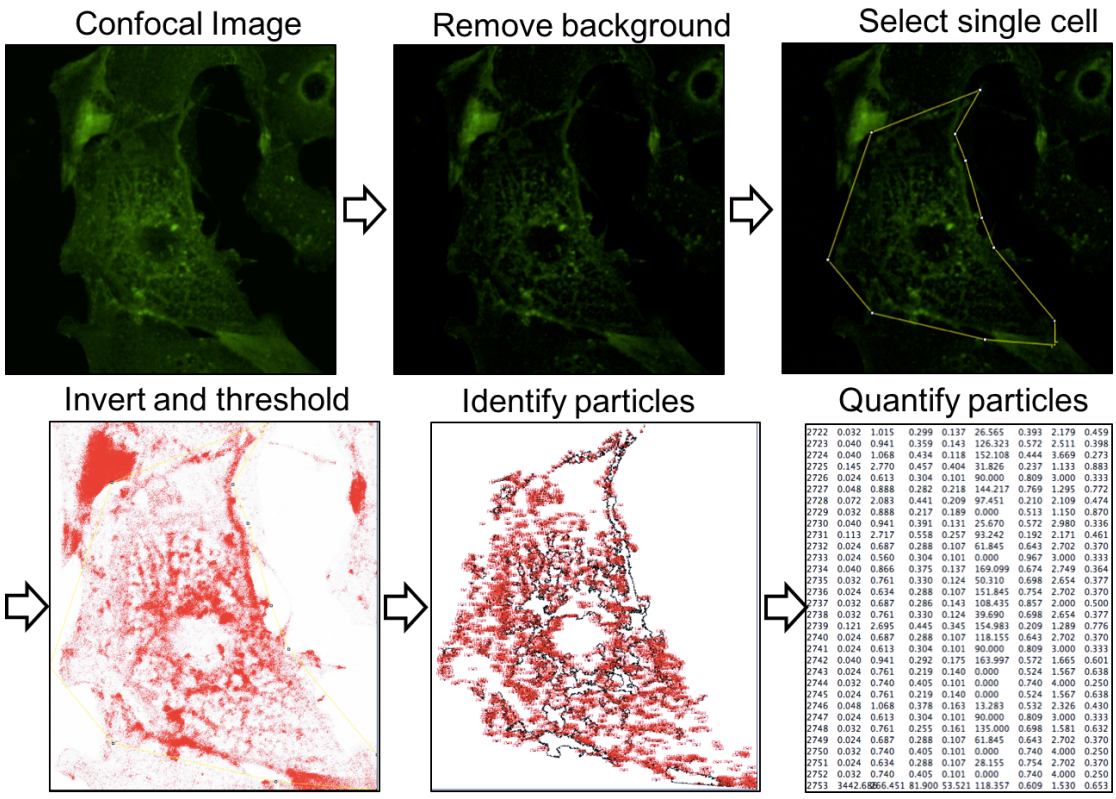

Figure 2-5: Quantification of LC3-B or FLNC puncta.
Schematic detailing the stages of puncta quantification in the method adapted from Dagda et al.[153]

Molecular Biology

Isolation of gDNA

Methods for extraction of gDNA from embryonic and adult zebrafish is detailed above. gDNA from cultured cells was isolated with DNEasy Kit (Qiagen).

Isolation of RNA and generation of cDNA

RNA was isolated with Trizol Reagent (Thermo) according to the manufacturer's instructions. cDNA was generated using 0.5µg RNA and the SuperScript VILO Kit (Thermo Fisher), according to manufacturer's instructions except that incubation at 42°C was increased from 60 to 120 minutes.

Quantitative RT-PCR (qPCR) analysis of gene expression in zebrafish

Zebrafish embryos or adult tissues were homogenized in Trizol (Invitrogen) and RNA was extracted according to manufacturer's instructions. The qPCR analysis was performed on a LightCycler 480 II (Roche) using LightCycler 480 Sybr Green master mix (Roche). Primer sequences are provided in Table 2-4. Relative gene expression was determined as described[154].

Immunoprecipitation of HSPB7

HL-1 cells were lysed on ice in a modified RIPA buffer (20mM Tris pH7.5, 150mM NaCl, 1% NP-40) with cOmplete mini protease inhibitor (Roche). Debris was cleared from lysed cells by centrifugation (21,000*g*, 10 minutes, 4°C) and protein concentration was calculated with QuickStart Bradford Protein Assay kit (BioRad). Lysates were precleared by incubation with 1:10 dilution of Protein G Dynabeads (Invitrogen, 30 minutes, 4°C) and then incubated overnight with 1:100 anti-HSPB7 (ab150390, Abcam) or control rabbit IgG whole molecule (Jackson). Complexes were precipitated with 1:10 Protein G Dynabeads (120 minutes, 4°C) and eluted into Western buffer (65% modified RIPA, 25% NuPAGE Sample Buffer, 10% NuPAGE Reducing Agent (both Invitrogen) by incubation at 95°C for 10 minutes. Residual Protein G Dynabeads were removed with DynaMag 2.0 (Thermo).

Western Blotting

Samples for western blotting were initially lysed as described above. Resultant lysates were diluted with 25% NuPAGE Sample Buffer and 10% NuPAGE Reducing Agent and incubated at 95°C for 10 minutes. 20µl per sample was loaded onto a 10%, 12% or a 4-12% Bis-Tris Acetate Gel‡‡ (Thermo) and run in 800ml 1X MOPS

‡‡ Gel density is altered according to the size of the protein one is blotting for. 10% gel for 30-150kDa, 12% gel for <30kDa, 4-12% gel for >150kDa.

buffer with 500µl NuPAGE Antioxidant (100V for 1-2 hours). For transfer of large proteins, post-elecrophoresis gels were incubated for 30 mintues in an Equilibration buffer (10% Methanol, 2X MOPS and 1:1000 NuPAGE Anti-oxidant). Westerns were transferred using the iBlot Dry Blotting System (P3, 5-8 minutes[§§]). Following transfer membranes were processed as follows:

- Rinse with PBST
- Block with 3% IgG-free BSA in PBST for 30 minutes at room temp, rocking
- Wash once in TBST
- Cut off irrelevant areas of gel and discard
- Incubate overnight in heat-sealed bag at 4°C, rocking in primary antibody in 3% IgG-free BSA in PBST
    - Mouse anti-cardiac troponin (13-11, 1:500, Thermo)
    - Rabbit anti-HSPB7 (ab150390, 1:250, Abcam) for mouse/human
    - Rabbit anti-HSPB7 (15700-1-AP, 1:200, ProteinTech) for zebrafish
    - Mouse anti-β-Actin (A1978, 1:2000-1:3000, Sigma)
    - Rabbit anti-cofilin-1 (ab11062, 1:500, AbCam)
    - Rabbit anti-GAPDH (ab9484, 1:5000, AbCam)
    - Mouse anti-FLNC (HPA006135, 1:200, Sigma)
- Wash 3X 5 minutes in TBST
- Apply secondary 1:2000 in 5% milk in TBST[***] for 1 hour at room temp, rocking.
    - Goat anti-mouse IgG HRP conjugate (170-6516, 1:2000, BioRad)
    - Goat anti-rabbit IgG HRP conjugate (170-6515, 1:2000, BioRad)
- Wash 3X 5 minutes in TBST
- Incubate protein side up 5 min in plastic box with ~1ml Pierce West pico pipetted directly onto membrane.

[§§] Transfer timing was altered according to protein size. 7 minutes for 30-150kDa, 5 minutes for <30kDa and 8 minutes for >150kDa.

[***] Change from milk to 3% IgG-free BSA in TBST for anti-goat secondaries.

- Image with c-DiGit Western Blot Scanner (Licor) for 12 minutes (high sensitivity).

Densitometry analysis of Western blots was performed with ImageJ software.

In gel trypsinolysis and mass spectrometry.

Samples for in gel trypsinolysis were initially processed as described for Western Blot. Following electrophoresis, gels were incubated with 1X Coomassie Brilliant Blue (Thermo) for 15 minutes, and then rinsed with distilled water to remove background staining. Visible bands of interest were excised with a clean scalpel and processed with In-Gel Tryptic Digestion Kit (Sigma) according to manufacturer's instructions. Reduction and alkylation steps were performed as recommended to optimize sequence recovery.

Peptide samples were eluted with 1% TFA and subsequently vacuum-centrifuged at 60°C to near-dryness in a SpeedVac. Remaining sample was diluted to 30µl with 0.1% TFA for analysis by liquid chromatography-tandem mass spectrometry.

Mass spectrometry and subsequent peptide identification was performed as described[155]. Briefly, peptides were analyzed using a 6520 accurate-mass quadrupole-time of flight (Q-TOF) mass spectrometer coupled to a chip cube with an on-chip C18 column (Agilent Technologies, Santa Clara, CA). The mobile phases were 0.1% formic acid in water (solvent A) and 0.1% formic acid in 90% acetonitrile (solvent B). Peptide elution utilized solvent gradient 3–40% solvent B for 52 min. Non-eluting peptides were then displaced by treatment with 90% solvent B for 2–5 min.

Mass spectra were acquired in automated data-dependent acquisition mode at 0.5s intervals, and MS/MS scans were performed on the four most intense ions for

each MS scan. Peptides were identified using Spectrum Mill software version A.03.03 (Agilent). Peptide files were searched against a regularly updated Swiss-Prot database, with a peak intensity threshold of 50%, precursor mass tolerance of 20 ppm and a product mass tolerance of 50 ppm. In each search, a fixed modification was set for dimethylated N-terminal residues and variable modifications for carbamidomethylated Cys residues, oxidized Met residues and dimethylated Lys residues. For all searches, peptides with a Spectrum Mill score of 9 or higher were considered valid.

Filter Trap Assay

The filter trap assay was performed as described[127]. In brief, cells were counted and a fixed number were lysed in 200µl FTA buffer (10mM Tris-HCl, pH8.0, 150mM NaCl) containing 2% SDS. Samples were boiled for 10 minutes and loaded onto a pre-washed (FTA, 0.1% SDS) 0.2µm cellulose acetate filter (GE Healthcare) with supporting filter paper (Bio-Rad) in Bio-Dot 96 well filtration system (Bio-Rad). Suction was applied to filtrate the samples. Following loading, membranes were processed as described above in Western Blotting.

Table 2-2: CRISPR and TALEN sequences.

CRISPR Sequences		
Gene	**Species**	**gRNA Targeted Sequence (PAM)**
Hspb5b	Zebrafish	5'- ACGTGATCTCCTCATTGTAC(**TCC**)-3'
HSPB7	Human	5'-(**CCC**)ACTCGGAGCCCCTGGCCTTC-3'
Gata5	Zebrafish	5'- GGGCGCGAGTGTGTGAACTG(**CGG**)-3'

TALEN sequences			
Gene	**Species**	**Targeted Sequence**	**RVD sequences**
Hspb7	Zebrafish	5'-CCTCCTCATCTTCATCCTCT-3'	HD HD NG HD HD NG HD NI NG HD NG NG HD NI NG HD HD NG HD NG
		5'-TACATGGAGAAGAGCCGAGG-3'	HD HD NG HD NN NN HD NG HD NG NG HD NG HD HD NI NG NN NG NI
Gata4	Zebrafish	5'-GCGTCCAGGCGGGTGG-3'	NH HD NH NG HD HD NI NH NH HD NH NH NH NG NH NH
		5'-GTCAGACTACCACAAC-3'	NH NG NG NH NG NH NH NG NI NH NG HD NG NH NI HD
Gata6	Zebrafish	5'-CTTCCTCCCGGCGGATCGGA-3'	HD NG NG HD HD NG HD HD HD NH NH HD NH NH NI NG HD NH NH
		5'-TGTCAGACGAGCACCACAAC-3'	NH NG NG NH NG NH NH NG NH HD NG HD NH NG HD NG NH NI HD

Table 2-3: Genotyping primers

Genotyping				
TE #	**Species**	**Gene**	**Sequence**	**Use Details**
5669	Human	HSPB7	AAGATTTCCAGCCCCCTCT	HSPB7 CRISPR 1-3
5670	Human	HSPB7	ACCTGTTTTCATGGCCACAT	HSPB7 CRISPR 1-3
5671	Human	HSPB7	GTGGGCTGTAGGAATGAGGA	HSPB7 CRISPR 4
5672	Human	HSPB7	CCCTGGAAGAAAGGATCTGG	HSPB7 CRISPR 4
5675	Human	HSPB7	CAGGGACAGTCGGCCTTAT	HSPB7 CRISPR 1-3
5676	Human	HSPB7	ACCTGTTTTCATGGCCACAT	HSPB7 CRISPR 1-3
5785	Human	HSPB7	CTCACAGCAGCCCATCCC	HSPB7 CRISPR 4
5786	Human	HSPB7	CTTCTCAGCCCGCACCTC	HSPB7 CRISPR 4
5789	Human	HSPB7	GTGGCCACATCTGTCTTGGT	HSPB7 CRISPR 1-3
5012	Zebrafish	hspb7	GCCTCATGCAGCTGACATATT	Hspb7 TALEN
5013	Zebrafish	hspb7	CTAATGAGCGCGAGCAATTC	Hspb7 TALEN
5168	Zebrafish	hspb7	TGAGAAAGCTGCTGAGTGGA	Hspb7 TALEN
5169	Zebrafish	hspb7	ATCCAAAGTCGTCAGCGAAG	Hspb7 TALEN
5673	Zebrafish	gata4	TTTTGCATGCCTATTCCTTTG	Gata4 TALEN
5674	Zebrafish	gata4	GGGTTTGGTTTTGCTGATGT	Gata4 TALEN
5734	Zebrafish	gata6	CCGCCAGTAATTGATCACAA	Gata6 TALEN
5735	Zebrafish	gata6	GATTGTCCTTCGGCTTGGTA	Gata6 TALEN
5885	Zebrafish	hspb5b	TGCAGTGAAAGAGGCAAATG	Hspb5b CRISPR 12
5886	Zebrafish	hspb5b	ACGCGTGACTCCTCAACTTT	Hspb5b CRISPR 12
5887	Zebrafish	hspb5b	TGAAAACCATGCTGCCTGTA	Hspb5b CRISPR 12
5888	Zebrafish	hspb5b	CGTCCTGTGTGTAAAAAGAAACA	Hspb5b CRISPR 12
5990	Zebrafish	gata4	TCACTGCTCTCTCCCCCTTT	Gata4 TALEN
5991	Zebrafish	gata4	GTTGCAGACTGGCTCTCCTT	Gata4 TALEN
5992	Zebrafish	gata6	TGCATGCCTGGACACTTTTT	Gata6 TALEN
5993	Zebrafish	gata6	CTCTCCCTCCGCGTTTCTG	Gata6 TALEN
5994	Zebrafish	gata6	GGACTGTCATGCGCAAACT	WC7, negative
5995	Zebrafish	gata4	GGTGGGTTTATCCTGCACA	WC5, WC6, F, negative

Table 2-3: Genotyping primers continued.

5996	Zebrafish	gata4	GTCTGACAGTTTGTAAACCCAGT	WC6 R, positive
5997	Zebrafish	gata4	GGACCCCAGATTAATATGTGG	indel, F, positive
6074	Zebrafish	gata5	CAAGTCGCACCTTGAAAACA	Gata5 CRISPR
6075	Zebrafish	gata5	TGGCTAGGTTTAAACAGGACAA	Gata5 CRISPR
6076	Zebrafish	gata5	TGCTTCATTGACTTTGTTGTCA	Gata5 CRISPR
6077	Zebrafish	gata5	ACCATGCAGCCTCTCAAAAT	Gata5 CRISPR
6311	Zebrafish	gata4	TTGCAGTGATTATTTATGCACATT	Gata4 TALEN
6312	Zebrafish	gata4	CAGCAGACAGGACACTCACC	Gata4 TALEN
6313	Zebrafish	gata6	AAATATTTGTGGAATTGATGATCC	Gata6 TALEN
6314	Zebrafish	gata6	TGTTCAAAGCAAAGGGAGAG	Gata6 TALEN
6346	Zebrafish	gata5	CGCGAGTGTGTGAACTGC	WC8, 10, 11, F, negative
6347	Zebrafish	gata5	GAAGGGCGCGAGTGTGT	WC9, F, negative

Table 2-4: qPCR Primers

qPCR				
TE #	**Species**	**Gene**	**Sequence**	**Use Details**
4522	General	eGFP	GCAGAAGAACGGCATCAAGGT	Forward
4523	General	eGFP	ACGAACTCCAGCAGGACCATG	Reverse
5642	Human	HSPB7	CAGGCAACATCAAGACCCTA	Forward
5643	Human	HSPB7	CTTGTGAGCGAAGGTGTTCA	Reverse
5644	Human	FLNC	GTGTCCTATCTGCCGACTGC	Forward
5645	Human	FLNC	CGGTGATCTTCAGTGACACG	Reverse
5646	Human	FLNC	CACATCAAGCTCGTGTCCAT	Forward
5647	Human	FLNC	CTGCTTGGGCGTCTGTTT	Reverse
6121	Human	HSPB5	CTTTGACCAGTTCTTCGGAG	Forward
6122	Human	HSPB5	CCTCAATCACATCTCCCAAC	Reverse
6123	Human	HSPB8	CAGAGGAGTTGATGGTGAAGAC	Forward
6124	Human	HSPB8	GTTGAGTAAGGAGGGACCTG	Reverse
6125	Human	FLNC	ACAACCATGACTACTCCTACAC	Forward
6126	Human	FLNC	GTTCACAGAGAATGCTTGTTCC	Reverse
6127	Human	BAG3	GCCTGTGTACCACAAGATCC	Forward
6128	Human	BAG3	AGTTTCTCGATGGGTCATGG	Reverse
6129	Human	CTGF	TTGGCCCAGACCCAACTA	Forward
6130	Human	CTGF	GCAGGAGGCGTTGTCATT	Reverse
6131	Human	XBP1t	CGCTGAGGAGGAAACTGAA	Forward
6132	Human	XBP1t	TGTTCCAGCTCACTCATTCG	Reverse
6133	Human	XBP1s	CTGAGTCCGCAGCAGGTG	Forward
6134	Human	XBP1s	ACTGGGTCCAAGTTGTCCAG	Reverse
6135	Human	CHOP	GCACCTCCCAGAGCCCTCACTCTCC3	Forward
6136	Human	CHOP	GTCTACTCCAAGCCTTCCCCCTGCG3	Reverse
6137	Human	GRP78	ATCATCAACGAGCCTACGG	Forward
6138	Human	GRP78	CGCTGGTCAAAGTCTTCTCC	Reverse
6139	Human	LC3A	TCCCGGACCATGTCAACAT	Forward
6140	Human	LC3A	ACCATGCTGTGCTGGTTCAC	Reverse
6141	Human	LC3B	ACCATGCCGTCGGAGAAG	Forward
6142	Human	LC3B	ATCGTTCTATTATCACCGGGATTTT	Reverse

Table 2-4: qPCR Primers continued

6143	Human	HSF1	CCGGCGGGAGCATAGACGAGAGG	Forward
6144	Human	HSF1	GACGGAGGCGGGGGCAGGTTCACT	Reverse
6304	Human	HSPB5	ATTGGGTGTGGACAGAAAGC	Forward
6305	Human	HSPB5	AGGCAGGGTAGGAAAGGAAA	Reverse
6306	Human	HSPB5	CTGACCCCTCACACTCACCT	Forward
6307	Human	HSPB5	AGAAGTTAGGGGACGGAGGA	Reverse
4664	Mouse	HSPB7	GCCAAGGAAACATCAAGACC	Forward
4665	Mouse	HSPB7	TTCATGACTGTGCCATCAGC	Reverse
5529	Mouse	FLNC	GGAGTCCTTTCCCTGTCCAT	Forward
5530	Mouse	FLNC	GACCTTTGACGGTGACCTTG	Reverse
5531	Mouse	FLNC	CCCATGGCTCCTGGTAACTA	Forward
5532	Mouse	FLNC	GGATGTTTCGTGAAGGCTGT	Reverse
5533	Mouse	YAP	TTCAATGCCGTCATGAACC	Forward
5534	Mouse	YAP	GAGTGAGCTCGAACATGCTG	Reverse
5535	Mouse	TAZ	GCAGACATCTGCTTCACCAA	Forward
5536	Mouse	TAZ	TTCCCTTCTGGGAAGATGTG	Reverse
5537	Mouse	FLNA	GAAAGCCAGTGAAGCACACA	Forward
5538	Mouse	FLNA	GGCCAGCTTCAGTACAATCC	Reverse
5539	Mouse	BAG3	GCTGGGAGATCAAAATCGAC	Forward
5540	Mouse	BAG3	TTGGCTGAAGATGCAGTGTC	Reverse
1586	Zebrafish	gata5	TCAACAGTGTCTGGCGCTAC	Forward
1587	Zebrafish	gata5	GCCTGCATATGGAGAAGCTG	Reverse
1588	Zebrafish	gata6	ATGGACTCAGCCGACCATTA	Forward
1589	Zebrafish	gata6	ACAGTGTTGTGGTGCTCGTC	Reverse
1849	Zebrafish	b-actin	GACAACGGCTCCGGTATG	Forward
1850	Zebrafish	b-actin	CATGCCAACCATCACTCC	Reverse
2357	Zebrafish	18S	TCGCTAGTTGGCATCGTTTATG	Forward
2358	Zebrafish	18S	CGGAGGTTCGAAGACGATCA	Reverse
2361	Zebrafish	gata4	AACCACCTCCTATAACTCAAGCA	Forward
2362	Zebrafish	gata4	GTTAACGGAGGACTGGTGGA	Reverse
2666	Zebrafish	eomesa	CATCGCTGTAACGGCTTACC	Forward
2667	Zebrafish	eomesa	TCGCTCTCTGGAGCTGTGTA	Reverse

Table 2-4: qPCR Primers continued.

2668	Zebrafish	eomesb	CGCAGGTGTATCTCTGCAAC	Forward
2669	Zebrafish	eomesb	CGTCATGTTGAAGCTGAGGA	Reverse
4453	Zebrafish	hspb7	GATCTTTCATGTGTCCGAAGG	Forward
4454	Zebrafish	hspb7	GATTGTTTGAGGTGGTGACG	Reverse
4526	Zebrafish	hspb12	TAACCTGGAGACGGACATCAG	Forward
4527	Zebrafish	hspb12	TCCGGGGATGTAGTACTTCTGG	Reverse
4754	Zebrafish	bax	GAGCTGCACTTCTCAACAACTTT	Forward
4755	Zebrafish	bax	CTGGTTGAAATAGCCTTGATGAC	Reverse
4756	Zebrafish	hsp70	CATCGACGCCAACGGG	Forward
4757	Zebrafish	hsp70	CCAGGGAGTTTTTAGCAGAAATCTT	Reverse
5541	Zebrafish	flnca	CCAGCTCTATGCCAACATCA	Forward
5542	Zebrafish	flnca	CTAGGACCGTGGACACCAAC	Reverse
5543	Zebrafish	flncb	GGCCCTACAAAGTGGACATC	Forward
5544	Zebrafish	flncb	CTTCAAACCAGGCCCATAAG	Reverse
5545	Zebrafish	titin	AATTTCGGAGGATGATGTGC	Forward
5546	Zebrafish	titin	GGAATCGTTTTGTTCCCTCA	Reverse
5547	Zebrafish	titin	CCAACAGTCTCCCTCTCCTG	Forward
5548	Zebrafish	titin	TCATCACAGGGGACTTGACA	Reverse
5549	Zebrafish	yap	GGTTGAGAAAGCTGCCAGAC	Forward
5550	Zebrafish	yap	AGTGCACCAGGAGAAACTGC	Reverse
5551	Zebrafish	taz	TTTCACTCCAGTTTCTTCAGCA	Forward
5552	Zebrafish	taz	CCTTGATTCAGCCTTTCCAA	Reverse
5626	Zebrafish	map1lc3a	CGAGTCGACCGACAATTTAGC	Forward
5627	Zebrafish	map1lc3a	TCCTTGCAACGATCAGCGAA	Reverse
5628	Zebrafish	map1lc3b	AATGTGACGATTGGACACGAGT	Forward
5629	Zebrafish	map1lc3b	AGTACAACAGCTCACGGTTATGC	Reverse
5691	Zebrafish	hspb1	ATGAACACGGCTTCATTTCC	Forward
5692	Zebrafish	hspb1	GCGGAGCTTCAACAGTCAGG	Reverse
5693	Zebrafish	hspb8	ACCGACCAAAGTGAGAGGTG	Forward
5694	Zebrafish	hspb8	GCATTTACGGAGCTCTGAGG	Reverse
5695	Zebrafish	hspb11	AGAGCTCGCCGTTAAACAAG	Forward
5696	Zebrafish	hspb11	AATAGGATCCCTTCCCATCG	Reverse

Table 2-4: qPCR Primers continued

5697	Zebrafish	hspb5a	CCCAGGCTTCTTCCCTTATC	Forward
5698	Zebrafish	hspb5a	GTGCTTCACATCCAGGTTGA	Reverse
5699	Zebrafish	hspb5b	CCTACTGACGGCCAAATGTT	Forward
5700	Zebrafish	hspb5b	GGCATCAGCAGCAGACAATA	Reverse
5710	Zebrafish	ctgfa	GTGTGATTGCTCTGCTGTTCC	Forward
5711	Zebrafish	ctgfa	GGTGAACACTGGGGCGGC	Reverse
5712	Zebrafish	ctgfb	CTGGAACAGCATTCACCAGAG	Forward
5713	Zebrafish	ctgfb	CTCGTCTGGGCAATCACAGG	Reverse
5854	Zebrafish	bip	AAGAGGCCGAAGAGAAGGAC	Forward
5855	Zebrafish	bip	AGCAGCAGAGCCTCGAAATA	Reverse
5856	Zebrafish	ddit3	AAGGAAAGTGCAGGAGCTGA	Forward
5857	Zebrafish	ddit3	TCACGCTCTCCACAAGAAGA	Reverse
5858	Zebrafish	dnajc3	TCCCATGGATCCTGAGAGTC	Forward
5859	Zebrafish	dnajc3	CTCCTGTGTGTGAGGGGTCT	Reverse
5860	Zebrafish	edem1	ATCCAAAGAAGATCGCATGG	Forward
5861	Zebrafish	edem1	TCTCTCCCTGAAACGCTGAT	Reverse
5862	Zebrafish	xbp1t	GGGTTGGATACCTTGGAAA	Forward
5863	Zebrafish	xbp1t	AGGGCCAGGGCTGTGAGTA	Reverse
5864	Zebrafish	xbp1s	TGTTGCGAGACAAGACGA	Forward
5865	Zebrafish	xbp1s	CCTGCACCTGCTGCGGACT	Reverse
5866	Zebrafish	xbp1t	GAGGAGCCCACAAAGTCCTC	Forward
5867	Zebrafish	xbp1t	CGAAGTGCTTTTTCCTCTGG	Reverse
5868	Zebrafish	rpp0	CTGAACATCTCGCCCTTCTC	Forward
5869	Zebrafish	rpp0	TAGCCGATCTGCAGACACAC	Reverse
6287	Zebrafish	hur	TGGTTGTTGCAGTTTTATCAGG	Forward
6288	Zebrafish	hur	CCTATTCACCTGAATCTCTGGG	Reverse
6289	Zebrafish	hur	ATTTGTGTAGATTGGGAATGGC	Forward
6290	Zebrafish	hur	TCCACATTGACTTCCACAAAAG	Reverse
6291	Zebrafish	hur	CTTTTGTGGAAGTCAATGTGGA	Forward
6292	Zebrafish	hur	TCATTTACAAACCTGATGCCTG	Reverse

Table 2-5: Sequencing Primers

Sequencing				
TE #	**Species**	**Gene**	**Sequence**	**Use Details**
5668	General	TracR	AAAAGCACCGACTCGGTGCC	iCas CRISPR
px330	General	px330	GACTATCATATGCTTACCGT	px330 plasmid
px330new	General	px330	TTTCTTGGGTAGTTTGCAGTTTT	px330 plasmid
T7	General	T7	TAATACGACTCACTATAGGG	
5027	Mouse	hspb7	CCTACGAGAGGATGGTAGCC	mORF plasmid 6478663
5028	Mouse	hspb7	GGGAAGCCAGAGAGATAGCC	mORF plasmid 6478663

CHAPTER 3: KNOCKDOWN OF HSPB7 IN ZEBRAFISH EMBRYOS LEADS TO DEFECTS IN CARDIOGENESIS AND ASYMMETRY

Introduction

The zinc finger protein Gata4 is known to have roles in cardiac morphogenesis in human, mouse and zebrafish. Previous work by the Evans laboratory has demonstrated that in both *gata4* morphants[156], and in embryos expressing a dominant negative Gata4[87], heart tube looping is disturbed. This indicates that following specification of cardiomyocytes, Gata4 is required for cardiomyocytes to correctly interpret morphogenetic cues. As discussed in Chapter 1, depletion of Gata4 leads to defective heart development and subsequent progressive cardiac pathologies. It follows that the genes regulated by Gata4 in the developing embryo contribute to both cardiomorphogenesis and continued cardiac function. However, as a master transcription factor, Gata4 regulates a large number of genes, the identity and functions of many of which remain to be uncovered.

A previous graduate student in our laboratory, Gabriel Rosenfeld, performed a screen for genes that are regulated by *gata4* in developing zebrafish heart, and identified a list of candidates. The small heat shock protein *hspb7* was a member of this list and proved interesting for further study for a number of reasons. First, *hspb7* is expressed exclusively within striated muscle, most abundantly in the heart, suggesting that it fulfils a muscle-specific function[123,128,132]. Second, the role of *hspb7* in muscle was not at all well delineated, but *in vitro* studies had suggested that it was able to prevent buildup of protein aggregates[126,127]. Third, and excitingly, a number of genome-wide association studies had linked

polymorphisms in human *HSPB7* with alteration in the risk of cardiac pathologies in various human populations[157–161]. We hypothesized that *hspb7* played an important role in heart development and/or function, and set out to investigate the phenotype of *hspb7* depletion in the zebrafish.

The studies described in this chapter were performed in collaboration with Gabriel Rosenfeld, PhD and are published[120]. All of the work presented herein was performed by myself except where noted in the figure legends.

Hspb7 is expressed in the developing zebrafish heart

As *hspb7* has not previously been comprehensively studied in zebrafish, we wished to better understand the temporal and spatial expression pattern of *hspb7* during zebrafish development.

Gabriel performed whole mount *in situ* hybridization (WISH) for *hspb7* and observed that *hspb7* is ubiquitously expressed during somitogenesis and is then specifically upregulated in the developing cardiac mesoderm at 25 somites (Figure 3-1B). *Hspb7* is specifically expressed in the heart tube during jogging and looping (Figure 3-1C,D). By qPCR, I confirmed initial upregulation of *hspb7* during segmentation stages (Figure 3-1E).

We did not detect *hspb7* expression during gastrulation, however another group was able to demonstrate the presence of *hspb7* transcripts at shield stage, and in the Kupffer's Vesicle, by ISH with a different probe[162]. This suggests that our WISH probe was not sensitive enough to pick up the earliest expression.

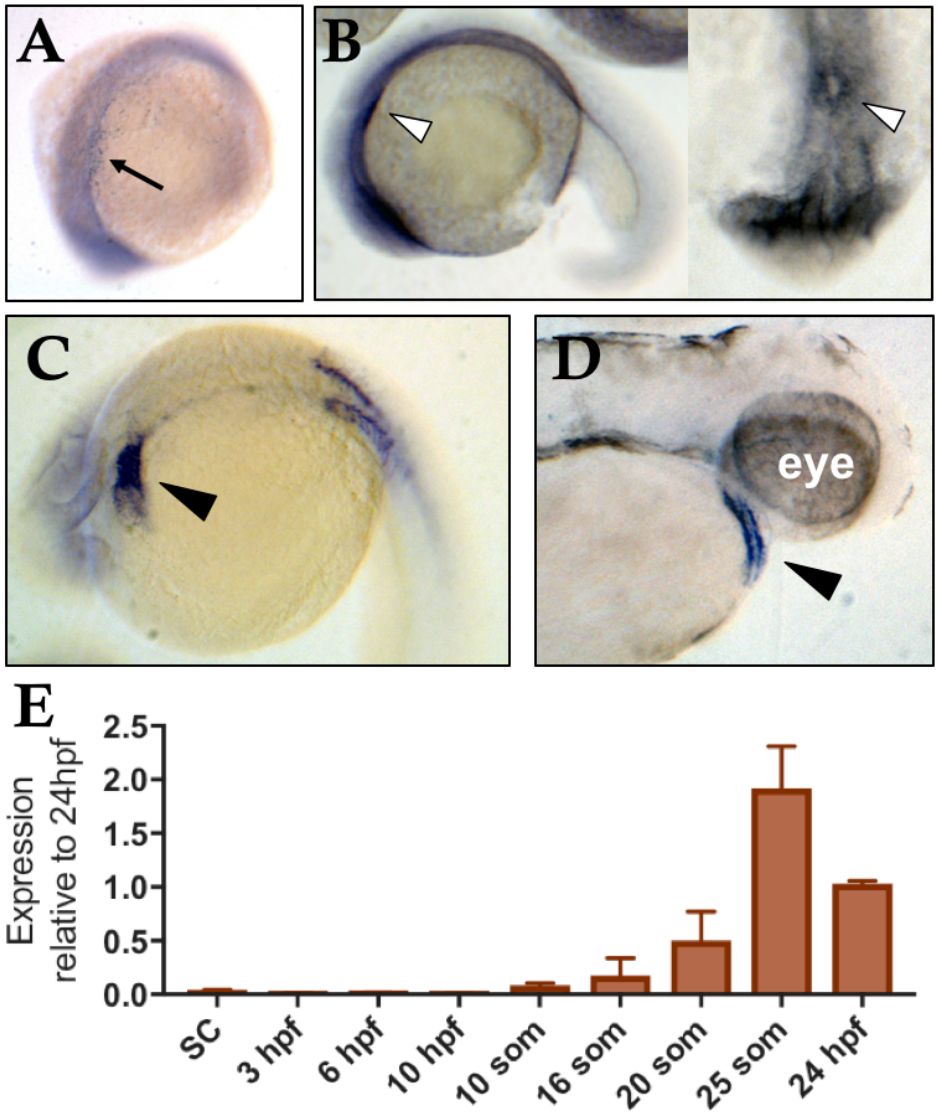

Figure 3-1: Expression of hspb7 during zebrafish development.
In situ hybridization at 14som (A), 22hpf (B), 24hpf (C) and 48hpf (D) shows hspb7 expression in the developing cardiomyocytes (arrow), cardiac cone (white arrowhead) and developing heart (black arrowhead). (E) qPCR expression for hspb7 identified upregulation of transcript commencing at the 10som stage. In situ hybridization studies were performed in collaboration with Gabriel Rosenfeld, PhD.

Defects in cardiomorphogenesis in *hspb7* morphants

Since *hspb7* is specifically expressed in the developing heart, we hypothesized that depletion of *hspb7* would lead to defects in cardiomorphogenesis. In order to

answer this question, Gabriel designed morpholinos targeting the start codon (7MO) or a splice site (7MOs) of *hspb7* (Figure 3-2A). I injected increasing concentrations of 7MO and 7MOs into wildtype zebrafish fertilized eggs and observed the effect of *hspb7* knockdown on embryonic phenotype. We identified a cardiac phenotype which presented as abnormal heart morphology. By 3dpf, morphant embryos had a variety of phenotypes including malformations, in particular atrial ballooning, as well as failure to loop resulting in a linear heart tube (Figure 3-2B,C).

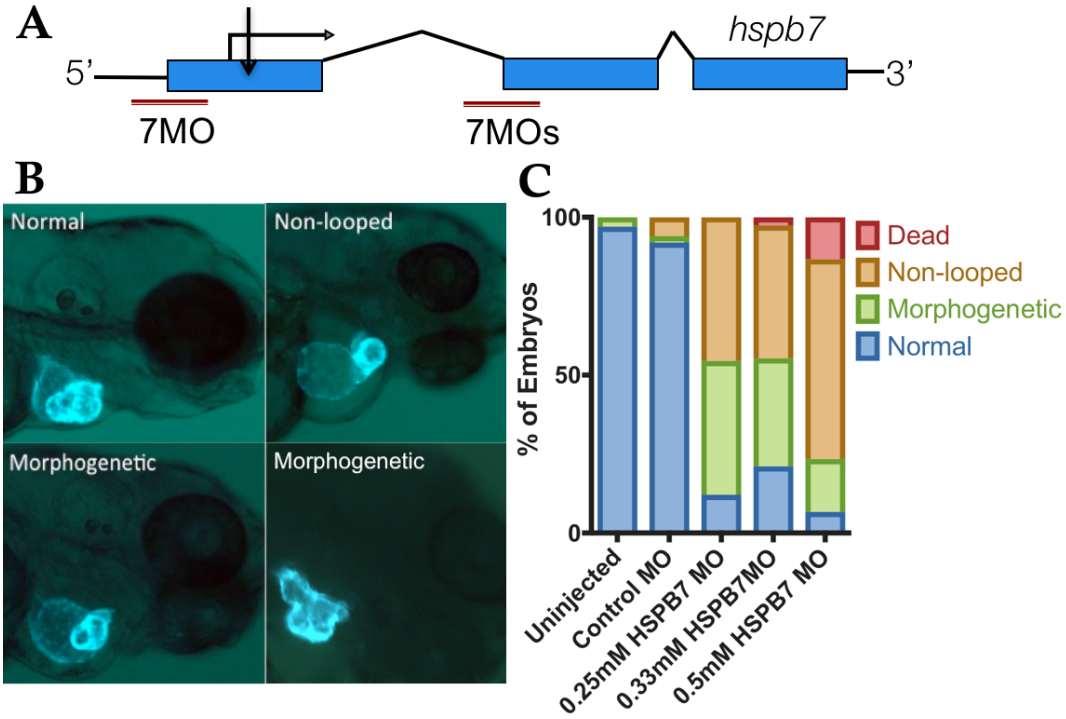

Figure 3-2: Knockdown of hspb7 with morpholinos leads to defects in cardiomorphogenesis.
(A)*Structure of* hspb7 *gene showing targeting location of morpholinos 7MO and 7MOs. (B) Representative cardiac phenotypes at 72hpf in tg(myl7::gfp) embryos injected with 0.5mM 7MO. (C) Quantification of cardiac phenotypes at 72hpf.*

Closer analysis by Gabriel Rosenfeld identified decreases in ventricular cardiomyocyte size, but not number, in *hspb7* morphants[†††].

Alteration in jogging in *hspb7* morphants

When monitoring the development of the heart in embryos injected with 7MO, I observed that in a significant percentage of morphant embryos, the heart tube either failed to jog left and remained central, or jogged to the right (Figure 3-3). In order to facilitate easy visualization of the heart, this experiment was performed in the *tg(myl7:gfp)* transgenic line, which expresses green fluorescent protein (GFP) under the control of the cardiac myosin promoter.

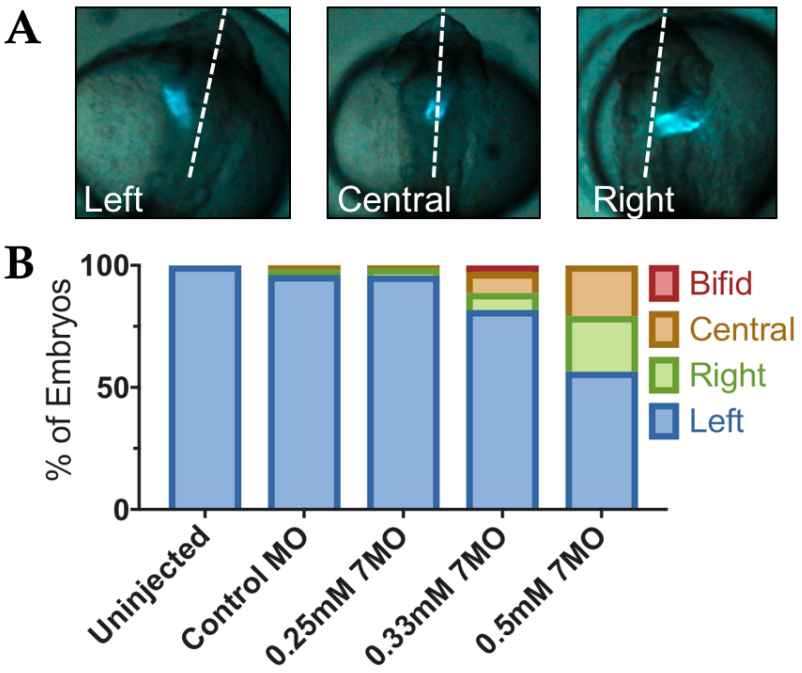

Figure 3-3:* Hspb7 *depletion leads to randomization in cardiac jogging.
(A) Representative images of 32hpf tg(myl7:gfp) embryos injected with 0.5mM 7MO. Dotted line marks the midline. (B) Quantification of jogging phenotypes.

[†††] Ventricular cardiomyocyte size was decreased at 48hpf when analyzed in *tg(myl7:mKate-caax)* embryos. Myocyte shape was also altered. It is important to note that decrease in size may be secondary to other defects in cardiomorphogenesis or to defects in cytoskeletal function.

Interestingly this phenotype was exaggerated with concomitant depletion of Gata4[120], indicating the two genes may genetically interact.

Randomization of jogging in *hspb7* morphants is suggestive of a role for *hpsb7* either in establishment of asymmetry, or the ability of cardiomyocytes to follow patterning cues. Early patterning in the zebrafish is directed by a transitory organ called the Kupffer's vesicle (KV), which is analogous to the murine node. I performed *in situ* for an early marker of the establishment of asymmetry, *southpaw (spaw)* which is predominantly expressed on the left-hand side of normal embryos at the 18 somite stage. In embryos injected with 7MO, *spaw* expression was altered with most embryos exhibiting bilateral expression (Figure 3-4). This indicates early disturbance to the establishment of asymmetry in the *hspb7* morphants.

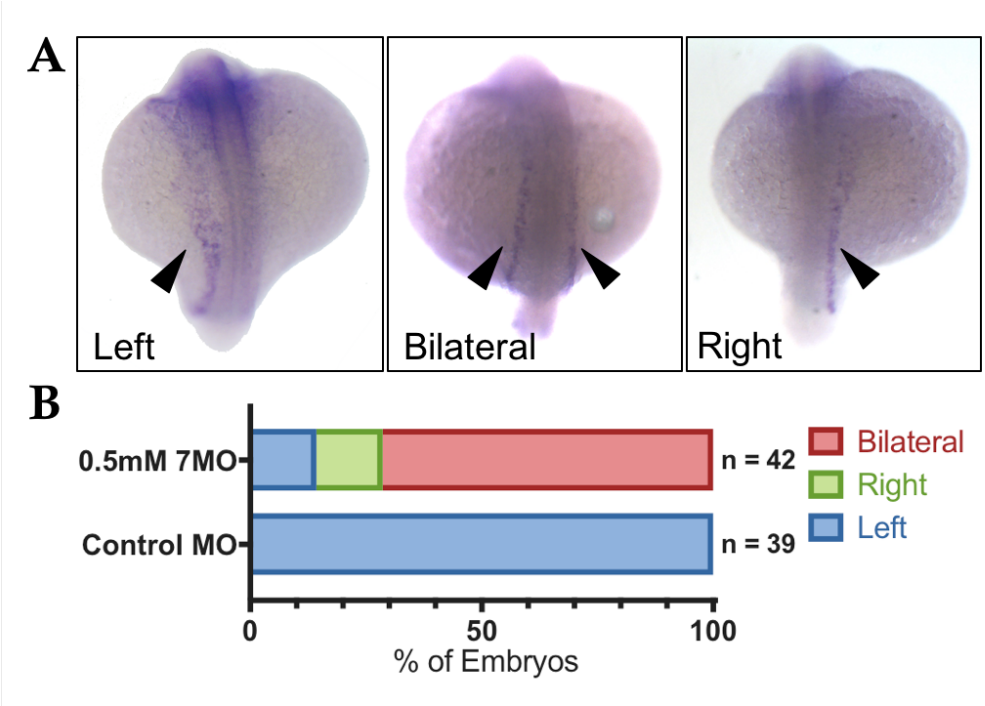

***Figure 3-4: Expression of the early marker of asymmetry,* spaw, *is altered in embryos depleted of* hspb7.**
(A) Representative dorsal images of in situ hybridization for spaw *performed in 18 somite stage embryos injected with 0.5mM 7MO. (B) Quantification of spaw expression patterns in* hspb7 *morphants shows that the majority no longer exhibit asymmetric expression.*

Closer analysis by Gabriel Rosenfeld revealed defects in the function of the KV of *hspb7* morphants. As discussed earlier, the Marvin laboratory published data to visualize *hspb7* expression in the KV[162], strengthening the evidence for this role.

Discussion

In this chapter, we used a morpholino-based knockdown approach to investigate, for the first time, the role of the small heat shock protein *hspb7* during development. Our inquiries generated some interesting insights.

First, we found that knockdown of *hspb7* in the developing zebrafish precipitated defects in cardiogenesis. This is indicative of a role for *hspb7* in myocyte differentiation, ability to follow morphogenetic cues or in myocyte function. Both the expression pattern and morphant phenotype we observed allow us to conclude that *hspb7* is not required for cardiomyocyte specification. Initial heart tube formation (Figure 3-3), chamber specification and cardiomyocyte proliferation are grossly successful, allowing us to presume that *hspb7* depletion does not interfere with a number of pathways that have been implicated in these early steps of cardiomorphogenesis[163]. We observed that ventricular myocyte size and shape, and overall cardiac morphology (Figure 3-2), are compromised. Studies into similar phenotypes have ascertained that these defects can arise as a consequence of alterations in either blood flow or cardiac contractility[18]. Based on the expression pattern of *hspb7*, it is a strong hypothesis that alteration in contractility may be responsible for the defects in cardiomorphogenesis we observed. It is also interesting that the phenomenon of altered contractility is also associated with the types of the human heart disease linked with *HSPB7* polymorphisms through GWAS studies[158–160].

In addition to the defects in cardiomorphogenesis, we identified that knockdown of *hspb7* leads to defects in the establishment of left-right asymmetry. Alterations in heart tube jogging were visualized and quantified (Figure 3-3), and disturbance of the underlying signaling pathways were confirmed with ISH for markers including *spaw* (Figure 3-4), *lefty1* and *lefty2*[120]. In an observation that may at first seem surprising, mis-expression of asymmetry markers was found in over 80% of morphants whereas alteration of jogging was only seen in around 50%. However, in human and mouse disease with failure to correctly establish left-right signaling cues, *situs inversus* is seen in around 50% of affected individuals[164]. This suggests that additional signaling cues control downstream patterning, allowing asymmetrical organ development on either the right or left in a stochastic manner. Thus, from our data, 20% of morphants retain normal left-hand signaling, and of the 80% with aberrant establishment of asymmetry we expect half to jog left anyway.

We ascertained that the asymmetry and defective cardiomorphogenesis phenotypes are independent of each other[120], however, there are some interesting overlaps between the mechanics of the KV and of the cardiomyocyte that allow us to speculate regarding the molecular role of *hspb7*.

Previous work has demonstrated that overexpression of Hspb7 prevents the formation of F-actin stress fibers in cultured cardiomyocytes[126]. In both the cardiomyocyte and the beating cilia of the KV, the actin cytoskeleton retains cell shape and function in a high-motion environment. If *hspb7* has a role in the maintenance of the actin cytoskeleton, or in the regulation of signaling pathways or structures that interact with the actin cytoskeleton, loss of *hspb7* might be expected to cause problems for both of these contracting cell types. A role

regulating cytoskeletal dynamics would be in keeping with published roles for a number of other members of the HSPB family[165]. Although all cell types have an actin cytoskeleton, given the expression pattern of *hspb7*, we would expect that this role is either specifically required in continuously contracting cells, or is fulfilled by a different protein in alternate organs.

The findings discussed in Chapter 4 were replicated shortly after their publication by a separate published study from the Marvin laboratory[162].

CHAPTER 4: *HSPB7* MUTANT ZEBRAFISH EXHIBIT CARDIAC PATHOLOGIES THAT SENSITIZE THEM TO EXERCISE STRESS

Introduction

As discussed in Chapter 3, the initial work that I completed with Gabriel Rosenfeld appeared to confirm our hypothesis that *hspb7* has an important role in the developing zebrafish cardiomyocyte. However, we had not established the molecular role of *hspb7*. In addition, there are several important caveats that must be noted of morpholino studies. The first is that the morpholino has a limited time frame in which it is able to effectively deplete the expression of its target protein. Eventually, the morpholino is depleted through dilution by cellular proliferation or degradation. Secondly, some morpholinos are associated with a number of common side effects, including cardiac malformation. Of key importance, comparisons of morphant and mutant phenotypes have exposed discrepancies[166]. Therefore, it was important to validate the observations we had made in the morphant model. Recent advances in genome editing technologies such as TALEN and CRISPR have made it feasible to generate targeted mutations in the zebrafish[60,62,167]. With these tools in hand, I next sought to generate and characterize *hspb7* mutant zebrafish.

Generation of mutant hspb7 lines

We generated mutant *hspb7* alleles using Transcription Activator-Like Effector Nuclease (TALEN) technology. In the absence of information regarding critical functional domains of Hspb7, Gabriel designed TALENs to target mutations near the 5' end of the gene, reasoning that an indel leading to an early frameshift was

likely to cause a deleterious mutation (Figure 4-1). By exploiting the presence of a HpyCH4V restriction site in the wildtype allele, I was able to monitor the generation and transmission of mutant alleles by RFLP analysis of PCR products that included the predicted TALEN cut site.

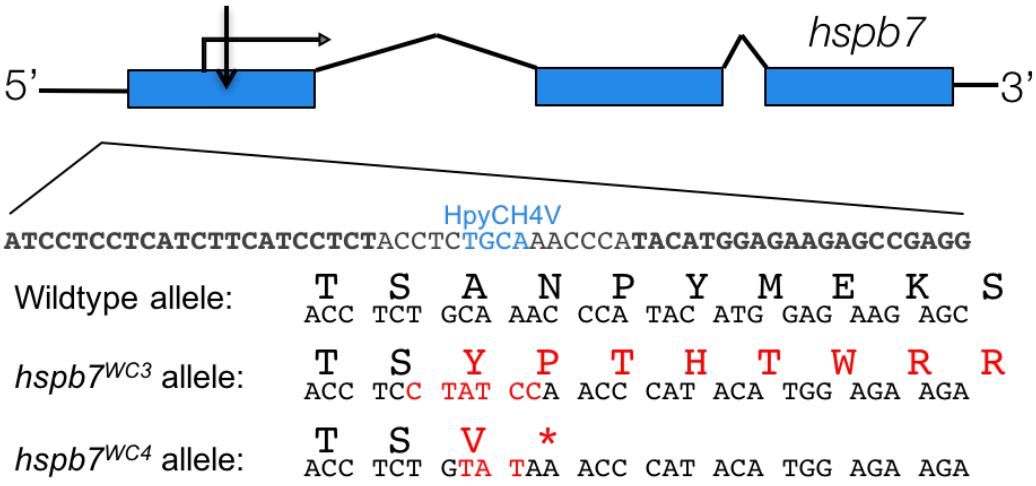

Figure 4-1: Generation of mutant* hspb7 *alleles.
Structure and partial sequence of the hspb7 gene, showing TALEN targeting proximal to the start codon and resultant mutant alleles WC3 and WC4.

I recovered two mutant alleles from separate founder fish that were predicted to encode proteins missing a large proportion of the normal Hspb7 protein (Figure 4-1). Both alleles generate a frameshift immediately after a polyserine stretch near the N-terminus of *hspb7*. The first allele, *hspb7*^{WC3}, is expected to result in the synthesis of an almost entirely novel predicted protein approximately half the mass of wildtype Hspb7. The second frameshift allele causes an early stop codon, truncating the predicted protein to only 27 amino acids, and was named *hspb7*^{WC4}. Both mutations lie in the middle of exon 1 and are not predicted to interfere with splicing of *hspb7* mRNA. I tested if the premature stop codons predispose mutant *hspb7* mRNAs to nonsense-mediated decay, but qPCR analysis indicated that *hspb7*^{WC3} and *hspb7*^{WC4} transcripts are expressed at levels similar to wildtype *hspb7*

(Figure 4-2B). Since both transcripts still encode the N-terminal of the Hspb7 protein, this is not unexpected.

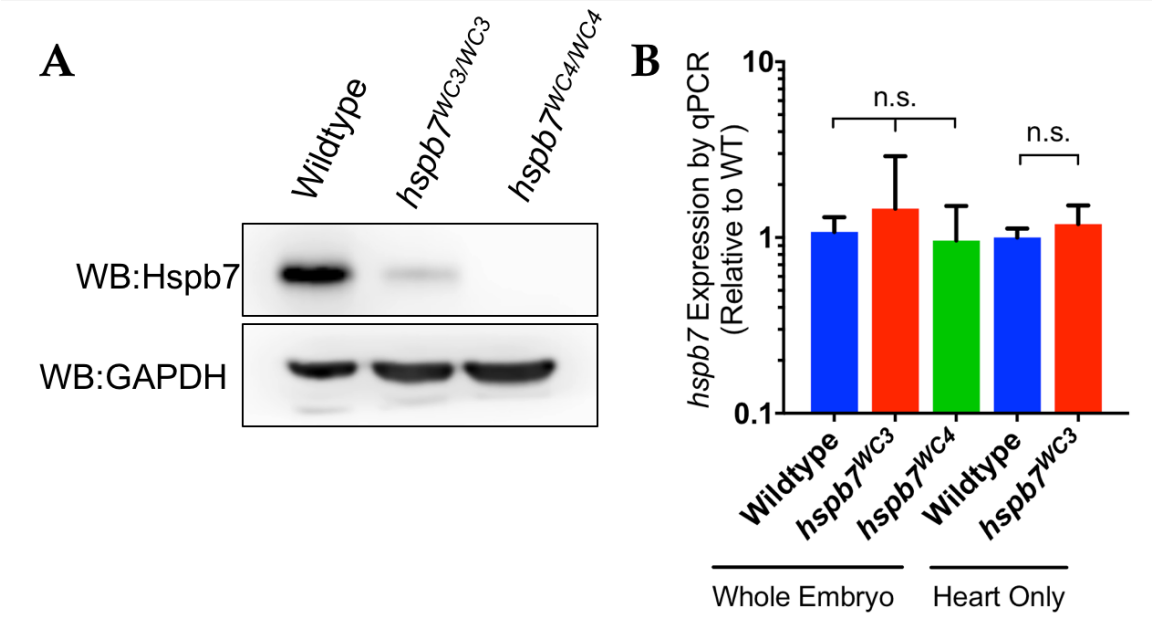

Figure 4-2: Loss of* Hspb7 *expression in mutant embryos..
(A) Western blot of protein lysates from adult zebrafish hearts shows loss of Hspb7 protein in animals homozygous for either of the hspb7 *mutations. (B) qPCR data showing that hspb7^{WC3} and hspb7^{WC4} are expressed at levels comparable to wildtype hspb7 in 5dpf zebrafish embryos.*

I also performed western blotting experiments and confirmed that Hspb7 protein was absent in the hearts of adult zebrafish homozygous for either of *the hspb7* mutant alleles (Figure 4-2A). Thus, I demonstrated that both *hspb7^{WC3}* and *hspb7^{WC4}* represent null alleles of *hspb7* and that these lines will be deficient for any normal role of Hspb7 in the zebrafish.

Zebrafish tolerate *hspb7* mutant alleles

Embryos homozygous for the mutant *hspb7* alleles were recovered from crosses of heterozygous fish in the expected Mendelian ratios (Figure 4-3).

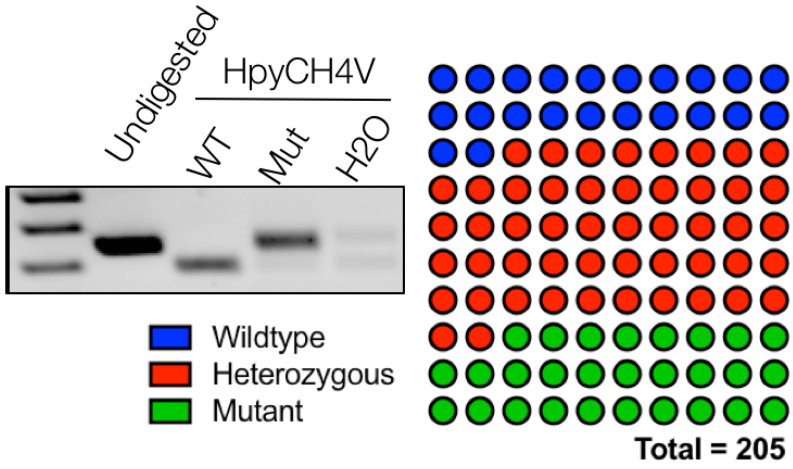

Figure 4-3: Genotyping of embryos from a* hspb7 *heterozygous incross.
Left: Example PCR demonstrating genotyping strategy for hspb7 alleles. The restriction site for HpyCH4V is lost in the hspb7 mutant allele. Quantification of embryonic genotypes demonstrates that hspb7$^{WC3/WC3}$ alleles are transmitted at expected Mendelian ratios (21.9% Wildtype, 50.3% Heterozygous, 27.8% Mutant).

Homozygous *hspb7^{WC3}* or *hspb7^{WC4}* mutants showed no gross morphological defects (Figure 4-4A). In order to better visualize the hearts of *hspb7* mutant fish, I crossed the *hspb7^{WC3}* allele onto the *Tg(myl7::gfp)* background and observed cardiac development across the first week of life. In the absence of Hspb7, the vast majority of hearts were seen to undergo timely jogging and looping and to have normal size and morphology (Figure 4-4A,B), although there is a variable increase of 0-20% in cardiac abnormalities in *hspb7* maternal zygotic (MZ) mutants. Fish homozygous for either of the two mutant *hspb7* alleles were viable to adulthood and fertile. These findings were surprising given our previous morphant data. However, as our lab, and others, have repeatedly observed compensatory mechanisms in play in zebrafish mutants, I hypothesized that something similar may be offsetting the loss of *hspb7.* This is further explored in Chapter 6.

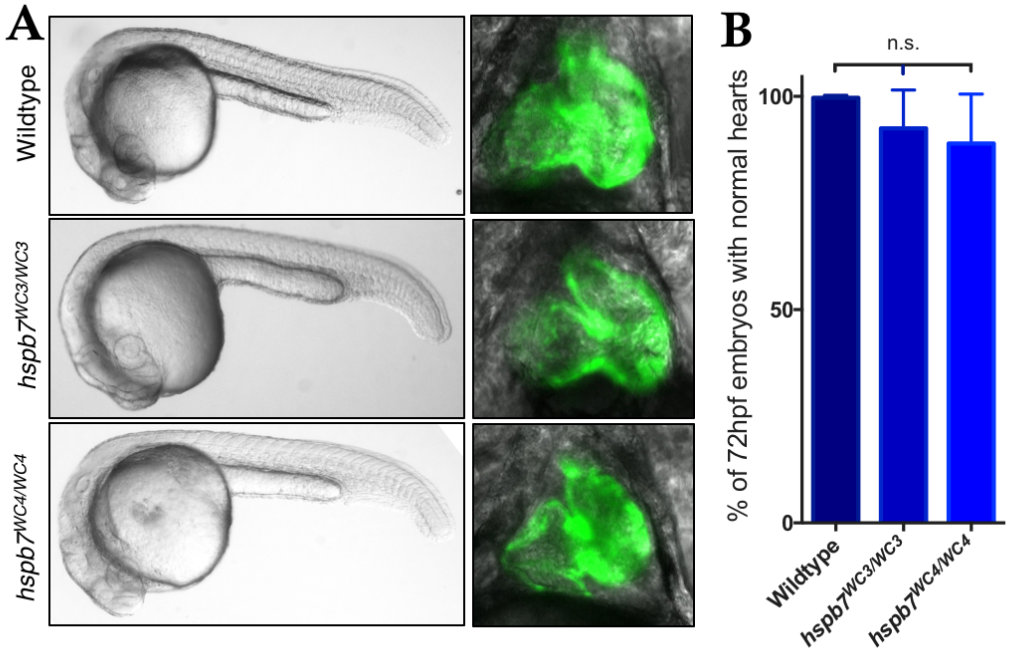

Figure 4-4: Phenotyping of* hspb7 *mutant embryos.
(A) Representative brightfield images of wildtype or homozygous hspb7 mutant 24hpf embryos. Also shown are representative 72hpf hearts from wildtype or hspb7 mutant lines crossed onto a tg(myl7:gfp) background. (B) Quantification of normal hearts at 72hpf in wildtype or homozygous hspb7 mutant animals (n=200)

Normal response to heat stress in *hspb7* mutants

Although expression of *hspb7* is not upregulated during heat shock[123], I reasoned that, as a heat shock protein, its role is likely to be more important during periods of cardiac or general stress. I asked whether *hspb7* mutant animals were less able to deal with a generalized heat challenge. I incubated embryos at the raised temperature of 32°C following gastrulation. There was not an increase in cardiac abnormalities in *hspb7* mutants that was greater than that seen in wildtype controls, nor was there a greater increase in randomization of cardiac jogging (Figure 4-5). However, I did notice that an increase in temperature led to a notable increase in right-jogging heart tubes in embryos of all genotypes. To my

knowledge, this finding has not been previously reported and may be of interest to those studying the pathways that control the establishment of left-right asymmetry.

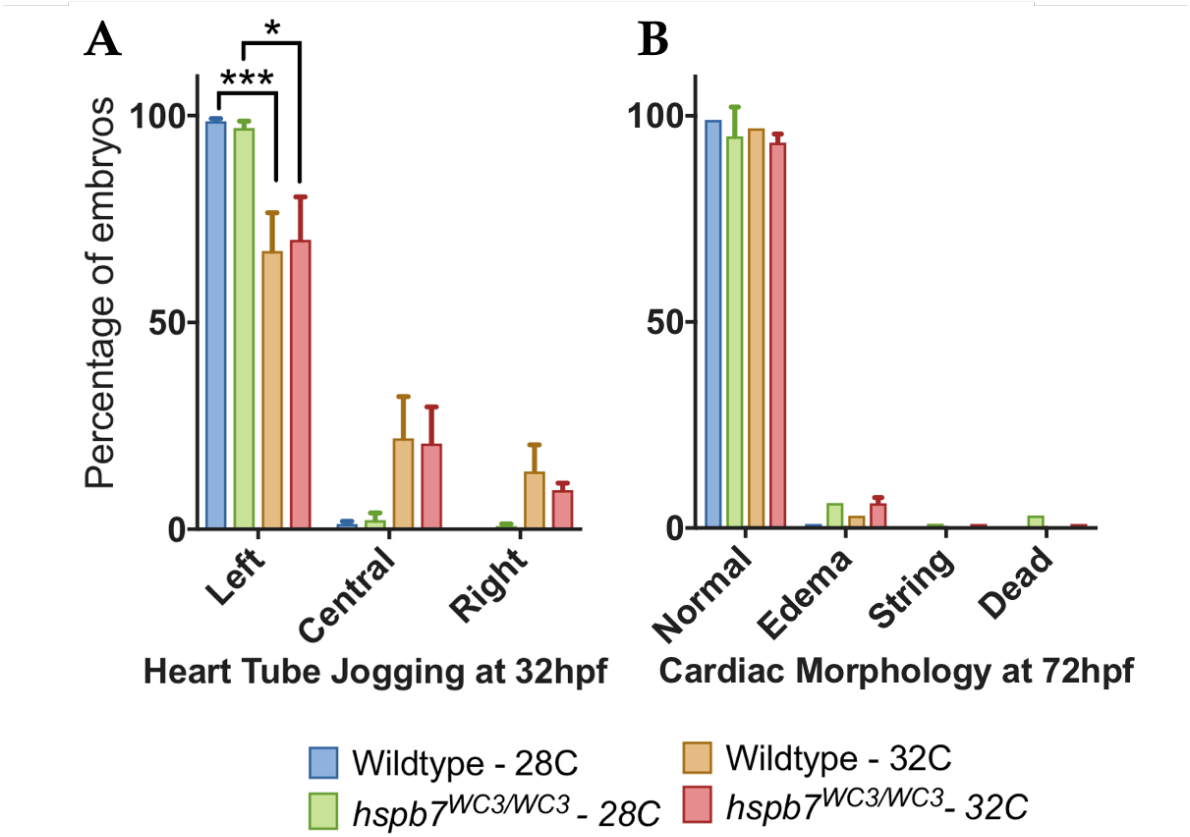

Figure 4-5: Phenotyping of wildtype and hspb7 mutant embryos incubated under normal (28C) or heat shock (32C) conditions.
(A) Heat shock leads to partial randomization of heart tube jogging in both wildtype and hspb7 mutant embryos. (B) Heat shock does not lead to increases in cardiac malformations.

Adult *hspb7*$^{WC3/WC3}$ fish have increased susceptibility to exercise-induced stress

When I bred homozygous null animals, I noticed a statistically significant increase in mortality rate in male fish (Figure 4-6). I reasoned that the mating process, particularly for the vigorously swimming male, represents a strenuous cardiovascular activity.

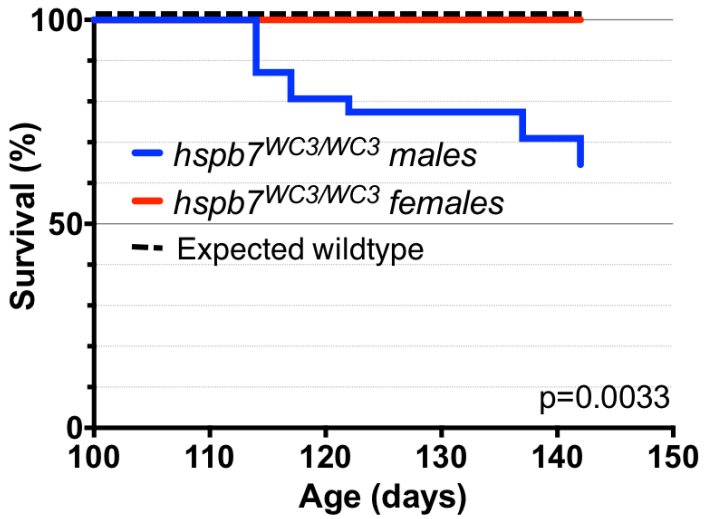

Figure 4-6: Tracking mortality of* hspb7 *mutants.
Kaplan-Meier curve showing survival of hspb7 mutant male and female animals following commencement of breeding at 105 days post fertilization.

I hypothesized that death indicated initial decreased capacity to cope with cardiac stress in *hspb7*$^{WC3/WC3}$ animals. To investigate the phenomenon in a controlled manner, batches of male and female adult zebrafish were subjected to an enforced swimming exercise paradigm. Genotyped groups of either *hspb7*$^{WC3/WC3}$ fish or wildtype controls were paced at 50 cms^{-1} for 30 minutes, every day for 5 days (Fig Figure 4-7A). This represents a high intensity anaerobic exercise regime, with a water flow approaching the critical swimming speed (U_{crit}) of zebrafish[168]. We observed that *hspb7* mutant animals spent a greater amount of time than wildtype

controls 'resting' at the back of the tank (23.37% of swim time for *HSPB7*$^{WC3/WC3}$ versus 2.78% of swim time for wildtype animals, Figure 4-7B,C).

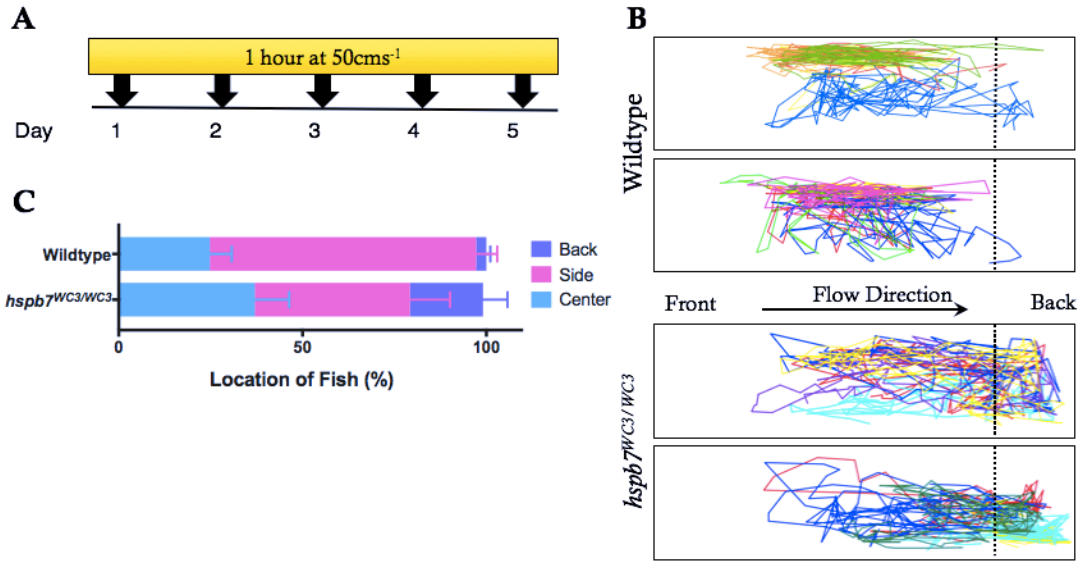

Figure 4-7:* Hspb7 *mutant adults are unable to maintain tank position during high-intensity exercise.
(A) High-intensity exercise paradigm for zebrafish. (B) Representative tracking of fish location in the tank during the final minute of exercise shows that hspb7$^{WC3/WC3}$ *fish are more likely to remain at the back of the tank. (C) Quantification of fish location.*

Strikingly, around 30% of *hspb7*$^{WC3/WC3}$ animals died during the first few days of enforced exercise (Figure 4-8).

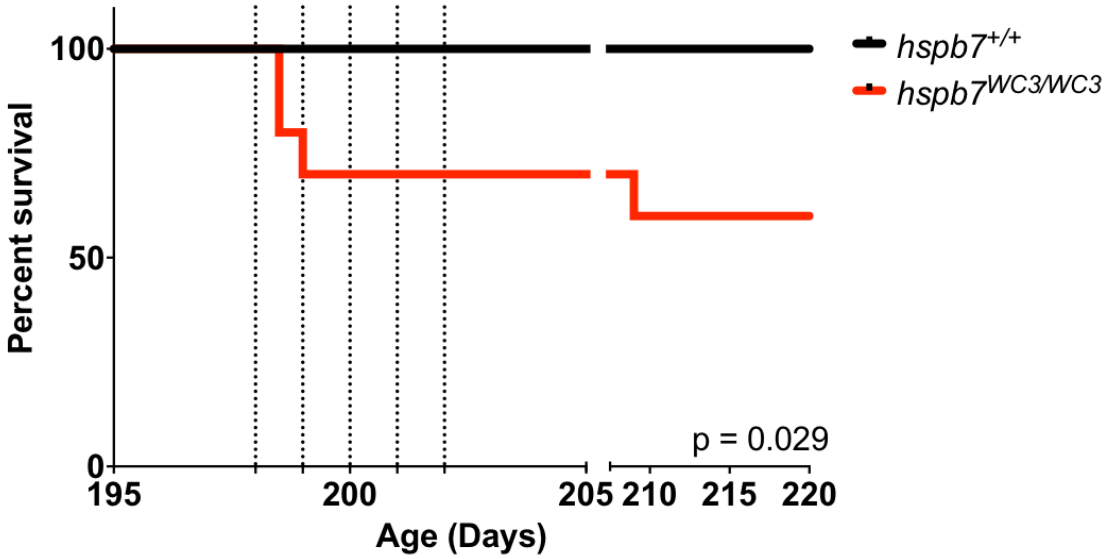

Figure 4-8: Increased mortality in* hspb7 *mutant animals subjected to a high intensity exercise regime.
Kaplan-Meier curve showing increase in mortality in hspb7$^{WC3/WC3}$ fish following commencement of exercise regime. Dotted lines indicate timing of exercise sessions (n=20)

However, 66% of animals that died were female, indicating that the gender bias we observed in post-mating mortality is more likely due to differences in behavior during mating rather than a gender-specific compromise of cardiac health.

Interestingly, I observed that *hspb7$^{WC3/WC3}$* animals consumed around 1.5 fold the amount of oxygen as wildtype controls when first exposed to exercise (Figure 4-9A). However, following repeated exposure to the exercise regime, the use of oxygen by *hspb7* mutant animals decreased to below that of wildtype controls (Figure 4-9B). It is important to note that the decrease in oxygen consumption coincides with the loss of ~30% of animals in whom the exercise machine induced mortality (after day 3 of exercise).

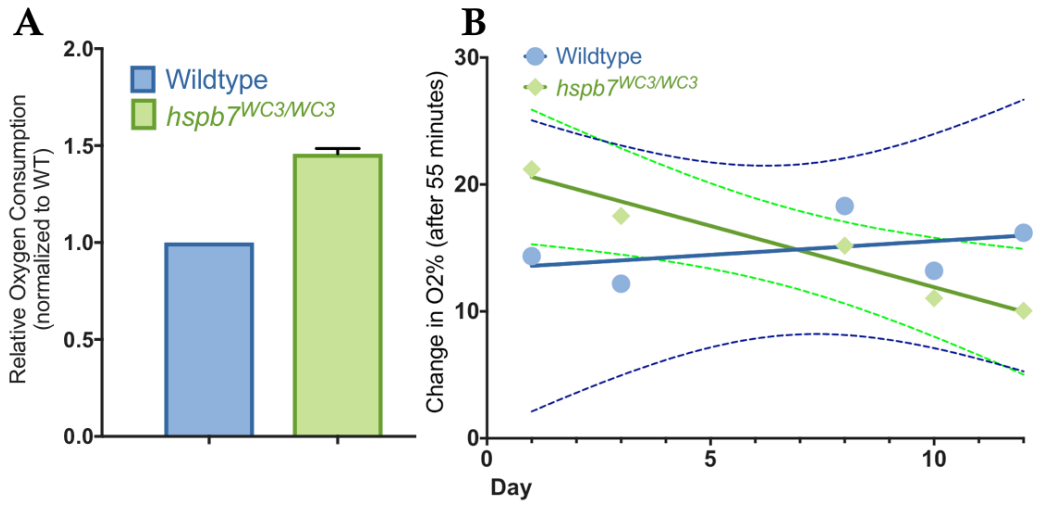

Figure 4-9: Oxygen consumption is altered in hspb7 mutants subjected to a high intensity exercise paradigm.
(A) Initially hspb7 mutants use around 1.4 fold the amount of oxygen as wildtype controls under the same swimming conditions. (B) Over time, the amount of oxygen used by hspb7 mutants decreases to levels equal to, or lower than, that of wildtypes. Solid lines represent line of best fit. Dotted lines represent 95% confidence intervals for the lines of best fit.

I hypothesize that inter-animal variation contributes to this phenomenon in one of two ways. Either the animals that die are those that are initially using much higher levels of oxygen than their siblings; or the animals that die are those that are unable to upregulate some compensatory pathway that allows them to tolerate the exercise stress – and in doing so decreases oxygen consumption. Since the relationship between oxygen consumption and cardiac function is exceedingly complicated, I opted not to further pursue this phenotype, but note it herein for the sake of completeness.

Hspb7$^{WC3/WC3}$ mutant adults exhibit heart pathology

I hypothesized that exercise stress may exacerbate a cardiac dysfunction that is not obvious in unstressed mutants. I dissected the hearts from adult zebrafish and quantified their size. I observed a striking and significant increase in ventricular

size in *hspb7*$^{WC3/WC3}$ and *hspb7*$^{WC4/WC4}$ adults when compared with wildtype animals or heterozygotes (Figure 4-10). Strikingly, the increase in mean ventricular area to body weight index (wildtype 3.01, *hspb7*^{WC3} 4.70, *hspb7*^{WC4} 5.16) exceeded the increase reported to be induced by cardiotoxin doxorubicin[56], suggesting that the *hspb7* mutants have a marked cardiomyopathy. Notably, the ventricles of *hspb7* mutants also appeared abnormally shaped, with a rounded appearance (Figure 4-10B) compared to wildtype controls (Figure 4-10A).

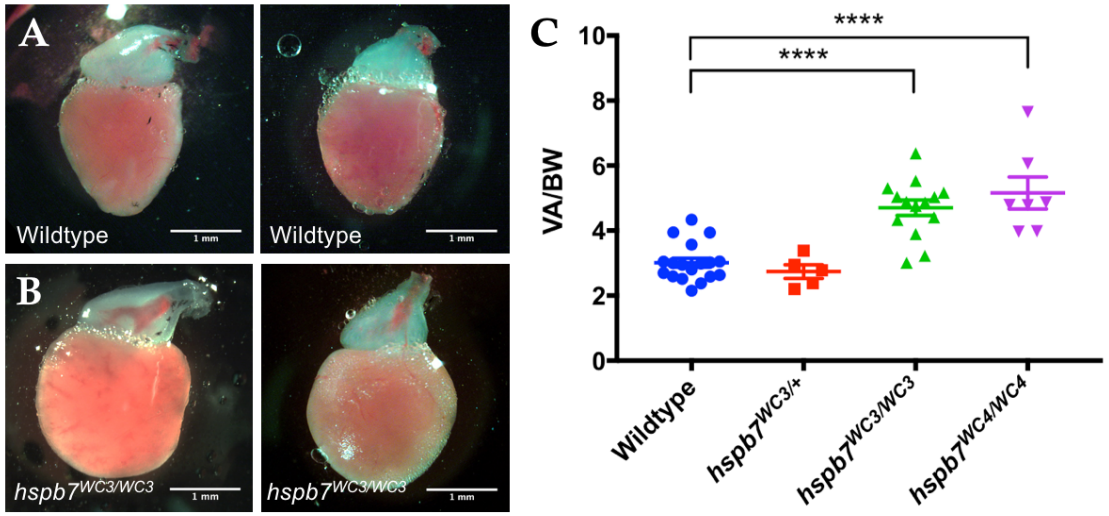

Figure 4-10: The hearts of* hspb7 *mutant adults are enlarged and abnormally shaped.

Representative images of dissected ventricles and outflow tracts from (A) wildtype and (B) hspb7$^{WC3/WC3}$ *adults. Shown are hearts from 10mo animals with the atria removed for clear viewing. (C) Quantification of ventricular area to body weight index (VA/BW) showed heart enlargement in animals homozygous for either of the* hspb7 *mutations. Each point represents one animal. Data combined for 10mo and 18mo zebrafish.*

In order to further explore the abnormalities in *hspb7* $^{WC3/WC3}$ hearts, I processed adult *hspb7*$^{WC3/WC3}$ mutant zebrafish for general histopathological analysis. Inspection of the gross anatomy by a pathologist revealed that 60% of mutant fish exhibited hearts that appeared rounded when compared with wildtype controls. Notably, 80% of mutant fish were found to exhibit diffuse, marked hepatocellular vacuolation (Figure 4-11A,B). This phenotype might be indicative of hepatic injury downstream from cardiac dysfunction[169,170169,170].

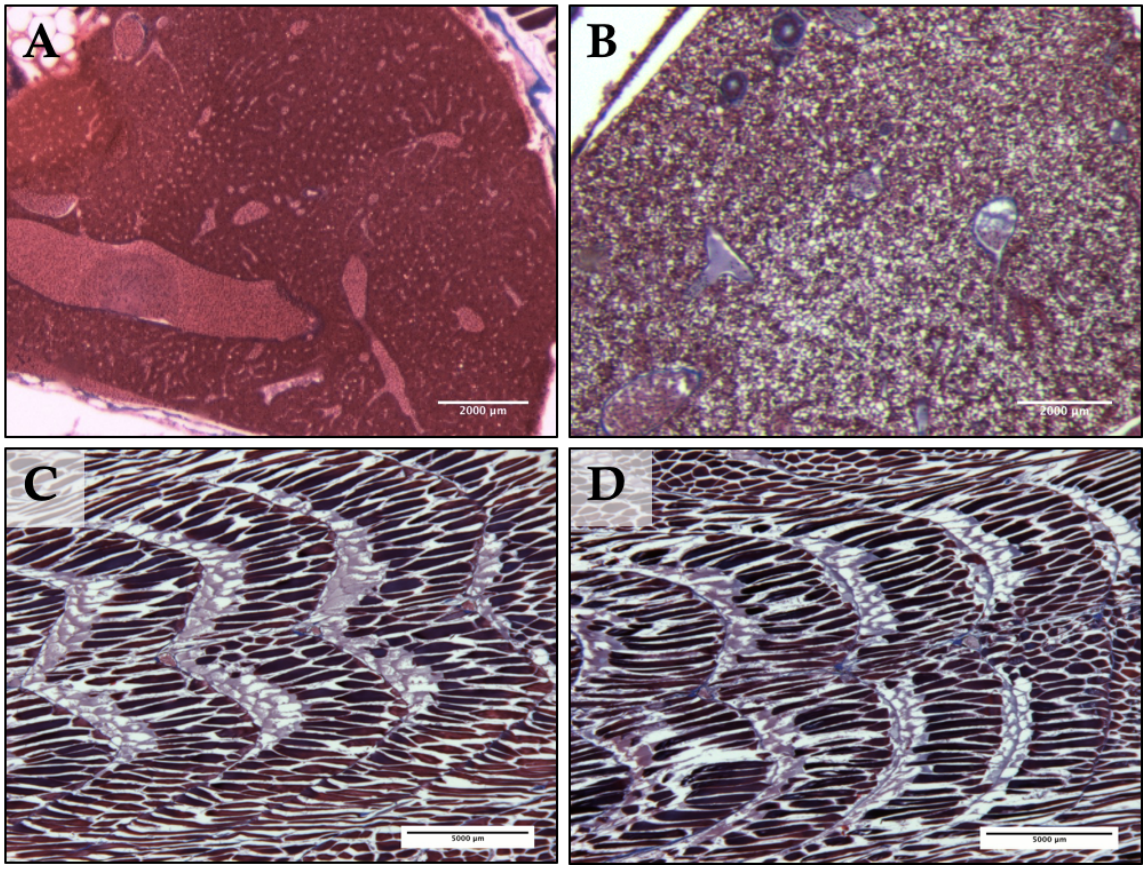

Figure 4-11: Abnormal liver histology in* hspb7 *adults.
Trichrome-stained images of adult (A,C) wildtype and (B,D) hspb7$^{WC3/WC3}$ *zebrafish liver (A,B) and skeletal muscle (C,D). Representative images.*

The skeletal muscle of *hspb7*$^{WC3/WC3}$ animals did not exhibit fibrotic lesions (Figure 4-11C,D), allowing me to conclude that differences in ability to maintain swim speed are not secondary to skeletal muscle dysfunction.

Heart pathology was evaluated comparing trichrome stained cardiac sections from mutant or wildtype animals. This revealed mild multifocal cardiac fibrosis in 100% of *hspb7*$^{WC3/WC3}$ hearts, which was not seen in control wildtype hearts (Figure 4-12A,B).

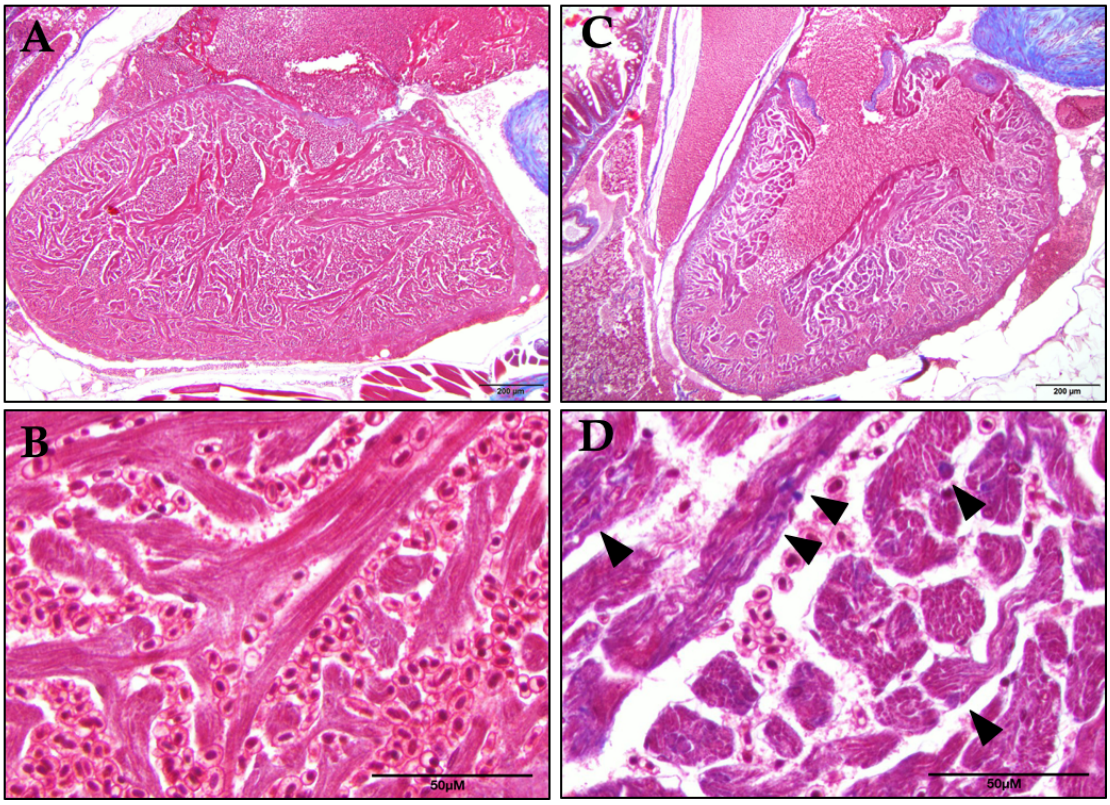

Figure 4-12: hspb7$^{WC3/WC3}$ adult hearts exhibit fibrosis.
Trichrome staining of 3 month old wildtype (A,B) and hspb7 mutant (C,D) hearts. Focal fibrotic lesions (arrowheads) are seen in all (5/5) hspb7 mutant but never in wildtype samples. Representative images.

For closer observation of abnormalities in the myocardium of *hspb7* mutants, hearts were dissected from adult mutant or wildtype zebrafish and analyzed by transmission electron microscopy (TEM), which revealed sarcomeric disarray in homozygous mutant hearts (Figure 4-13). This suggests that in the absence of Hspb7, there is an underlying cardiopathology, which likely predisposes mutant animals to exercise-induced stress that can lead to cardiac failure.

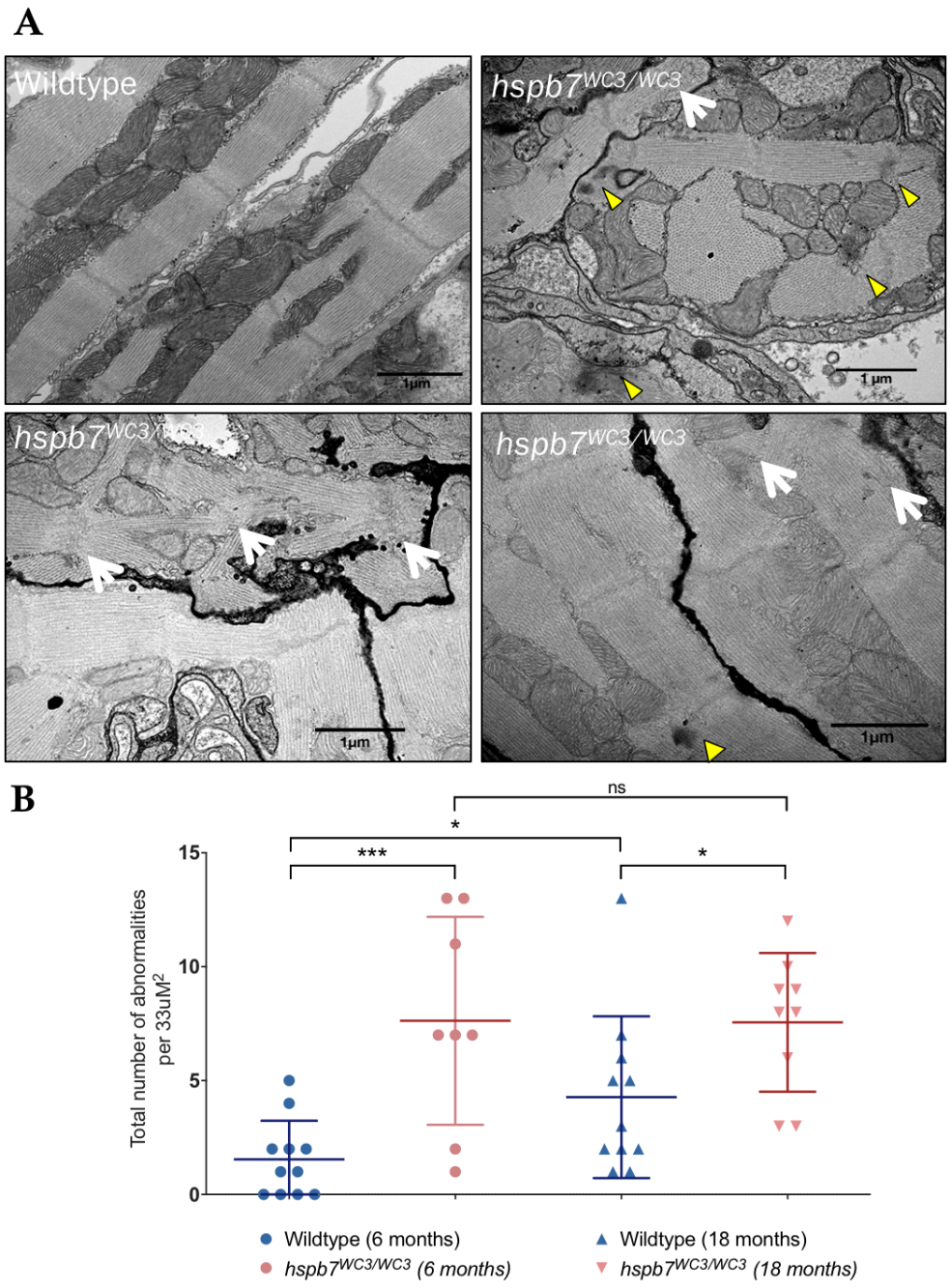

Figure 4-13: hspb7 mutant hearts exhibit abnormalities visible by TEM.
TEM images of 3-month-old wildtype and hspb7$^{WC3/WC3}$ hearts. Wildtype hearts exhibit repeated, regular sarcomeric striations with organized mitochondria. Hspb7 mutant hearts show defects including breakdown of sarcomeric organization (white arrows) and electron-dense dark-staining areas (arrowheads) indicative of the presence of aggregates. (H) Quantification of abnormalities from blinded analysis of TEM images. Each dot represents a unique 25000X image.

Discussion and Future Directions

Hspb7 mutant zebrafish develop normally.

I used TALEN technology to generate *hspb7* mutant zebrafish lines, which I initially hypothesized would corroborate the data myself, and others, had generated by morpholino depletion of *hspb7* (see Chapter 3). Surprisingly, global loss of *hspb7* is tolerated during zebrafish embryogenesis and *hspb7* mutants are viable and fertile. This is particularly unexpected in light of data that *hspb7* is very abundantly expressed in adult zebrafish heart, in particular in the ventricle (Table 4-1,[24]).

Table 4-1: Differential expression of* hspb7 *in adult zebrafish heart chambers.

Gene	Atrium FPKM (Rank)	Ventricle FPKM (Rank)	Bulbus Arteriosus FPKM (Rank)
myl7	11238.9 (#2)	36297.9 (#2)	1001.8 (#84)
hspb7	756.4 (#116)	3633.7 (#32)	228.1 (#254)
hspb1	658.8 (#132)	2512.6 (#65)	663.1 (#122)
hspb5b	-	23.6 (#3595)	-

Analysis of data from chamber-specific RNAseq in the adult zebrafish heart (Singh et al. *2016[24]) showing high expression of* hspb7 *in the ventricle. Myl7 and other small heat shock proteins included for comparison of FKPM values.*

Despite the lack of strong phenotype in the *hspb7* mutant embryo, I am confident that the *hspb7*^{WC3} and *hspb7*^{WC4} mutant alleles lead to complete loss of Hspb7 protein. There is a small amount of residual signal when Western blotting for Hspb7 in mutant heart (Figure 4-2), however, the antibody used to perform this assay is a polyclonal mix that likely recognizes the N-terminal of the protein, which would still be translated from either of the mutant alleles. The WC3 allele goes out of frame but continues to encode an amino acid sequence. The resultant protein is predicted to have a mass only 7kDa less than the wildtype Hspb7. Thus, it is a reasonable hypothesis that the residual signal might be from the polyclonal

antibody recognizing the N-terminal of this 'junk' peptide. The low level of signal compared with wildtype (around 10%) suggests that this peptide is much less stable than Hspb7.

As mentioned briefly above, one possible explanation for the lack of developmental defects is that the zebrafish compensate for loss of *hspb7* through upregulation of compensatory pathways and/or genes that attenuate any cardiac pathologies. This idea is explored in Chapter 5 and in Appendix A.

Discovery of exercise-induced mortality in *hspb7* mutant adults.

Despite normal development, I discovered that high-intensity exercise, which would cause an acute increase in cardiac workload, leads to exercise-induced mortality in around 40% of adults. I uncovered a mild cardiac pathology in *hpsb7* mutants, which is grossly asymptomatic until the animal is subjected to stress. The requirement for an additional stressor to precipitate a phenotype in the *hspb7* mutant zebrafish is particularly exciting as it better models the complex pathogenesis seen in much of human heart disease, in which environmental stresses and individual genetic variation impact disease severity and outcome.

It is interesting that the majority (~60%) of *hspb7* mutants tolerate the exercise insult despite the fact that all mutant hearts examined exhibited around the same mild level of fibrosis, and most had increased in ventricular size. One possibility is that additional inter-animal variation accounts for this variability. This could be due to differential inheritance of alleles of modulator genes. Our wildtype zebrafish lines are generated from crossing two unique strains (AB and Tubingen), allowing for substantial genetic variability.

Potential causes of cardiomegaly and sarcomeric abnormalities in *hspb7* mutants.

The generation of *hspb7* mutant lines was not as informative as I had originally hoped regarding the molecular role of Hspb7 within the cardiomyocyte. The mechanism behind the cardiomegaly, mild fibrosis and increased mortality that I observed is less easy to predict than would be the pathway behind a specific malfunction in cardiogenesis. However, the literature does provide some possible hints.

Cardiac enlargement in humans is most commonly caused by growth of existing individual myocytes rather than their proliferation[4]. However, the zebrafish heart has an increased regenerative capacity. The ventricles of adult zebrafish subjected to high intensity exercise regimes exhibit increase in both heart size and number of cardiomyocyte nuclei, indicating that the zebrafish compensates for cardiac overload through hyperplasia rather than hypertrophy[171]. The zebrafish is also able to retain normal physiological function following exercise overload-induced cardiomegaly, whereas human hearts typically have decreases in measures of cardiac function, such as fractional shortening[4]. In contrast, cardiomegaly of the zebrafish heart following treatment with the cardiotoxin doxorubicin leads to pathological alterations in these functional measurements[56]. These divergent findings make it difficult to immediately interpret the observation of cardiomegaly in *hspb7* mutant animals. However, the >50% increase in mean VA/BW that we

observed is larger than that recorded in either of these two prior studies[‡‡‡]. Since the increases caused by cardiotoxins are higher and closer to the increases we observed, and given the concomitant cardiac fibrosis, we hypothesize that cardiomegaly in the *hpsb7* mutants is pathological and is having an adverse effect on cardiac function. Recordings of functional parameters such as fractional shortening, or re-expression of atrial natriuretic factor in the adult heart would help to confirm this.

Through high magnification imaging of *hspb7* depleted cardiomyocytes by electron microscopy we were able to observe some abnormalities, including sarcomeric disarray. This phenomenon is most often observed in hypertrophic cardiomyopathy caused by mutation of genes that encode sarcomeric proteins, predominantly *MYH7* and *MYBPC3*[5]. This observation leads us to suggest a model whereby *hspb7* depletion leads to loss of sarcomeric integrity resulting in myofiber dysfunction and subsequent hypertrophic cardiomyopathy. Closer assessment of ventricular wall thickness in our mutants should allow us to observe whether the observed increase in ventricular area resembles hypertrophic cardiomyopathy.

Potential causes of cardiac fibrosis in *hspb7* mutants.

We also observed increases in cardiac fibrosis in *hspb7* mutant animals. Cardiac fibrosis is a hallmark of heart disease and is found in heart failure driven by

‡‡‡ Increase of around 20% (VA/BL increase from 5 to 6) for exercise and 30% (VA/BW increase from 4.0 to 5.1) for doxorubicin treatment. Raw data was not provided so these numbers are estimated from graphed data.

mutations in cytoskeletal components, calcium modulators, epigenetic regulators and transcriptional factors as well as following cardiac infarction[4]. The deposition of extracellular matrix within the muscle leads to impairment of muscle contractility and ultimately decreases in the ability of the heart to pump blood. Thus, the phenomenon is both a symptom of and a contributor to pathology. The mechanisms involved in the stimulation of cardiac fibrosis are not fully understood. The TGFβ signaling pathway is known to be a driver of fibrotic deposition in many tissue types, including collagen-producing cardiac fibroblasts[172]. TGFβ signaling leading to fibrosis in the heart is believed to be predominantly activated by TGF-β_1, secreted by cardiac fibroblasts. Expression of TGF-β_1 is known to be increased in response to Angiotensin II signaling, downstream of renin release by the kidneys. Decrease in renal perfusion leads to renin production, leading to a potential systemic pathology whereby loss of *hspb7* leads to a decrease in cardiac output, resulting in decreased kidney perfusion and increased renin production, driving TGF-β signaling and causing cardiac fibrosis. Cardiac fibrosis further compromises cardiac output, worsening the situation.

An interesting additional hypothesis is that loss of *hspb7* affects the cardiac fibroblasts in a cell autonomous manner. *Hspb7* is expressed in cardiomyocytes, but unvalidated RNAseq data found in the literature indicates that it is also expressed in adult cardiac fibroblasts[173§§§]. Cell-type specific depletion of *hspb7* would best answer this question.

§§§ *HSPB7* counted at 17.4FKPM in adult human cardiac fibroblasts and 1.99FKPM in fetal human cardiac fibroblasts, indicating that it is upregulated with age. These counts are considerably lower than those found in whole zebrafish ventricle, which is composed of both myocytes and fibroblasts.

Conclusions

In conclusion, these studies are the first to generate and characterize an *hspb7* mutant model system. I identified a cardiac pathology in adult *hspb7* mutant zebrafish that was lethal in a subset of mutant animals exposed to exercise stress. Careful phenotyping of the hearts of adult *hspb7* mutant zebrafish revealed cardiomegaly, sarcomeric abnormalities and cardiac fibrosis.

These observations demonstrate that the *hspb7* mutant zebrafish has a cardiomyopathy in which genetic and environmental interaction determines disease outcome. The contributions of multiple small influences on overall pathology is a phenomenon that is also observed in human complex cardiac disease, suggesting that the *hspb7* mutant zebrafish will be a useful tool for future identification of modifier genes and pathways that can influence the development and progression of cardiomyopathy.

Finally, by considering the observed phenotypes in the context of the larger literature surrounding cardiac pathologies, I was able to generate testable hypotheses regarding the molecular role of Hspb7 in the cardiomyocyte, which are explored in the following Chapter.

CHAPTER 5: HSPB7 BINDS TO THE SARCOMERIC PROTEIN FLNC AND PREVENTS ITS AGGREGATION

Introduction

In order to make testable hypotheses regarding the role of HSPB7 in the heart as a whole, and to understand the pathology in *hspb7* mutant zebrafish, it is important to better understand its function at a cellular and molecular level. For this purpose, a model system was required in which HSPB7 is expressed, and in which it would be possible to successfully perform biochemical experiments. The zebrafish is not ideally suited to this purpose, due to the small size of the heart and the general lack of zebrafish protein-specific antibodies.

HSPB7 is expressed in the murine HL-1 cell line

I initially turned to the murine atrial cardiac cell line HL-1, which is the only available cardiac cell line that can be maintained and beats spontaneously in culture[68]. I confirmed by Western blotting experiments and by immunofluorescent staining (IF) that HSPB7 is indeed expressed in HL-1 cells (Figure 5-1). Using IF I observed that HSPB7 is expressed throughout the cytoplasm of the HL-1 cell, but does not appear to be completely excluded from the nucleus. This finding is in keeping with previously published staining for a tagged HSPB7 isoform expressed ectopically in 293T cells[174]. The appropriate expression and localization of HSPB7 in HL-1 cells, in combination with the fact that these cells also express other cardiac proteins and form functional sarcomeres[175], recommended this cell line to me as an appropriate choice for further biochemical studies.

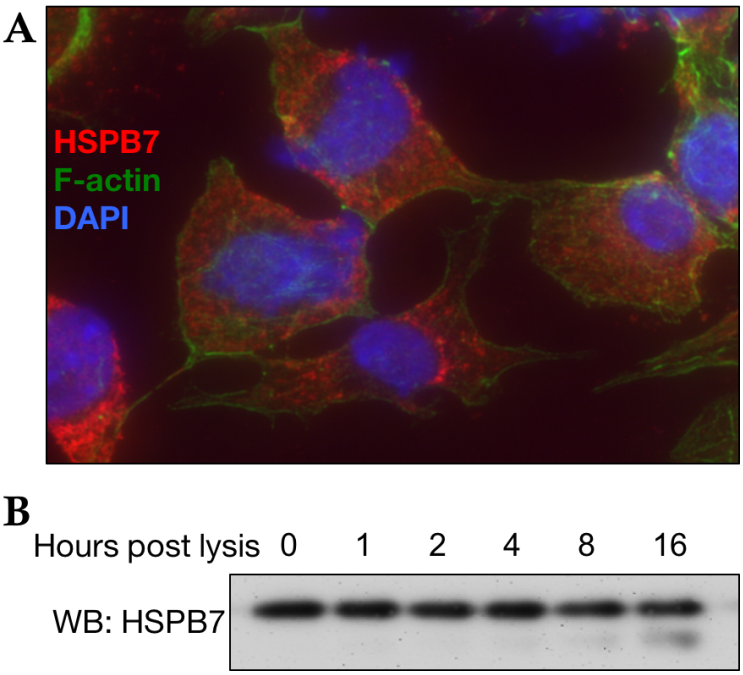

Figure 5-1: HSPB7 is expressed in HL-1 cells.
(A)Immunofluorescent staining for HSPB7 (red) shows a predominantly cytoplasmic localization. (B) Western blot for HSPB7 in HL-1 cell lysate. The protein is relatively stable at 4℃ for 16 hours post-lysis.

HSPB7 binds to large cytoskeletal proteins FLNC and TITIN

Although the cellular function of HSPB7 is unclear, it has been shown capable of preventing aggregation of certain proteins by *in vitro* assays[126,127], contingent on the presence of intact cellular autophagic machinery[127]. Seeking clues to its function, I sought to identify proteins that HSPB7 can bind in cardiomyocytes. I first ascertained that HL-1 lysates could be incubated overnight at 4°C with minimal degradation of HSPB7 (Figure 5-1B). I immunoprecipitated HSPB7 from HL-1 lysates and confirmed capture of the majority of the protein by Western blotting experiments (Figure 5-2A). In order to confirm that I could detect proteins pulled down specifically with anti-HSPB7, and not with a control IgG, I

electrophoresed the lysates following precipitation and assessed pull-down results with a silver stain of the gel (Figure 5-2B).

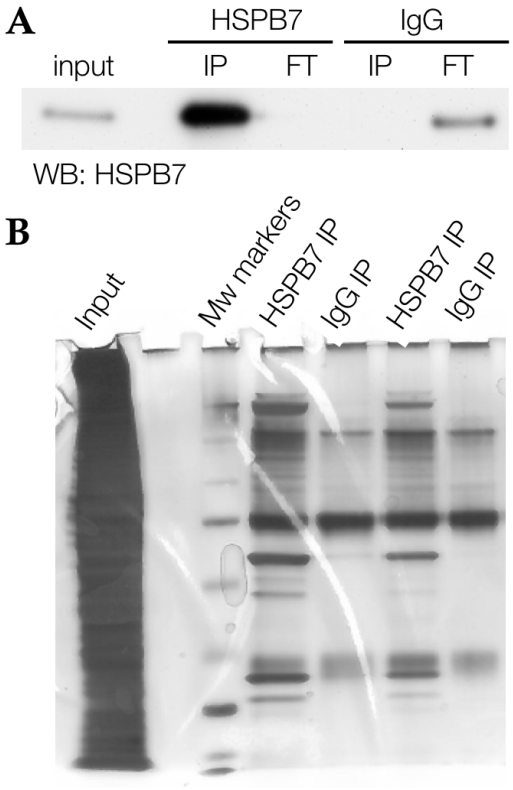

Figure 5-2: Successful immunoprecipitation of HSPB7 and associated complexes from HL-1 cells.
(A) Western blot showing specific and near-complete capture of HSPB7 protein from HL-1 lysates following overnight immunoprecipitation at 4°C. (B) Silver stain of immunoprecipitated proteins visualizes a number of protein bands that are specifically pulled down with anti-HSPB7 and not with an isotype matched control.

Protein bands that precipitated specifically with anti-HSPB7 and not with an IgG control were subjected to in-gel trypsinolysis and identified by unbiased tandem mass-spectrometry (Figure 5-3). Bands were identified using the less specific Coomassie stain, due to the unsuitability of silver-stained gels for processing for mass spectrometry. I identified the large cytoskeletal proteins Filamin and TITIN as potential HSPB7 binding partners. Although Titin is an interesting target which

has been shown to be indispensable for myofibrillogenesis and cardiomyocyte function[176,177], it is also the largest protein encoded by the genome. The enormous technical challenge of conducting biochemical experiments with a protein of this magnitude biased my decision to investigate the relationship between the Filamins and HSPB7 more closely.

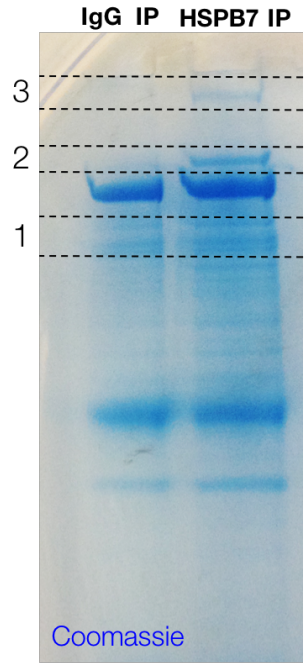

Band	HSPB7 1	HSPB7 2	HSPB7 3	IgG 1	IgG 2	IgG 3
1-acyl-sn-glycerol-3-phosphate acyltransferase GN=AGPAT1					1	
Alpha-actinin-1 GN=ACTN1	3					
Desmoplakin GN=DSP		5				
Filamin-A GN=FLNA		**8**				
Filamin-B GN=FLNB		**5**				
Filamin-C GN=FLNC		**90**				
Ig gamma-1 chain C region GN=IGHG1				1		
KN motif and ankyrin repeat domain-containing protein 2 GN=Kank2	6					
Myosin-1 GN=MYH1					3	
Myosin-13 GN=MYH13					4	
Myosin-4 GN=Myh4 PE=1 SV=1					1	
Myosin-6 GN=Myh6 PE=1 SV=2	1	3		1	15	
Myosin-XVIIIa GN=MYO18A					11	
Sorbin and SH3 domain-containing protein 2 GN=Sorbs2	1					
Spectrin beta chain, brain 4 GN=SPTBN5			1	1		5
Spectrin beta chain, brain 4 GN=SPTBN5					1	
Splicing factor, proline- and glutamine-rich GN=SFPQ	5					
Titin GN=Ttn			**86**			

Figure 5-3: Identification of binding partners of HSPB7.
Coomassie-stained gel with bands specific to immunoprecipitation of HSPB7 identified and labelled. Unbiased mass spectrometer-based peptide identification identifies Filamin-C and Titin as HSPB7 interaction partners.

HSPB7 was reported previously to bind the ubiquitous isoform Filamin A[132]. However, note that coverage for peptides from FLNC was extensive (Figure 5-3), while the few peptides mapped by mass spectrometry as coming from Filamin A or Filamin B are completely conserved in FLNC. Furthermore, I was able to confirm through western blotting experiments that HSPB7 co-immunoprecipitated with FLNC, but strikingly not the A isoform (Figure 5-4).

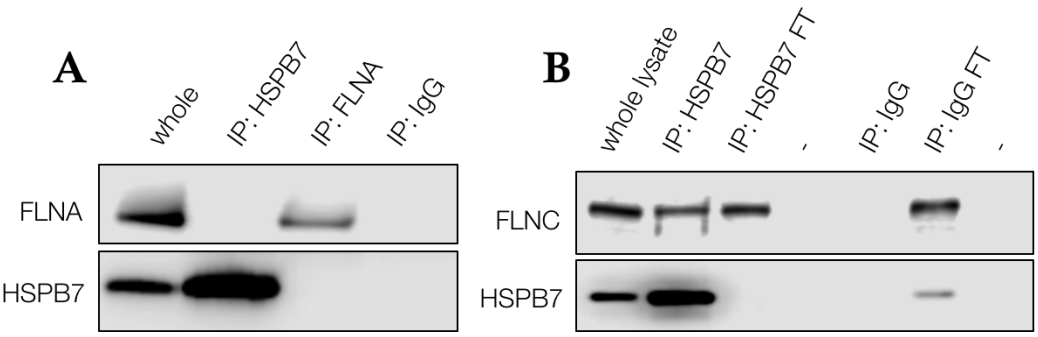

Figure 5-4: HSPB7 binds specifically to FLNC.
(A) Immunoprecipitation of HSPB7 or Filamin-A from HL-1 cells demonstrates that they do not interact. (B) Filamin-C is co-immunoprecipitated with HSPB7 from HL-1 cells.

FLNC is the muscle-specific isoform of filamin, with roles in myogenesis[178] and sarcomeric maintenance[8,35,179]. Given that HSPB7 is expressed exclusively in striated muscle and at a higher level in the heart, FLNC is an excellent candidate for a functional chaperone target, and HSPB7 may aid in either protecting FLNC and other large sarcomeric proteins from damage, or facilitating the processing of these proteins after damage has occurred. I reasoned that the cardiac phenotype I had observed in *hspb7* mutant zebrafish might potentially be caused by alterations in FLNC activity or regulation. Mutations in FLNC that affect its function or predispose it to aggregation are associated with a range of myopathies in human patients[8], including some cases that are restricted to the heart[7,180]. Interestingly, recent modelling of one of these mutations in mice revealed that the myopathy is exaggerated by acute exercise[181].

HSPB7 is not required for HL-1 cell survival but appears to sensitize the cells to stress.

In the human and mouse diseases discussed above, the filaminopathy leads to cellular phenotypes including the formation of aggregates within the cardiomyocyte and progressive degenerative myofibrillar changes. In order to

assess whether these alterations are found in HSPB7 null cardiomyocytes, I first asked whether HSPB7 is a required protein in the HL-1 cell. The data generated in the zebrafish suggested that HSPB7 is not required for cardiomyocyte survival or proliferation. I utilized siRNA to knock down HSPB7 (Figure 5-5) and did not observe alterations in cell survival (as assessed by trypan blue staining) when compared with a control siRNA.

Given both the role of HSPB7 as a chaperone protein, protecting cells from protein damage; and the requirement for external stress to precipitate a phenotype in the *hspb7* mutant zebrafish, I hypothesized that the phenotype of HSPB7 would be most apparent under conditions of stress. HL-1 cells were treated with increasing concentrations of the cardiotoxic drug doxorubicin, and their survival was assessed by trypan blue staining. Cells that had been transfected with siRNA targeted against *HSPB7* appeared to be more sensitive to doxorubicin than those that had not (Figure 5-5B). However, the percentage of surviving cells seemed to vary from treatment to treatment.

When considering the potential reasons for this heterogeneity, I considered more carefully the model system in which I was working. Whilst the HL-1 cell line is routinely used in the field, it has a number of caveats. First, the cardiomyocytes are not fully differentiated (which allows them to proliferate and be passaged), which means that sarcomeric structures are incompletely formed. Second, within a culture of HL-1 cells there is heterogeneity in cell shape, size and beating frequency.

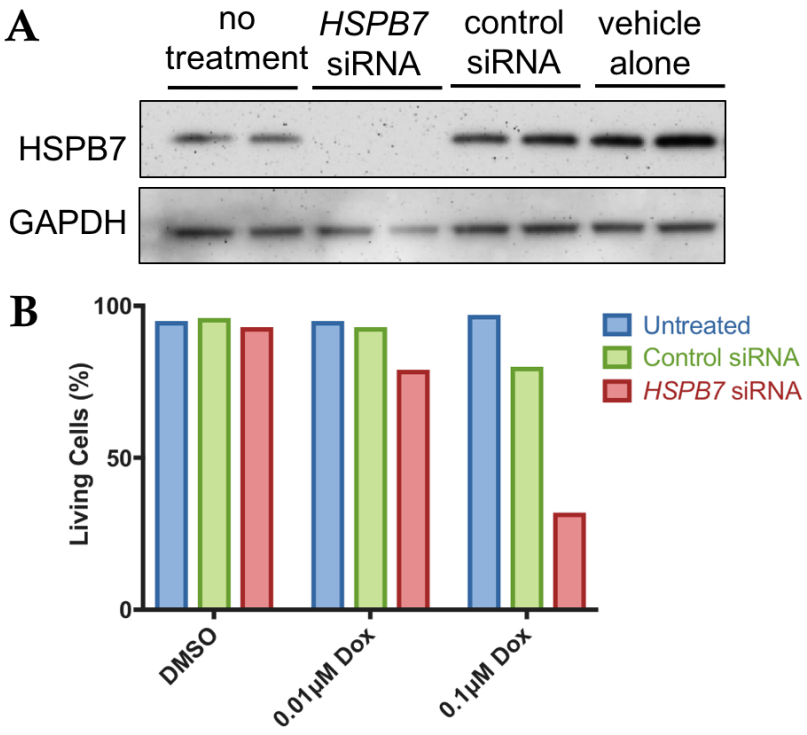

Figure 5-5: HL-1 cells survive in the absence of HSPB7 but are more sensitive to toxic insult.
(A) Western blot for HSPB7 shows loss of protein at 72 hours post transfection with specific siRNA. (B) Quantification of living cells using trypan blue, 3 days post-transfection with siRNA and following 12 hours treatment with doxorubicin hydrochloride or vehicle control.

This heterogeneity is also reflected in the transcriptome and proteome of these cells; most importantly for my purposes, only a subset of HL-1 cells were expressing HSPB7, confounding attempts to examine the effect of loss of HSPB7. A final consideration is that there are inherent differences between murine and human cardiomyocytes. For these reasons, I decided to generate a stable HSPB7 loss-of-function model in a system that better modeled cell biology of the human heart.

Generation of HSPB7$^{-/-}$ human ESC-derived CMs.

In order to test if HSPB7 function is conserved across vertebrate species, and to facilitate biochemical investigation into the molecular role of HSPB7 in a human cardiomyocyte, I used the inducible CRISPR/Cas9 system[145] to target mutations to the *HSPB7* locus in human embryonic stem cells (hESCs). I recovered clonal lines in which *HSPB7* was predicted to be homozygous null (Figure 5-6A). I also identified lines that had proceeded 'unsuccessfully' through CRISPR targeting, retaining wildtype *HSPB7,* and used these as control "wildtype" lines.

HSPB7 is not expressed in ESCs, and both wildtype and *HSPB7*$^{-/-}$ clones maintained normal ESC morphology, expressing comparable levels of pluripotency genes, including *SOX2*, *NANOG* and *KLF4* (Figure 5-6B).

I used a directed differentiation protocol (modified from Lian *et al* (2012)[149]) to generate beating cardiomyocytes from the hESC lines and was able to confirm through flow cytometry (Figure 5-6C,D) and IF (Figure 5-6E) successful generation of cardiomyocytes in numbers comparable in both wildtype and mutant *HSPB7* lines. IF in hESC-CMs also confirmed that HSPB7 protein is absent from the mutant cells (Figure 5-6E). *HSPB7* mutant cardiomyocytes were competent to differentiate to cardiac fate and observed to form beating sheets.

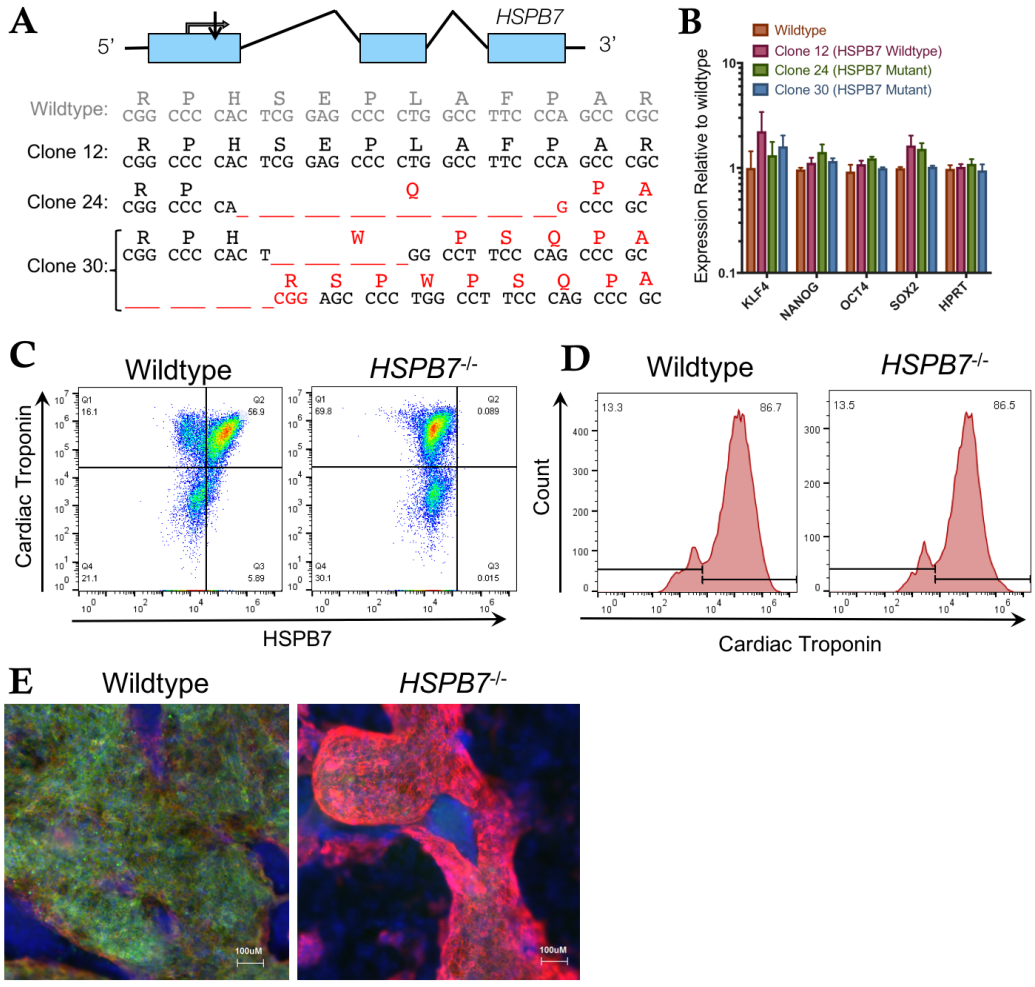

Figure 5-6: Generation of* HSPB7 *mutant hESC and hESC-derived cardiomyocytes.

(A) Structure and partial sequence of the human HSPB7 gene, showing CRISPR targeting immediately downstream of the start codon and resultant HSPB7 homozygous and compound heterozygous mutant clones that were recovered. (B) qPCR quantification of expression levels of pluripotency markers are normal in HSPB7 mutant hESC clones. HSPB7 mutant lines are competent to generate cardiomyocytes, and do not have HSPB7 protein as shown by flow cytometry (C,D) and immunofluorescence (E), both performed on day 10 of differentiation. (F) qPCR qunatification of cardiac HSPB family members in hESC-CMs.

This was not unexpected given that *hspb7* mutant zebrafish have functional hearts, and that knockdown of *HSPB7* in HL-1 cells did not lead to cardiomyocyte deterioration. Taken together, these findings lead to the conclusion that HSPB7 is not required for successful cardiomyocyte specification or basic cardiomyocyte function. However, if HSPB7 functions as a sarcomeric cytoskeletal chaperone protein, we considered that the differentiated mutant cells might display protein aggregation phenotypes.

FLNC aggregates in *HSPB7* mutant cardiomyocytes

To compare levels of aggregate formation, the filter trap assay was employed (Vos et al., 2010). Cardiomyocytes derived from *HSPB7* mutant hESC lines showed an increase in FLNC aggregates when compared with cardiomyocytes derived from wildtype control lines (Figure 5-7A,B). I also observed an increase in puncta when staining for FLNC by immunofluorescence.

These findings demonstrate abnormalities in human cardiomyocytes lacking HSPB7. However, the lack of overt pathology suggests that in human cardiomyocytes, as in zebrafish, the cell is able to tolerate the detrimental effect that absence of HSPB7 has on cardiomyocyte function, perhaps by upregulating pathways that remove aggregated proteins.

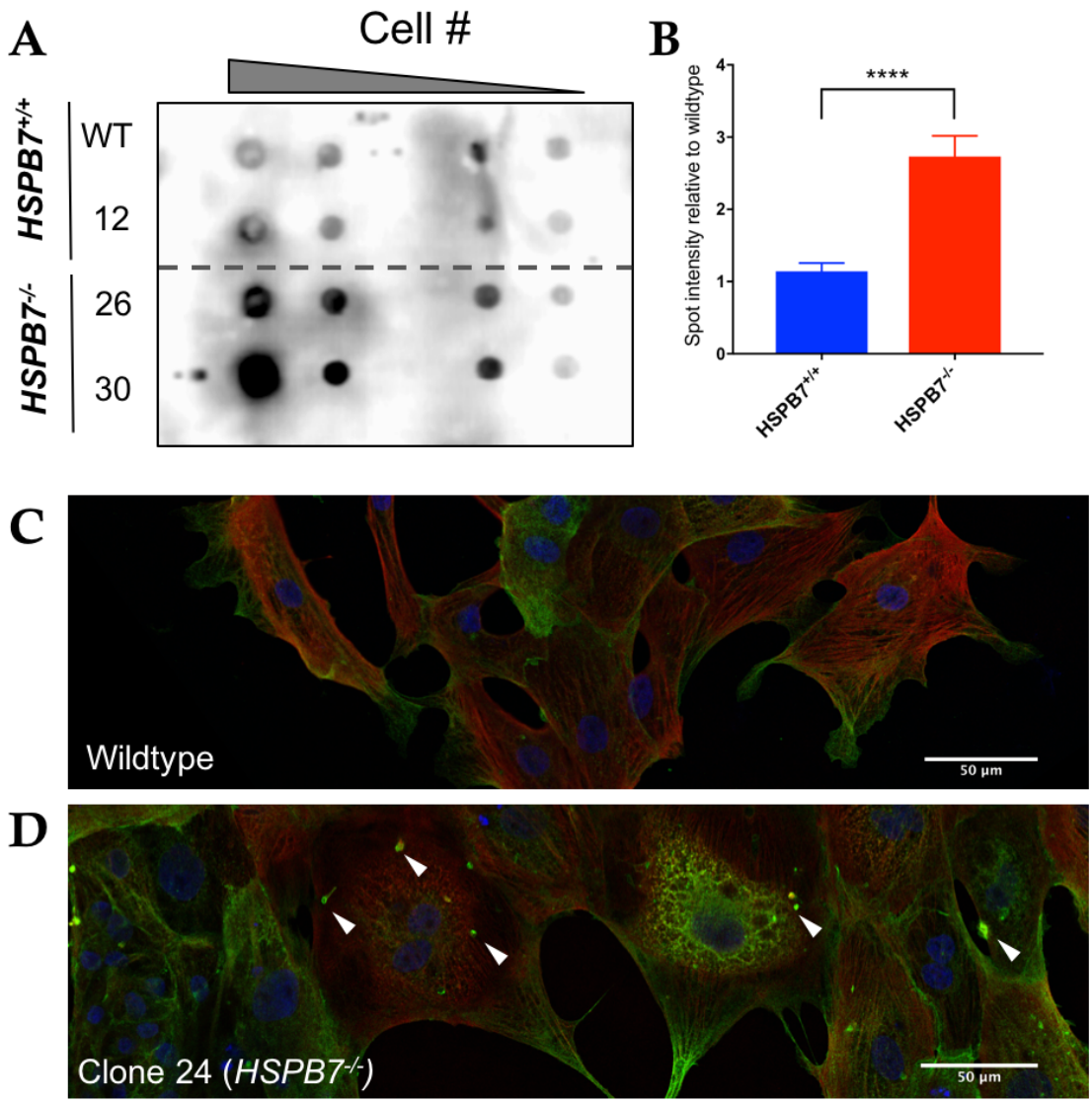

Figure 5-7: Increase in FLNC aggregation in* HSPB7*mutant hESC-CMs.
(A) Filter trap assay probing for Filamin C in lysates from day 10 hESC-CMs shows increase in FLNC-containing aggregates in HPSB7$^{-/-}$ cardiomyocytes when compared to wildtype. Representative image. (B) Quantification of filter trap assays. ***n=5.*** *Immunofluorescence for cardiac troponin (red) and FLNC (green) in hESC-CMs derived from HSPB7 wildtype (C) or HSPB7 (D) mutant lines. White arrowheads mark puncta.*

Autophagy is enhanced in *HSPB7* mutant cardiomyocytes

Some members of the sHSP family are known to be involved in protein degradation pathways, including specific types of chaperone-assisted autophagy[46]. HSPB7 has been linked to the autophagic process, because the ability of HSPB7 to prevent aggregation of poly-glutamate proteins was attenuated in the absence of the key autophagic protein Atg5[127]. Damaged FLNC has been recently shown to be degraded in a rat aortic cell line through the process of Chaperone Assisted Selective Autophagy (CASA), in which a CASA protein complex facilitates transport of the damaged protein to the autophagosome[46]. Given these links, we hypothesized that to compensate for loss of HSPB7, mutant cardiomyocytes might enhance autophagic processes to facilitate removal of damaged proteins. This was tested by measuring autophagy levels through visualization of the autophagy marker LC3. I stained differentiated wildtype and *HSPB7* mutant hESC-derived cardiomyocytes for LC3 (Figure 5-8A,B) and quantified the number and size of LC3 positive puncta as described[153]. I observed an increase in the number and size of puncta in *HSPB7* mutant cardiomyocytes when compared with control lines (Figure 5-8C), demonstrating an upregulation of autophagy in the absence of *HSPB7.*

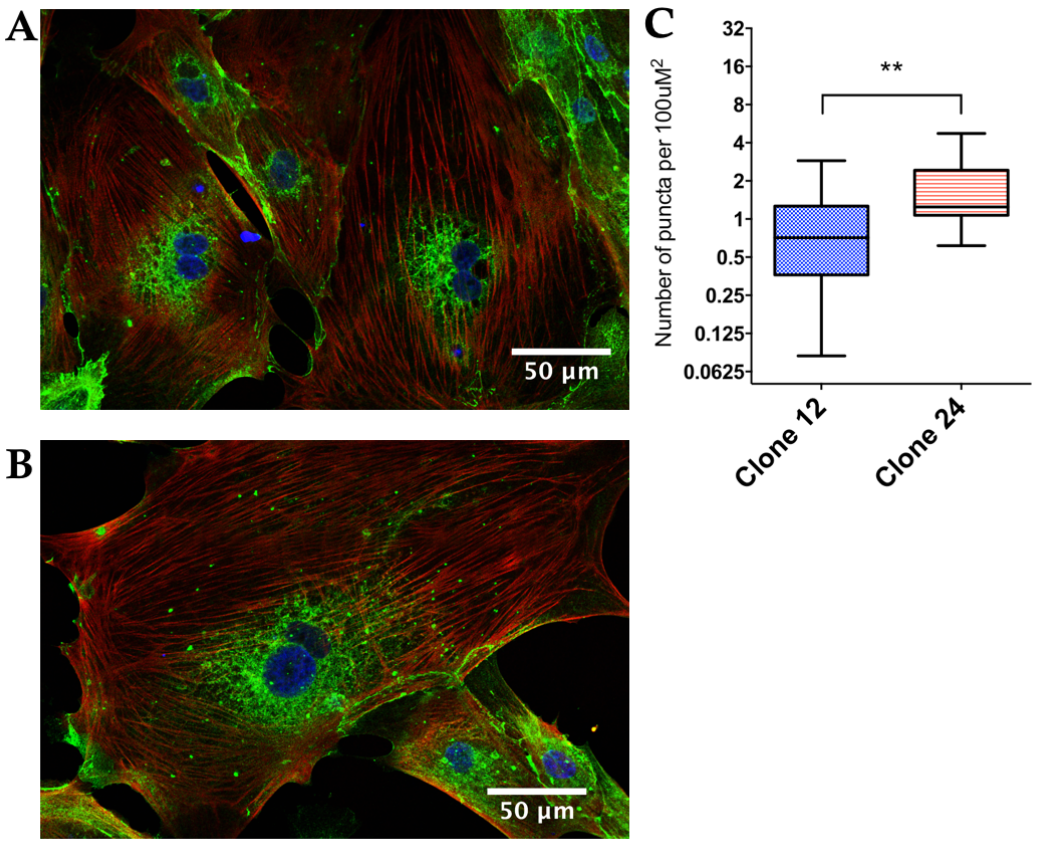

Figure 5-8: Upregulation of autophagic processes in HSPB7 null cardiomyocytes.
Representative images of immunofluorescence for LC3B (green) in wildtype (A) or HSPB7 mutant (B) hESC-CMs. Co-stained with anti-cardiac troponin T (red) and counterstained with DAPI (blue). (C) Quantification of LC3B puncta in hESC-CMs shows an increase in average puncta number in HSPB7 mutant cardiomyocytes.

Overall LC3B levels were seen to be slightly increased over wildtype by western blot in both *HSPB7* mutant hESC-CM and adult *hspb7*$^{WC3/WC3}$ zebrafish hearts (Figure 5-9). Increased LC3B protein level is not directly correlated with increased autophagy. However, in conjunction with the observation of increased LC3B puncta, this is strong evidence that the autophagic program is activated in *HSPB7* null cardiomyocytes.

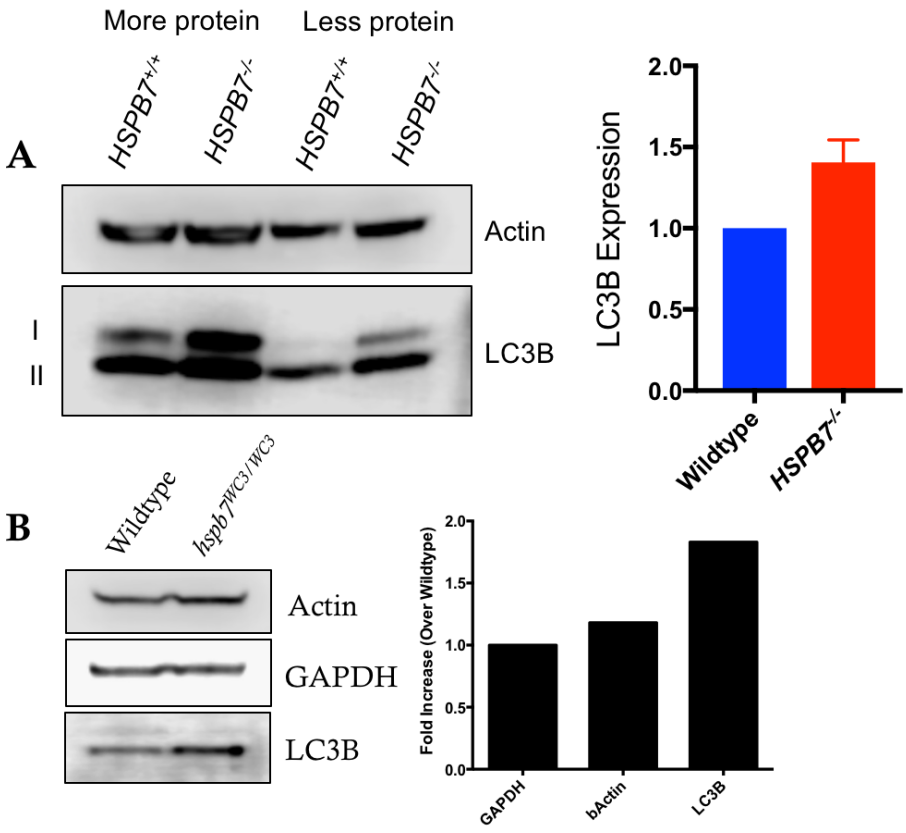

Figure 5-9: Autophagy marker LC3B is increased in* HSPB7 *mutant cardiomyocytes.
Western blot for LC3B in lysates from hESC-CM (A) or adult zebrafish heart (B). Quantification by densitometry (right) indicates a slight increase in LC3B in cells or hearts that are lacking HSPB7.

Upregulation of *FLNC* expression in *HSPB7* mutant cardiomyocytes.

A separate arm of the CASA process also leads to upregulation of expression of degraded proteins[46]. This is especially important in muscles for maintaining the stoichiometry of the sarcomere. Following on from our discoveries that FLNC is prone to aggregation in *HSPB7* null cardiomyocytes (Figure 5-7), and a concomitant upregulation in autophagy (Figure 5-8, Figure 5-9), we hypothesized that the CASA process is activated in these cells. I performed qPCR analysis and

discovered that expression of *FLNC* is upregulated in *HSBP7* null hESC-CMs (Figure 5-10).

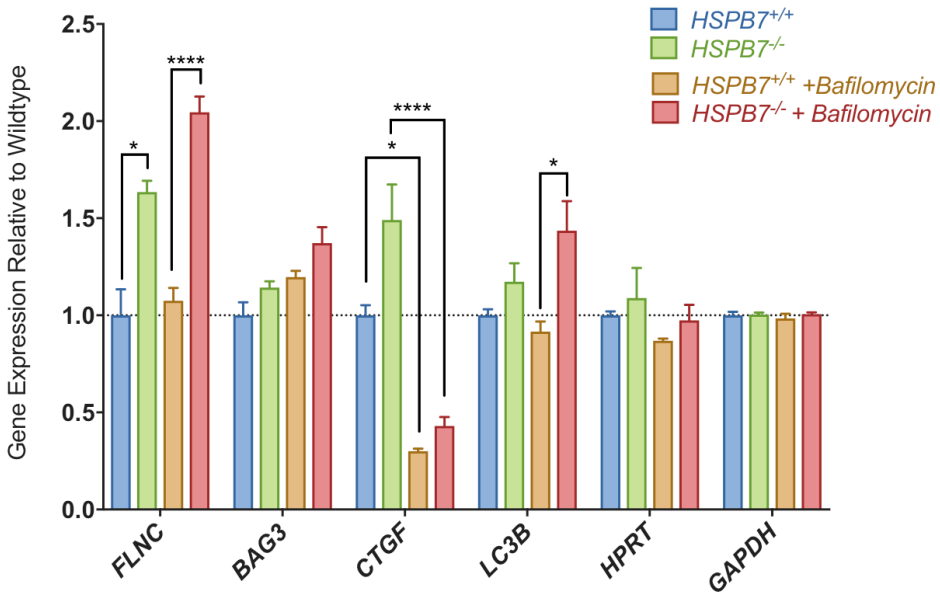

Figure 5-10:* FLNC *expression is upregulated in* HSPB7 *mutant hESC-CMs. *qPCR analysis of gene expression in hESC-CMs on day 15 of differentiation shows upregulation of* FLNC *expression in* HSBP7 *mutant cardiomyocytes. Data is pooled for Wildtype and Clone 12 (*HSPB7$^{+/+}$*) and Clone 26 and 30 (*HSPB7$^{-/-}$*).*

Homozygous *hspb7* mutant zebrafish embryos exhibit increased sensitivity to autophagy inhibition

The increase in autophagy measured in *HSPB7* mutant human cardiomyocytes indicates a requirement for activation of this pathway in order to maintain normal cardiac function. This could be one of the mechanisms by which zebrafish embryos compensate for the loss of Hspb7 during cardiogenesis. In this case, *hspb7* mutants are predicted to be hyper-sensitive to the loss of autophagy. To test this prediction, we exposed wildtype or *hspb7* mutant zebrafish embryos to a small molecular inhibitor of the pathway, Bafilomycin A1 (BafA). BafA prevents the fusion of autophagosomes with lysosomes, inhibiting the last step of autophagy. BafA treatment led to a dose-dependent increase in the incidence of cardiomyopathy in

both *hspb7*^{WC3} and *hspb7*^{WC4} homozygous mutants, but not in wildtype controls (Figure 5-11).

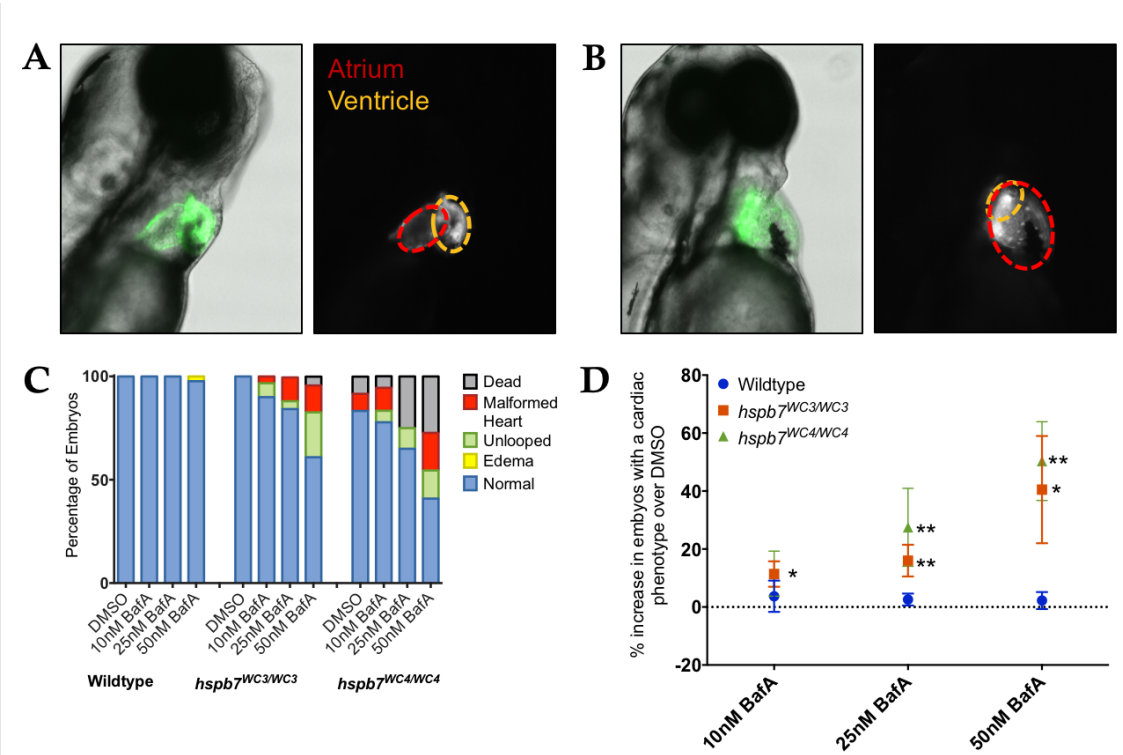

Figure 5-11: Inhibition of autophagy leads to cardiac malformation in* hspb7 *mutant zebrafish embryos.
Representative images of 72hpf, Bafilomycin A-treated wildtype (A) or hspb7$^{WC3.WC3}$ *(B) embryos which have been crossed onto a tg(myl7:gfp) background showing a cardiac malformation with expansion of the atrium and an undersized ventricle in the hspb7*$^{WC3/WC3}$ *fish. (C) Quantification of the percentage of embryos with cardiac abnormalities at 48hpf following 24 hours of treatment with increasing concentrations of Bafilomycin A. n=40 for each treatment group. (D) hspb7 mutant embryos consistently exhibit significant increases in cardiac abnormalities following treatment iwth Bafilomycin.*

We also exposed control or *hspb7* mutant embryos to chloroquine diphosphate (CQ) or 3-methyladenine (3-MA), autophagy inhibitors with different mechanisms of action. Similar to BafA, both CQ and 3-MA led to increases in cardiac defects in *hspb7* mutant embryos but not in wildtype controls. This confirms that normal cardiogenesis in *hspb7* mutant embryos is reliant on autophagy.

Discussion

To understand the role of HSPB7 in the cardiomyocyte, I used a range of model systems to best answer a number of specific questions.

I discovered that in cardiomyocytes FLNC is an endogenous binding partner of HSPB7 and that FLNC aggregates form in the absence of HSPB7. FLNC is a large sarcomeric protein that interacts with both Z-disc components and sarcolemma-associated proteins, leading to speculation that it may act as both an assembly point for myofibrils in early myogenesis[178,182] and as a mediator of signal transduction from the sarcolemma to the sarcomere[8,35], facilitating myofibril maintenance. Loss of FLNC is associated with defects in myogenesis[178], and human mutations are associated with a range of skeletal and cardiac myopathies[7,8,180,183], many of which are associated with the formation of pathological aggregates containing FLNC. I observed aggregates in cardiomyocytes lacking HSPB7, indicating that loss of HSPB7 may affect the stability or processing of FLNC. My data indicate that HSPB7 also binds to at least one other large sarcomeric protein, TITIN. Further studies are needed to determine if HSPB7 is a dedicated chaperone for these two, or if this role is generalized to many large sarcomeric proteins. My results are consistent with a recent report that HSPB7 can bind FLNC in skeletal muscle[136]. Knockout of *HSPB7* in skeletal muscle caused lethal progressive myopathy, found to be most severe in the diaphragm[136]. Contrary to this report, I did not observe hallmarks of progressive myopathy in the skeletal muscle of *hspb7* mutant zebrafish, but it is interesting to note that the diaphragm is the one muscle that, like the heart, must move continuously in order to maintain life. Either this function is not conserved in zebrafish (which of course lack a diaphragm), or loss

of Hspb7 is better compensated in the skeletal muscle of zebrafish compared with mouse.

I hypothesized that HSPB7 may bind to proteins that need to be processed by autophagy, since this function has been demonstrated for family member HSPB8[46], expressed more generally in all striated muscle. I found that autophagic processes are enhanced in HSPB7-depleted cardiomyocytes and that impairing autophagy during embryogenesis causes lethal cardiomyopathy in developing *hspb7* mutant embryos. Recent studies have suggested that damaged FLNC is among the proteins degraded by autophagy, a catabolic cellular process for the breakdown and recycling of extraneous or defective proteins and complexes[46]. The role of autophagy in the heart is known to be relatively complex. Key autophagic proteins are required for normal cardiac development[184], and autophagic turnover is known to occur in the healthy heart[185]. Increases in autophagy are seen in situations of cardiac stress, presumably in response to an increase in damaged and dysfunctional proteins downstream of mechanical or oxidative stressors. However, either too little or too much autophagy is pathological under conditions of cardiac stress[54,58,186], indicating that the process must be carefully balanced. A model consistent with my data is that the absence of HSPB7 leads to an increase in damage or unfolding of FLNC, resulting in compensatory activation of autophagic pathways to prevent aggregate formation.

A recent study also described a potential role for FLNC in the fast repair of myofibrillar microdamage[35], indicating a potential role as a signaling hub for the efficient reassembly of sarcomeric structures. Given this finding, a decrease in the availability of functional FLNC caused by mutation of *hspb7* could have effects on the ability of the myocyte to repair damage at multiple steps. The importance of

FLNC for both muscle function and repair could explain the increase in fibrosis and mortality observed in *hspb7* mutant zebrafish. I expect that FLNC depletion amplifies the effects of high intensity exercise to a pathological level, leaving cardiomyocytes with a burden of unstable sarcomeric lesions that results in death in a subset of mutant animals.

Conclusions

My study provides novel insight into how HSPB7 regulates proteostatic mechanisms that function in a cardiomyocyte, and a new model for human stress-dependent cardiomyopathy. Future studies need to investigate the relationship between HSPB7 and the delivery of FLNC to autophagic organelles. Given the complex role of autophagy in the sarcomere, direct therapeutic manipulation is likely to be inherently risky. However, by manipulating specific components like HSPB7 that have a regulatory role, redirection or optimization of autophagic processes might be achieved that will be clinically beneficial for patients with disorders of aggregation.

CHAPTER 6: GENERATION AND CHARACTERIZATION OF ZEBRAFISH WITH MUTATIONS IN *GATA4* AND *GATA6*

Introduction

The GATA transcription factors are a family of zinc finger transcription factors that regulate transcriptional programs in a number of developing organs. Our laboratory was interested in further investigating the roles of Gata4, Gata5, and Gata6 in the developing zebrafish. Previous work by both our own laboratory[82,154], and others[187], has utilized the morpholino system to knockdown *gata* family members in the developing zebrafish. Briefly, these studies identified roles for *gata4, -5 and -6* in the mesendoderm and mesendoderm-derived organs, which aligns with the roles of the murine and human homologues. Interestingly, studies in multiple systems have indicated redundancy between the GATA factors[92,108,109,116]. I set out to make use of novel genome editing technologies to generate zebrafish lines in which different combinations of *gata4, -5 and -6* had been mutated, allowing us to further investigate these redundancies. In addition, these lines will give us more information about the specific roles of each GATA protein at various points in development, and could reveal any previously-recorded phenotypes that were due to off-target effects of morpholinos, or are caused by acute knockdown but not genetic lesion.

Generation of *gata4* mutant fish

The DNA binding domain of the GATA factor proteins is composed of a highly conserved motif in which a series of cysteine residues coordinate a zinc ion, stabilizing the protein structure. Previous work from our laboratory has

demonstrated that mutation of a single C-X-X-C motif in the zinc finger closest to the C-terminal of a GATA protein leads to a complete loss of DNA binding activity[71], a phenomenon also seen in other zinc fingers[188]. Thus, I injected mRNA encoding TALENs targeted to the DNA encoding this same amino acid in zebrafish *gata4,* reasoning that even a small mutation would lead to complete loss of protein function (Figure 6-1A). Following breeding of founder zebrafish, I recovered a range of mutant *gata4* alleles predicted to interfere with protein function (Figure 6-1B). Moving forward, I chose to focus on an allele that encoded a premature stop codon, truncating *gata4* before the second zinc finger; and on a mutation that specifically deletes the C-X-X-C motif and two adjacent amino acids. These alleles will be referred to as *gata4^{WC6} and gata4^{WC5}.*

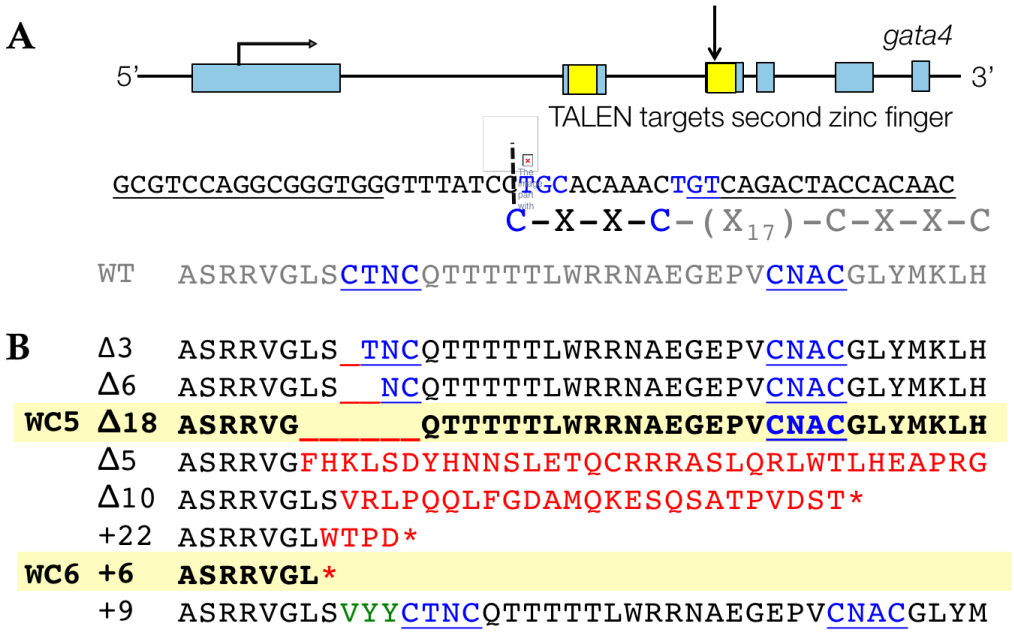

***Figure 6-1: TALEN-mediated generation of mutations in* gata4.**
(A) Structure and partial sequence of zebrafish gata4*. (B) Predicted protein sequences of recovered* Gata4 *mutants. Alleles WC5 and WC6 are of particular interest for further studies and are highlighted in bold.*

In the absence of the creation or loss of a unique restriction enzyme recognition sequence, I designed a PCR genotyping strategy for the *gata* alleles, which is detailed in Chapter 2 of this thesis.

Gata4 homozygous mutants develop normally but are recovered in lower than expected numbers.

To my surprise, unlike the *gata4* morphants, or previously detailed mutations in murine or human *GATA4,* zebrafish were able to tolerate homozygous mutation in *gata4.* Homozygous mutant animals were identified in clutches of embryos from heterozygous crosses and were viable to adulthood and fertile. Maternal-zygotic homozygous (MZ) mutant animals carrying either of the two *gata4* alleles developed normally and resembled wildtype embryos (Figure 6-2).

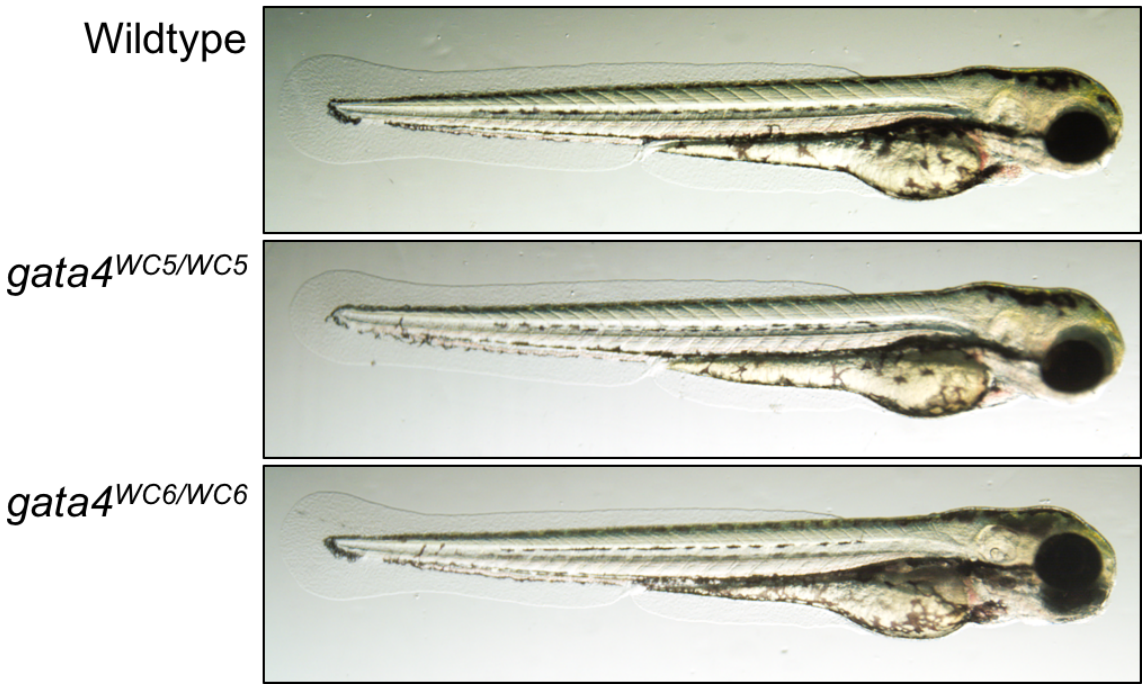

Figure 6-2:* Gata4 *mutant zebrafish have normal phenotypes during embryogenesis.
Brightfield images of wildtype and gata4 *mutant embryos at 3dpf.*

Despite a normal body plan and no gross developmental defects, I observed that 24hpf *gata4* mutants consistently appeared several hours less developed than wildtype embryos of the same age. I closely tracked the development of clutches of *gata4* mutant embryos and identified a very specific delay in their development which commenced at sphere stage (4hpf)[****] (Figure 6-3A).

The time taken for *gata4* mutants to achieve dome stage (4.33hpf) was significantly longer than that taken for wildtype embryos (Figure 6-3B). The delay increased from around 1 hour at dome stage to around 2 hours at shield stage (6hpf). Following shield stage, *gata4* mutants resumed normal rates of development, so that the 2-hour delay was retained at Prim 5 (24hpf). This suggests that specific processes occurring between sphere and shield stage are compromised by the lack of Gata4.

[****] Stages of zebrafish embryo development were named and given 'normal' timepoints as previously described[10].

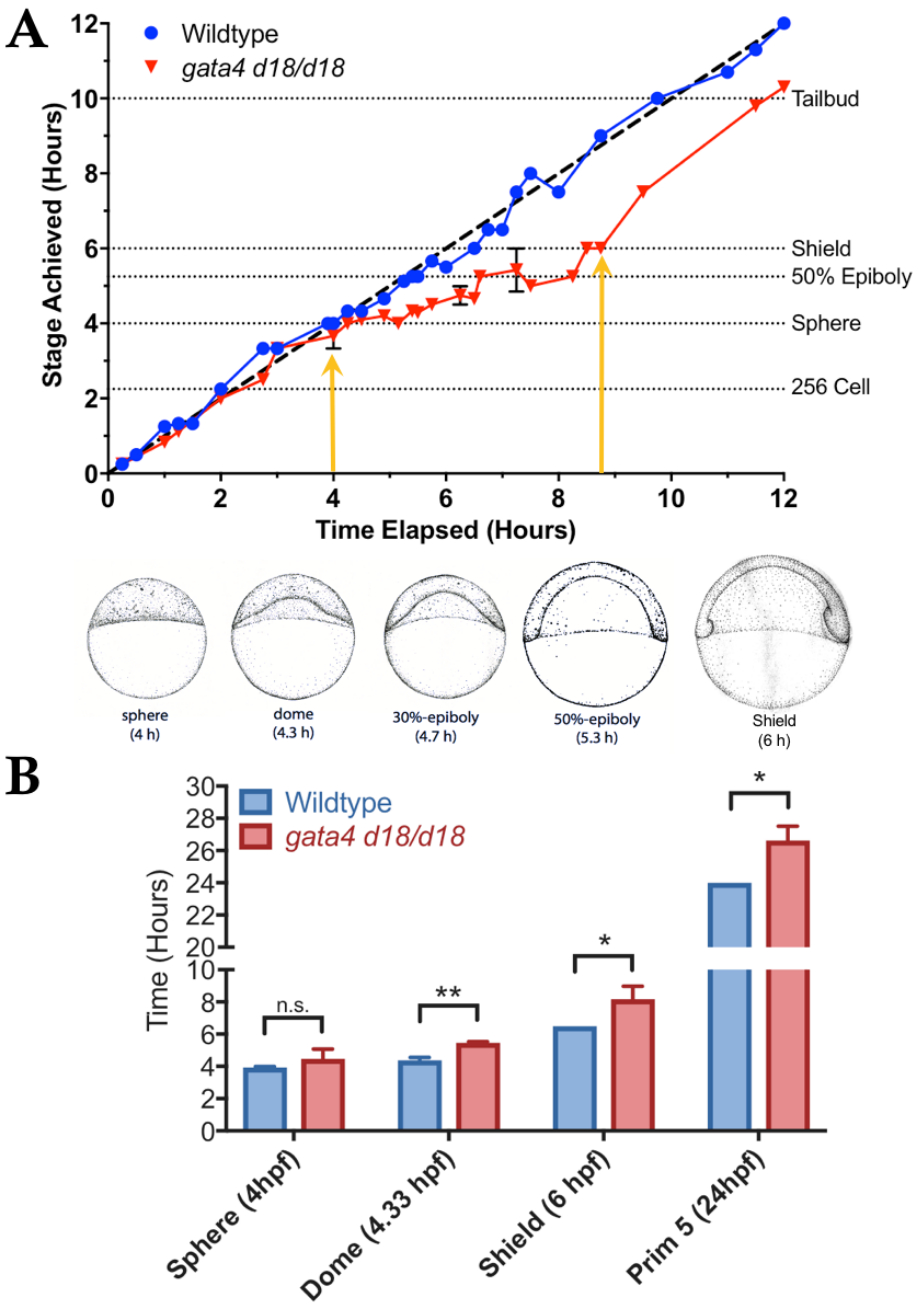

Figure 6-3: **Gata4** ***mutant embryos are developmentally delayed during early gastrulation.***

(A) Visualization of the time taken for batches of wildtype and gata4 *mutant embryos to achieve each developmental stage. Points are mean time ± S.D. Yellow arrows demarcate boundaries of delayed period. Sketch illustrations adapted from Kimmel* et al. (1995)[10]. *(B) Quantification of time taken to reach specific stages of development highlights significant delay in* gata4 *mutant embryos. (n=3 batches).*

Gata4 mutants are specifically delayed in early embryogenesis

The delay observed during gastrulation of the *gata4* mutants suggests that *gata4* is required during early embryogenesis in zebrafish. I wanted to discover whether loss of *gata4* may also lead to other earlier or later defects in some percentage of homozygous mutants. To identify broad periods of development in which *gata4* homozygous mutants might be lost, I genotyped the offspring from heterozygous crosses at 3dpf, and in adulthood. No abnormal embryo death was observed before 3dpf. I discovered that *gata4* homozygotes are not recovered at expected frequencies (Figure 6-4).

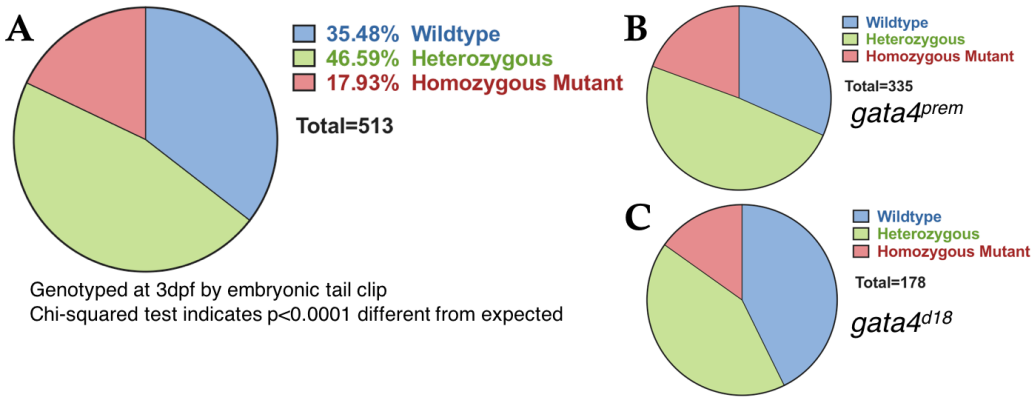

Figure 6-4: Homozygous* gata4 *mutants are not recovered in expected ratios. *(A) Quantification of genotypes of embryos from crosses of adults heterozygous for any* gata4 *mutation. Lower than expected recovery of homozygous* gata4 *mutants is observed regardless of where the* gata4^{WC6} (B) *or* gata4^{WC5} (C) *allele is considered.*

At 3dpf, we recovered 17.93% homozygous mutants, significantly different from the expected 25% (n=500, p<0.0001). Recovery of homozygous mutant genotypes fell further to 11.5% in adult animals (n=52, p<0.05), demonstrating an additional loss of *gata4* mutant animals after 3dpf.

These results suggest both an earlier and a later effect of *gata4* mutation than the developmental delay detailed above.

Overexpression of *gata6* in *gata4* mutant embryos

The overall normal development of *gata4* mutant embryos was unexpected, and I hypothesized that other *gata* factors may be compensating for the loss of *gata4.* As discussed above, this phenomenon has been previously observed, although never before to the extent of complete rescue. I extracted RNA from zebrafish embryos at timepoints during the first 3 days of development and quantified gene expression by qPCR. I observed upregulation of *gata6* in *gata4* null animals.

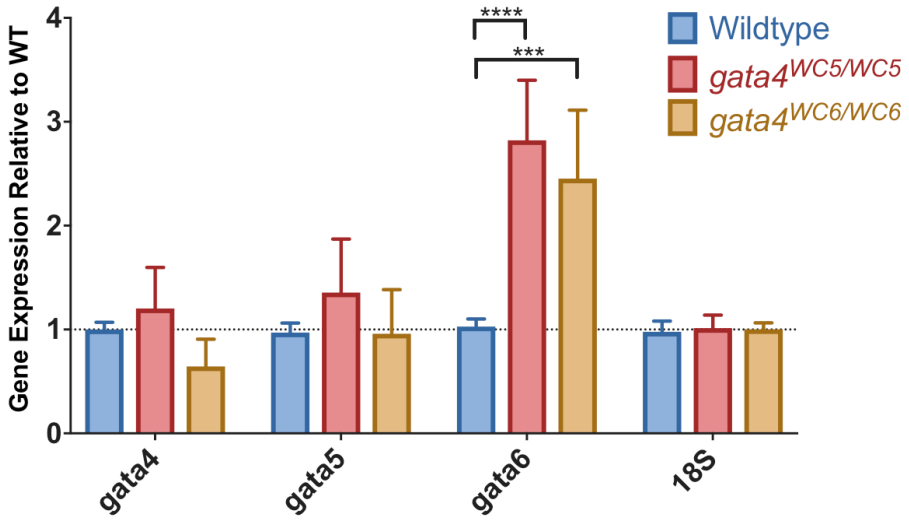

Figure 6-5:* gata6 *expression is upregulated in* gata4 *homozygous mutant embryos at 50% epiboly.
Quantification of expression of a subset of gata *factors in wildtype and* gata4 *mutant embryos at 50% epiboly by qPCR.*

Generation of *gata6* mutants

In order to study the role of *gata6* in the developing zebrafish embryo, we utilized the same strategy that we had applied for *gata4*. TALENs were designed to target the second zinc finger (Figure 6-6A) and I recovered animals harboring a *gata6* allele with a 14 base pair deletion leading to a frame shift (*gata6*^{WC7}), leading to loss of the second zinc finger and the C-terminal of the protein (Figure 6-6B). The same allele was recovered from multiple F0 injected animals and is likely the product of microhomology-mediated repair around the TALEN site.

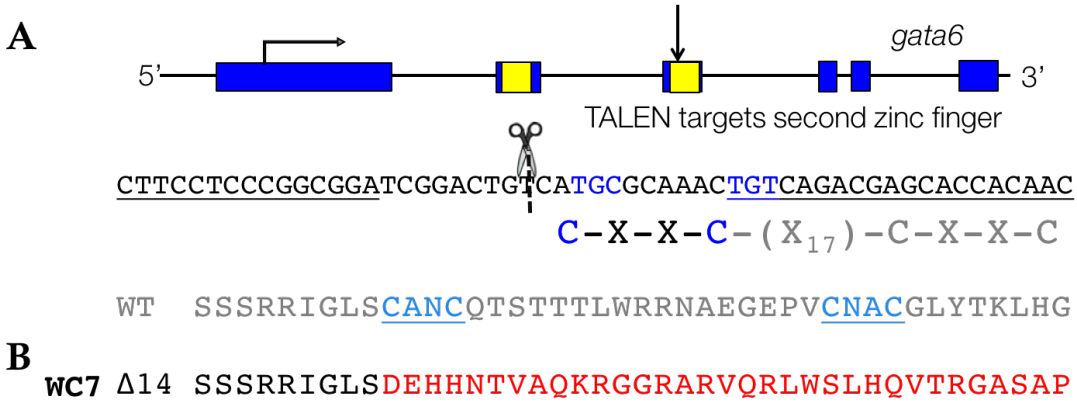

Figure 6-6: TALEN-mediated generation of a* gata6 *mutant allele.
(A) Structure and partial sequence of the zebrafish gata6 *gene. (B) Predicted protein sequence of a recovered* gata6 *allele.*

Abnormal development in *gata6* mutant zebrafish

Unlike *gata4* mutants, *gata6* mutants were recovered at much closer to expected ratios at 3dpf (Figure 6-7C), however they also presented with severe defects. Phenotyping of clutches of embryos from *gata6* heterozygous crosses revealed ~20% of embryos with abnormal phenotypes at 3dpf. By light microscopy we observed severe defects in cardiomorphogenesis with concomitant cardiac edema, yolk sac edema and an abnormally thin tail (Figure 6-7B,C).

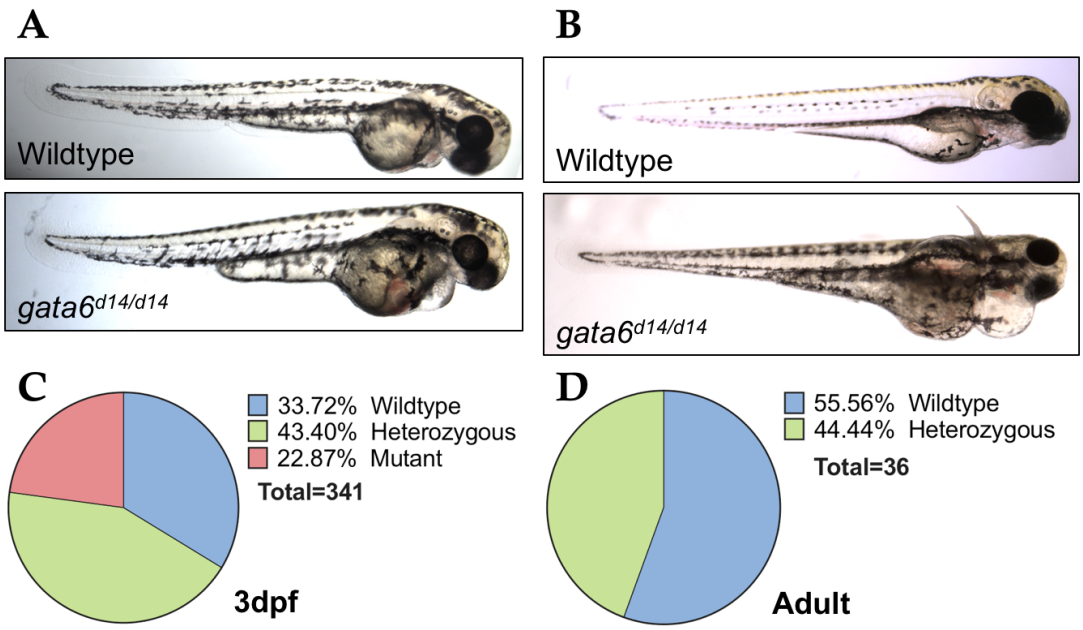

Figure 6-7:* Gata6 *mutation leads to lethal abnormalities.
Gata6$^{WC7/WC7}$ *embryos display developmental abnormalities by (A) 48hpf, which become more severe by (B) 72hpf. Representative images. Quantification of* gata6 *genotype in embryos from adults carrying heterozygous* gata6^{WC7} *alleles at (C) 3dpf and (D) 3 months.*

Genotyping of embryos revealed that 100% of embryos (8/8) presenting with this phenotype were homozygous for the *gata6*^{WC7} allele. However, around 25% of *gata6* homozygous mutants (3/11) appeared grossly normal. When adult animals from a heterozygous cross were genotyped, I did not recover any homozygous *gata6* mutants (Figure 6-7D), indicating that even those that appear normal at 3dpf subsequently perish. In addition, I recovered significantly less heterozygotes in the surviving animals than predicted by Mendelian genetics (44.4% instead of 66.7%, $p<0.01$). This suggests that haploinsufficiency for *gata6* is sufficient to lead to a failure to thrive phenotype.

Generation and phenotyping of *gata4/gata6* compound mutants

Given the normal phenotypes seen in around a quarter of *gata6* mutants and in almost all *gata4* homozygous mutants, and following leads from published literature, I hypothesized that these two transcription factors are compensating for each other. In order to investigate further their interactions, I bred *gata4* and *gata6* heterozygous animals and recovered compound heterozygous fish, which were predominantly phenotypically normal (Figure 6-8A), viable to adulthood, and fertile.

I phenotyped clutches of embryos from crosses of adult compound heterozygotes and observed striking phenotypes by 3dpf. Some embryos presented with exclusively cardiac malformation and edema, similar to the *gata6*$^{WC7/WC7}$ phenotype (Figure 6-7A,B), whereas others had a combination of abnormalities including cardiac malformation, edema, thin tails with somite abnormalities and craniofacial abnormalities (Figure 6-8A). I also observed compromised blood flow in some embryos, but this appears to be due to cardiac dysfunction rather than defects in blood or vascular development (data not shown). Finally, I noted that there appear to be abnormalities in the shape and positioning of melanocytes in many of these embryos, but this phenotype was not explored further at this time.

Genotyping of phenotyped embryos revealed that the abnormalities we observed were predominantly present in embryos with homozygous mutation of *gata6* (Figure 6-8B). However, as I observed previously, some animals carrying mutations only on both *gata6* alleles appeared normal. The percentage of 'normal'-looking *gata6* mutants decreased with concomitant loss of *gata4* alleles and 0% (7/7) of embryos carrying mutations on all 4 *gata* alleles presented with a normal

phenotype at 3dpf. This strengthens our hypothesis that *gata4* is able to compensate for *gata6* during early development in a relatively small percentage of zebrafish.

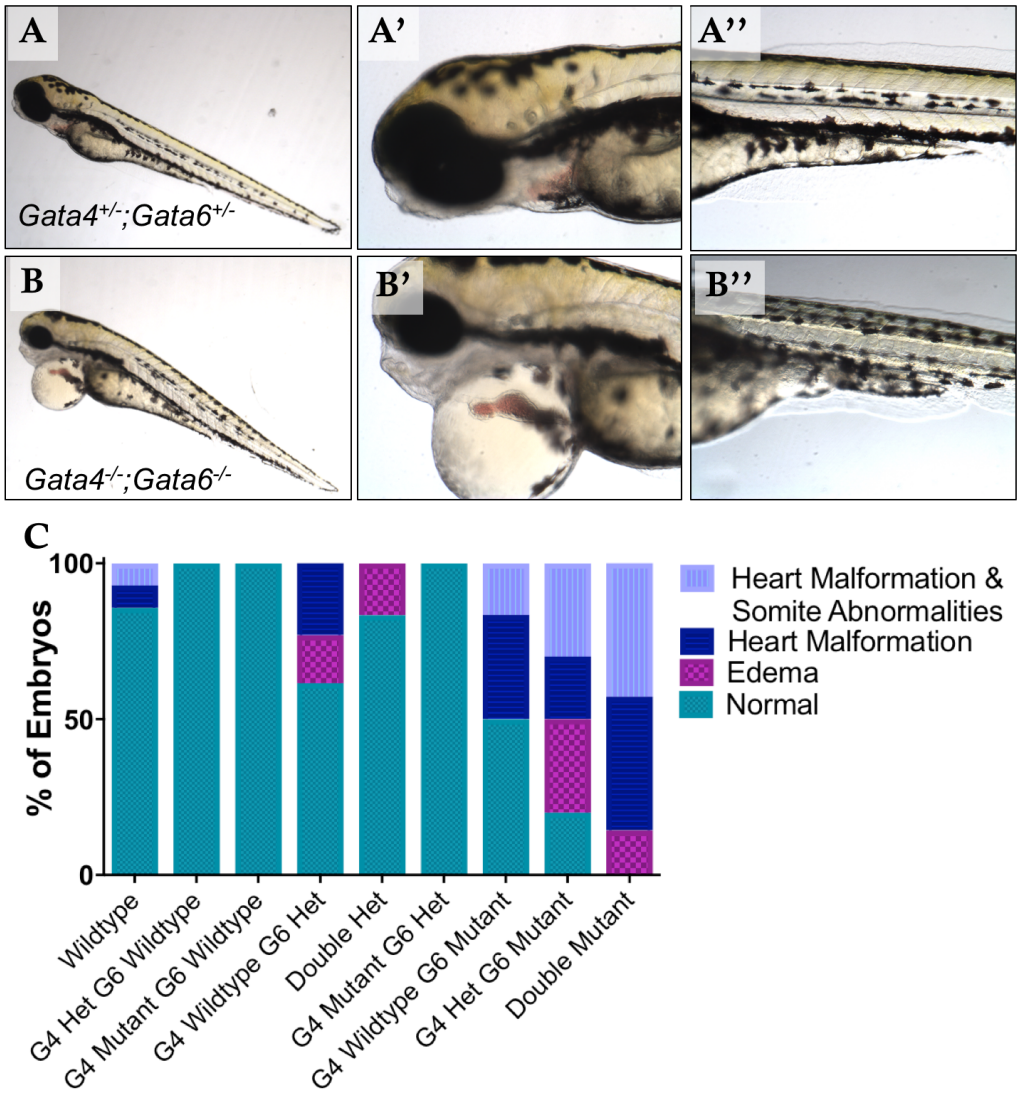

Figure 6-8: Progressive loss of* gata *factors leads to increasingly severe developmental abnormalities.
Brightfield phenotypes of embryos from a cross of gata4$^{WC5/+}$;gata6$^{WC7/+}$ *adults show (A) normal development of compound heterozygous embryos but (B') craniofacial and cardiac abnormalities and (B'') tail defects in embryos lacking both* gata4 *and* gata6*. Representative images. (C) Genotyping of embryos after phenotyping with light microscopy reveals that major defects are predominantly associated with homozygous* gata6 *mutation. Overall n=105.*

Defects in cardiac chamber specification and cardiac morphogenesis in *gata6* mutant embryos.

In order to better characterize the abnormal cardiac morphology seen in *gata6* mutant embryos, I performed wholemount in situ hybridization (WISH) to document the expression patters of chamber-specific cardiac markers. As seen by brightfield microscopy, I observed linear heart tubes in the majority of *gata6* mutant embryos with ISH for atrial marker *amhc* (Figure 6-9).

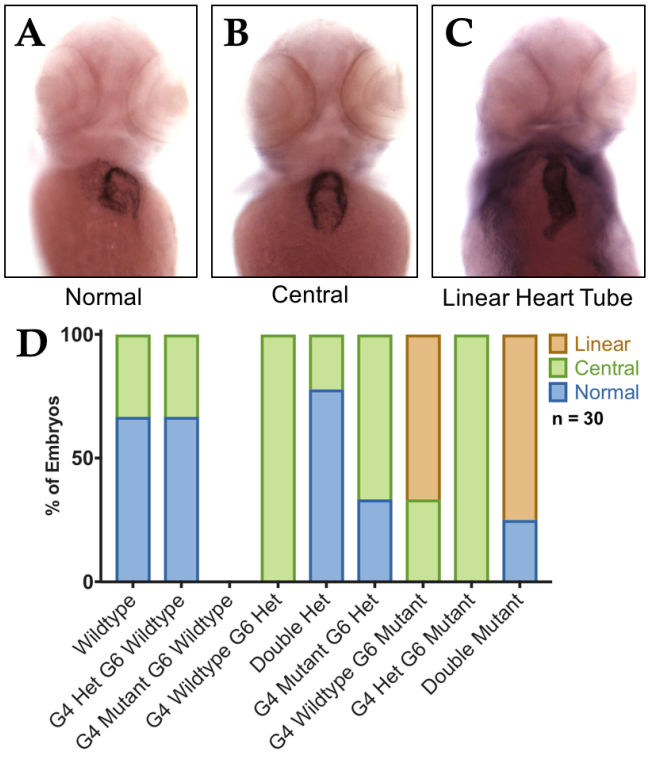

Figure 6-9:* Gata6 *mutant embryos have abnormally shaped hearts with ectopic* amhc *expression.
Amhc *staining patterns observed in 3dpf embryos from cross of* gata4$^{WC5/+}$;gata6$^{WC7/+}$ *adults show a range from (A) normal* amhc *expression through (B) D-looped hearts and (C) unlooped chambers to (D) linear heart tubes. Representative images. (E) Quantification of genotypes after assessment of* amhc *expression pattern indicates that abnormalities are predominantly associated with homozygous* gata6 *mutation.*

Interestingly, in most *gata4;gata6* homozygous mutants, *amhc* is highly expressed throughout the bulk of the length of the linearized tube. In contrast, when I performed WISH for *vmhc,* I observed a major reduction in staining in *gata6* mutant embryos (Figure 6-10).

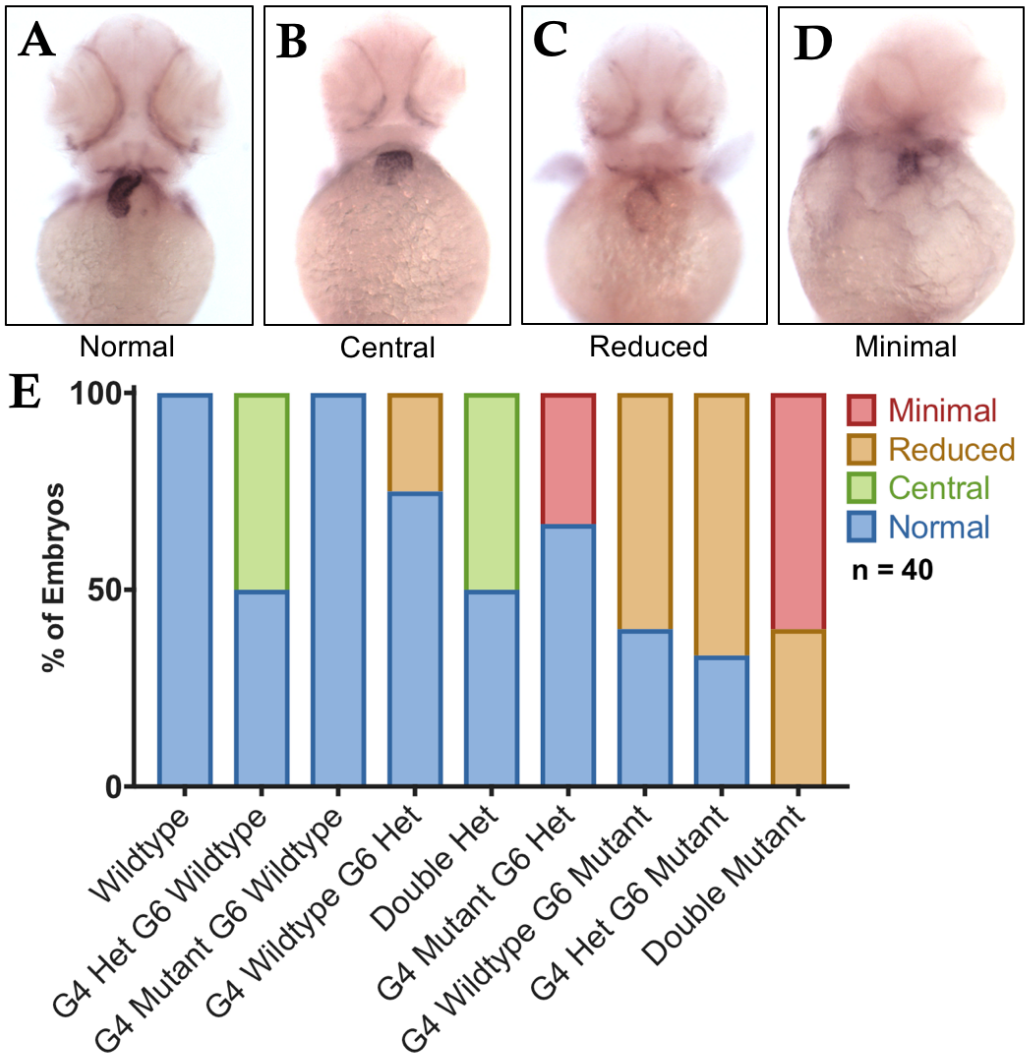

Figure 6-10: Decrease in* vmhc *expression in* gata6 *mutant embryos.
Vmhc staining patterns observed in 3dpf embryos from cross of gata4$^{WC6/+}$;gata6$^{WC7/+}$ adults show a range. Representative images of (A) normal staining, (B) central ventricle, (C) reduced staining, and (D) minimal staining. (E) Quantification of genotypes after assessment of vmhc *expression pattern indicates that decreases in* vmhc *expression are predominantly associated with homozygous* gata6 *mutation.* n=40

In combination, these observations suggest that that the ventricle either fails to properly specify or that ventricular progenitors fail to expand in *gata6* mutant embryos.

Loss of liver and pancreas in gata6 mutants

In addition to the easily observable defects in development in our compound mutants, we hypothesized that other organ systems may be compromised, and that these defects may explain the delayed demise of those mutant embryos that presented with a normal phenotype at the 3dpf time point.

GATA4 and *GATA6* are known to play roles in the development of the murine and human liver and pancreas[83,107,111,189]. In mice, the two transcription factors appear to be redundant for early specification of hepatic and pancreatic progenitors, and for pancreatic development[189], but have unique later roles in hepatic outgrowth[104,112]. We wanted to discover whether these organs develop normally in *gata* mutant zebrafish. Clutches of embryos from a compound heterozygous incross were fixed at 3dpf and we performed a triple WISH stain for markers of the liver (*lfabp*), pancreas (*insulin)* and thyroid (*tg)* and observed a range of abnormalities in triple WISH staining pattern (Figure 6-11). In some embryos, staining for the liver and pancreas was either completely misplaced into a 'speckled' pattern, or entirely absent (Figure 6-11D,E).

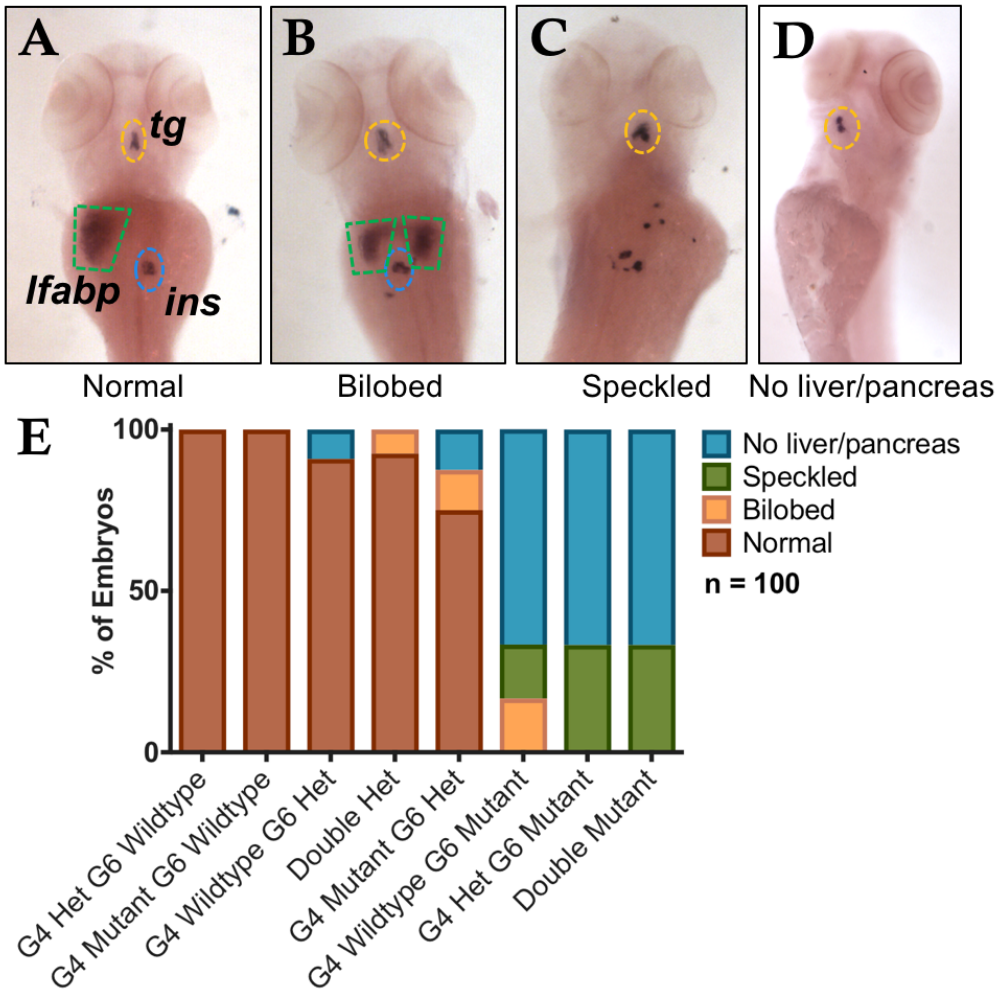

Figure 6-11: Hepatic and pancreatic agenesis in* gata4;gata6 *double homozygous mutants.

(A-E) Range of staining patterns observed with probes for tg *(yellow dashes),* lfabp *(green dashes) and* ins *(blue dashes) in 3dpf embryos from cross of* gata4$^{WC5/+}$;gata6$^{WC7/+}$ *adults. Representative images. (F) Quantification of genotypes after assessment of WISH phenotype reveals that loss of hepatic and pancreatic markers is associated with homozygous mutation of* gata6..

Randomization of asymmetry with decrease in wildtype *gata* alleles.

In addition to the abnormalities discussed above, I observed a consistent inversion of organ placement in a subset of embryos from the *gata4*$^{+/-}$;*gata6*$^{+/-}$ cross. This phenotype was consistent across all markers studied (A-D).

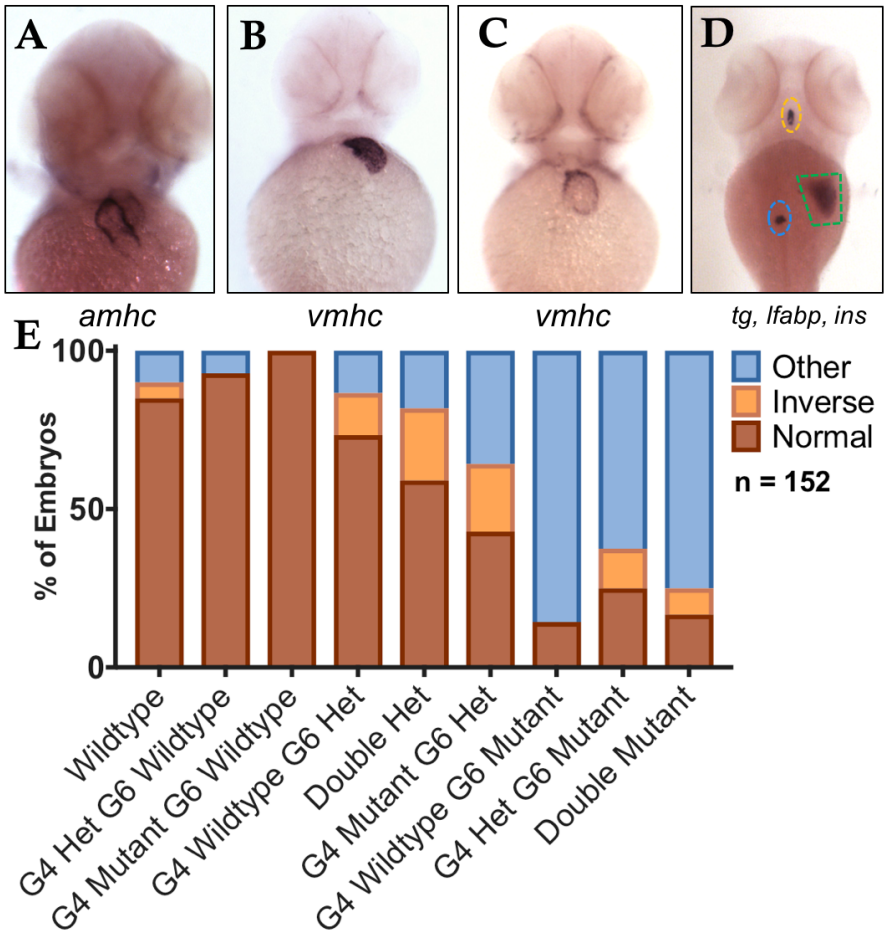

Figure 6-12: Inversion of organ location with loss of wildtype* gata *alleles.
Inverted staining patterns observed in (A) amhc, (B,C) vmhc and (D) triple WISH performed in 3dpf embryos from cross of gata4$^{WC5/+}$;gata6$^{WC7/+}$ *adults. Representative images. (E) Quantification of inversion phenotypes according to genotype. Genotyping was performed after phenotyping. 'Normal' refers to organ layout irrespective of intensity or shape of staining. 'Other' phenotypes include staining patterns for which the organ location was entirely abnormal or absent. For control WISH images see Figures 6-9, 6-10 and 6-11.*

For *amhc* (A) or *vmhc* (B,C) staining, the heart was normally shaped but a mirror image of the normal conformation. In some embryos, *vmhc* staining revealed both inversion and reduced signal (C). Inverted organs appeared predominantly in *gata6*$^{+/-}$ embryos, but with increasing numbers with progressive decrease in wildtype *gata4*, suggesting that overall *gata* load plays a role in randomization of left-right asymmetry. The more severe phenotypes in *gata6* homozygous mutants preclude observation of inversion with organ-specific markers and were designated 'other'.

Discussion and Future Directions

The zebrafish is able to tolerate mutation of *gata4.*

The relatively normal development of zebrafish homozygous for mutation in *gata4* (Figure 6-2) was an unexpected finding of this work, given the lethality of *GATA4* mutation in other species[83,86,112], and the severe defects identified in previous knockdown studies in zebrafish[82]. There are a number of possible explanations for this discrepancy. The first, and we believe most likely, hypothesis, is that the zebrafish is particularly well able to compensate for loss of *gata4* by upregulation of the alternative transcription factor *gata6.* Our initial analysis does indicate that *gata6* is upregulated in *gata4* mutants (Figure 6-5), and an observation of partial functional redundancy of the two proteins in the mouse has been observed in previous studies[108,111,112].

Complete rescue of *gata4* mutation by upregulation of *gata6* in most animals seems to be unique to the zebrafish system, despite comparable identity levels between the two proteins in different species††††. Reports of compensatory

†††† Zebrafish Gata4 and Gata6 have 33.7% identity compared with 33.6% identity for mouse.

pathways allowing zebrafish to tolerate mutant alleles are growing in the literature[190], making it tempting to hypothesize that the zebrafish is especially robust amongst the model systems used in the laboratory at recognizing and ameliorating the effects of genetic lesions.

Decreased recovery of *gata4* homozygous mutants may stem from alterations in germ cells.

The finding of normal development in *gata4* mutants is tempered by the observation that at 3dpf they are recovered at quantities around 25% lower than Mendelian genetics would predict (Figure 6-4). We did not observe lethal defects in embryogenesis between the 4-cell stage‡‡‡‡ and the 3dpf time point at genotypes were determined. Therefore, loss of *gata4* mutant alleles must occur either at the level of gamete generation or during initial cleavage. The former explanation is a tempting hypothesis, given reports of a role for *GATA4* in the testis[191,192]. We observe a slight decrease in recovery of heterozygous *gata4* mutants at 3dpf§§§§, strengthening this conjecture. Further careful genetic studies of pools of genotypes recovered from male and female heterozygote animals may be able to confirm which, if either, pool of gametes is affected.

Evidence for a larval or juvenile lethality in some *gata4* mutants.

There was also a 40% loss of homozygous mutants between 3dpf and 3 months post fertilization. We did not observe death of *gata4* mutants before day 10 of development, and hypothesize that loss of *gata4* may lead to minor defects in

‡‡‡‡ Clutches were sorted at the 4-cell stage to remove any unfertilized eggs from further observation.

§§§§ Given normal gameto- and embryogenesis, one would anticipate a 2:1 recovery of het:wildtype genotypes regardless of ratios of mutant genotypes. Applying this assumption, heterozygous embryos are recovered at around 15% lower than expected rates at 3dpf (46.6% instead of 54.6%, Figure 6-4).

overall growth or feeding behavior that disadvantage homozygous mutants when in competition with wildtype or heterozygous mutant siblings. This hypothesis is supported by preliminary observations of normal growth and survival of MZ *gata4* mutants raised separately from wildtype juveniles. We note that a similar failure-to-thrive phenotype may explain the low recovery of *gata6*$^{WC7/+}$ adults (Figure 6-7).

Potential alternative explanations are that mutant alleles, haploinsufficiency or even a dominant-negative mutant protein lead to later defects that present problems during larval or juvenile stages. Careful monitoring of growth and mortality rates of isolated mutants compared with wildtype siblings should be able to rule out these possibilities. As a final consideration, *gata4* is known to play a role in gut epithelium[76,156], which raises the possibility that any observed growth defects might be secondary to abnormalities in nutrient absorption.

Developmental delay in *gata4* mutants is suggestive of *gata4* target pathways.

Our ability to identify a finite period of delay in *gata4* mutant gastrulation is a testament to the particular benefits of the zebrafish model system, in which, unlike in mice, we are able to observe this process. It also gives us some clues to key processes that are particularly sensitive to loss of *gata4.* The affected period between sphere and shield stage (Figure 6-3) is a time associated with a complex rearrangement of the developing germ layers, requiring coordination of signaling cues and cytoskeletal rearrangements in the participating cells. The phenotype of developmental delay with ultimate recovery has been observed in previous studies, specifically in *claudine* morphants[193] and *eomesodermina*[194] mutants. The claudins are a family of junctional proteins that Gata4 has been shown to regulate

in the gut, suggesting that cell:cell junctions may be compromised during early epiboly in *gata4* mutant embryos. Eomesodermin is a transcription factor that is known to coordinate with Gata4 to regulate gene expression, leading us to hypothesize that alteration in regulation or cooperation with Eomes[*****] in developing *gata4* mutants may contribute to epiboly delay. These connections give us some interesting and likely avenues for further research. Preliminary experiments suggest that the expression levels of ClaudinE and Eomesa are altered in *gata4* mutants during early gastrulation (Figure 6-13) indicating that dysregulation of these pathways is likely responsibly for the observed epiboly delay (Figure 6-3).

Follow up experiments will confirm the finding of alteration in *claudine* and *eomesa* expression. Since Claudine is a junctional protein, experiments would ideally also determine whether its localization is altered. Elucidation of the alterations to these genes and the pathways by which they control epiboly will outline the role of Gata4 in gastrulation. Given a conserved requirement for Gata4 in early mammalian development[74,84] (a timepoint that this technically near-impossible to access), the zebrafish *gata4* mutant model provides an excellent model system in which to explore this role.

[*****] The zebrafish has two *eomes* genes (a and b). *Eomesa* has a role in the initiation and progression of epiboly, and is expressed from sphere stage onwards[200]. *Eomesb* is less well studied, although qPCR analysis suggests that it is also expressed during gastrulation.

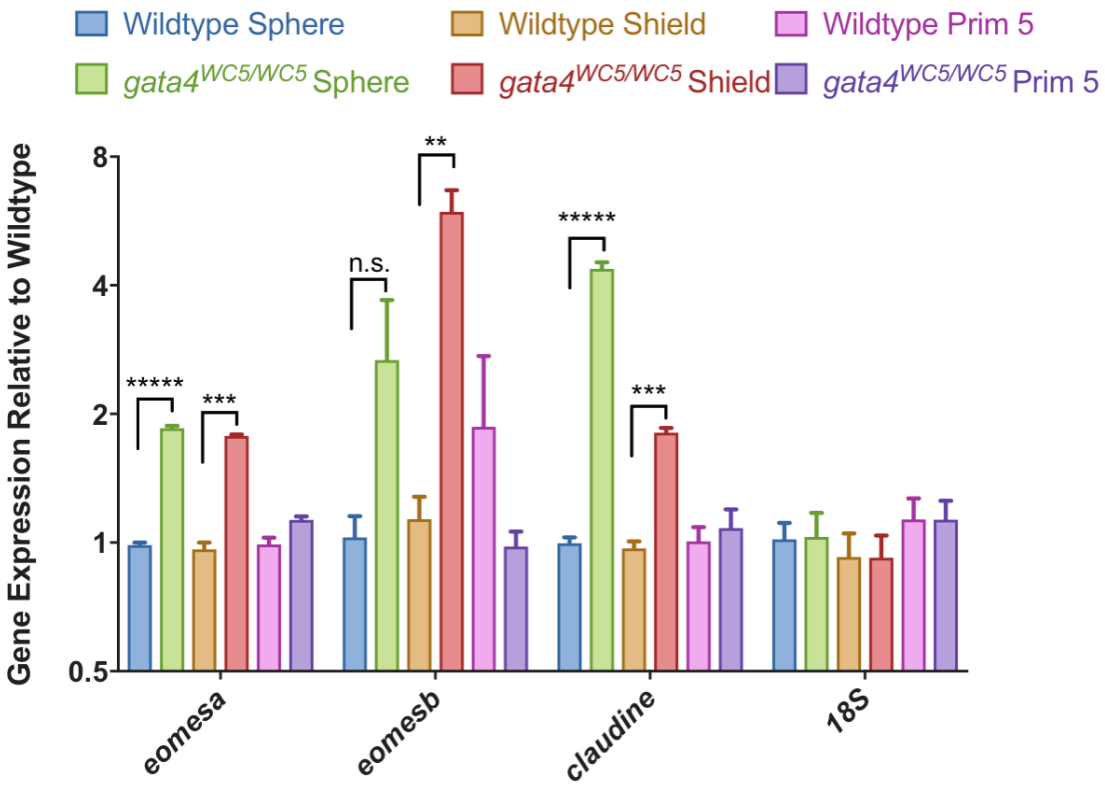

Figure 6-13: Dysregulation of* eomesa *and* claudine *expression in* gata4 *mutants.
qPCR analysis of wildtype or gata4 *homozygous mutant embryos at timepoints ranging from sphere to 24hpf (Prim 5). During gastrulation there is upregulation of* eomesodermin *genes and* cluadine *in* gata4 *mutant embryos.*

Regulation of ventricular identity by *gata6*.

An exciting, novel observation from my WISH studies is a decrease in *vmhc* expression in *gata6* mutant embryos (Figure 6-10). This suggests that loss of *gata6* compromises the identity of the ventricular cardiomyocyte and reveals Gata6 as a potential regulator of ventricular cardiomyocyte development. The expression of genes specific for ventricular versus atrial cardiomyocytes is known to be regulated by other cardiac transcription factors, including Tbx5[195] and the Nkx family[22], however the roles of GATA factors in this specification process is not known. However, in agreement with my finding in the zebrafish, work from our

laboratory suggests that *GATA6* overexpression may drive ventricular identity in hESC-CMs (Tang and Evans, Unpublished).

I did not note a concomitant decrease in *amhc* expression in normally-shaped *gata6* homozygous mutant hearts (Figure 6-9A). There are a couple of potential explanations for this discrepancy. First, there is a low level of *amhc* expression in the ventricle even in wildtype animals, which may obscure the observation of minor upregulation by WISH. Second, it may be that the cardiomyocytes in the ventricular portion of *gata6* homozygous mutant hearts are expressing neither *vmhc* nor *amhc.*

However, I did observe expansion of *amhc* expression across the whole of the linear heart tubes found in *gata4;gata6* double homozygous mutant embryos (Figure 6-9C). This mirrors the large reduction in *vmhc* staining observed in linear heart tubes in embryos of the same genotype, suggesting that in the absence of *gata4* and *gata6*, the heart is both misshapen and has expanded atrial identity. Moving forward, it will be important to confirm that the loss of *vmhc* and expansion of *amhc* are occurring in the same hearts through double WISH. Following this, the identity of the myocytes in both chambers needs to be better confirmed. This can be achieved through assessing the expression of alternate chamber markers such as *myosin binding protein 1 Hb* (atrium) and *actin, alpha 1a* (ventricle)[24]. Atrial and ventricular cardiomyocytes also have unique electrophysiology, which could be assessed by patch clamp.

Randomization of asymmetry in embryos with loss of multiple *gata* alleles.

An additional novel observation from these studies is the inversion of organ location that arises predominantly in *gata6*$^{+/-}$ embryos (Figure 6-12). The consistency of this phenotype across multiple organs (heart, liver, pancreas)

indicates an early disturbance in normal patterning. Interestingly, there are rare case studies in the literature in which mutation of *GATA4* leads to dextrocardia[196], suggesting that this role is conserved. To confirm the hypothesis that early patterning is disturbed, WISH for early markers of left-right asymmetry (*lefty1/2, spaw*) should be performed. In addition, the development and function of the Kupffer's vesicle (analogous to the mammanlian node), which establishes left-right patterning, can be analyzed.

The phenotype of inversion is seen increasingly with progressive loss of *gata4* in a *gata6* heterozygous background, suggesting that the two transcription factors may be able to compensate for each other in this pathway. It is less clear whether homozygous mutation of *gata6* also leads to alterations in early patterning due to the severe defects in organ development. However, the experiments suggested above are likely to clarify this point.

An intriguing hypothesis here is that the more severe defects in *gata6* mutants may also be due to the loss of patterning cues, which subsequently lead to failure in tissue-specific progenitors to migrate or differentiate appropriately. In the long term, tissue-specific and temporally controlled depletion of *gata6* and/or *gata4* in the instructional layers of the developing embryo, or within defined progenitor populations, might answer this question.

Incomplete penetration of *gata6* mutant phenotype indicates partial redundancy with *gata4*.

Despite the predominance of a severely abnormal phenotype in most *gata6*$^{WC7/WC7}$ embryos, around 30% of homozygous mutants appear normal at 3dpf. When we consider specific organ systems by WISH (Figure 6-9, Figure 6-10, Figure 6-11) we also observe normal expression of tissue markers. Interestingly, the percentage of

'normal' *gata6* mutants at 3dpf decreases progressively with additional loss of wildtype *gata4* alleles. This suggests that *gata4* is able to compensate for *gata6* in some embryos, although the rescue is clearly unable to sustain *gata6* mutants through the larval and juvenile stages.

A question that arises from the observations and hypotheses discussed above is why there might be an asymmetric relationship between *gata4* and *gata6*, in which the latter is able to compensate for the former, but not *vice versa.* One possibility is that the third transcription factor, *gata5,* is also playing an important compensatory role in *gata4* mutants, and that *gata4* and *gata6* thus have only partially overlapping roles. Although we do not see upregulation of *gata5* transcript at the timepoints we have so far considered (Figure 6-5), there may be transient or delayed upregulation of *gata5* transcript, or indeed stabilization or relocalization of Gata5. To begin to address this question, we are developing *gata5* mutant and combination *gata4, -5 and -6* mutant lines (see Appendix C).

Conclusions

In conclusion, these studies are, to our best knowledge, the first to generate and characterize zebrafish that harbor homozygous mutations in *gata4* and/or *gata6*.

We used light microscopy and WISH to detail abnormalities in the development of multiple organ systems in embryos harboring mutations in the *gata* genes. We capitalized on the ability to observe gastrulation in the developing zebrafish to pinpoint the precise period of delay in *gata4* mutant development, allowing us to make strong hypotheses about the pathways that *gata4* is regulating during early epiboly.

Finally, our findings uphold previously described roles for *gata6* in cardiac, hepatic and pancreatic development, but intriguingly suggest that *gata4* is dispensable in the zebrafish model system. This finding hints at a unique ability of the zebrafish to sense genetic lesion in, and compensate for, a master regulator transcription factor.

APPENDIX A: HSPB5 COMPENSATES FOR LOSS OF HSPB7 IN THE HEART.

Introduction

The findings of mild cardiac dysfunction in hspb7 mutant zebrafish, discussed in Chapter 4, are in contrast with those from previous studies, in which we[1] and others[2] used morpholinos to knock down Hspb7 during zebrafish embryogenesis and observed embryonic lethality with randomization of left-right asymmetry, cardiac malformation and a change in the size of ventricular cardiomyocytes. Discrepancies between morphant and mutant phenotypes are often reported in recent zebrafish literature[3]. As a result, debate has arisen over the accuracy of morpholino data. However, several groups, including our own, have identified compensatory mechanisms that arise following genetic mutation but not following acute knockdown of the same gene[4]. It is possible that the morphant phenotypes were caused by off-targeting effects, given recent reports that morphant and mutant phenotypes can be concernedly discordant[3]. Alternatively, consistent with other reports[4], it is possible that the mutants (but not morphants) compensate for loss of Hspb7. and discrepancies have been uncovered between morphant and mutant phenotypes for some genes[3].

Hspb5b/HSPB5 is upregulated in *HSPB7* mutant cardiomyocytes

In order to investigate whether an alternative small heat shock protein could be compensating for loss of *hspb7* in the zebrafish, I performed qPCR for a panel of small heat shock proteins that are known to be expressed in the heart[5]. I discovered that *hspb7* mutants show increased expression levels of *hspb5b*, a sister

sHSP gene that could conceivably compensate for loss of Hspb7 (Appendix Figure A-1A).

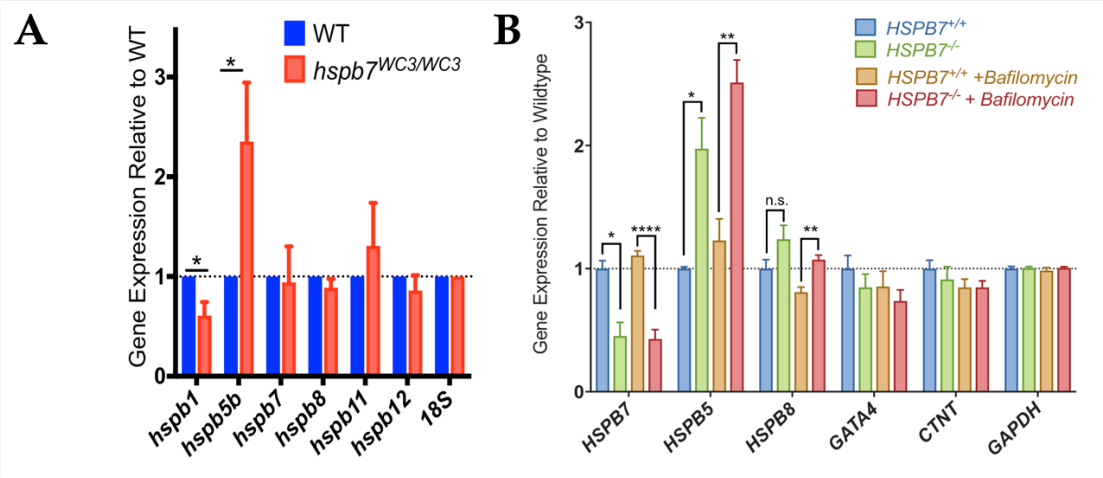

Appendix Figure A-1: Upregulation of* HSPB5 *in* HSPB7 *null cardiomyocytes
qPCR analysis of small heat shock and control mRNA expression in (A) embryonic zebrafish hearts isolated by microdissection and (B) hESC-derived cardiomyocytes on day 15 of differentiation. hESC-CM data is pooled for Wildtype and Clone 12 (HSPB7$^{+/+}$) and Clone 26 and 30 (HSPB7$^{-/-}$).

Excitingly, when I performed a matching qPCR analysis for small heat shock protein expression in wildtype or *HSPB7* null hESC-CMs, I observed a similar upregulation of the human *HSPB5* (also known as *CRYAB)* transcript (Appendix Figure A-1B). This suggests that *HSPB5* upregulation is a conserved response to loss of *HSPB7*.

HSPB5 is a more ubiquitously expressed member of the sHSP family. Important roles for HSPB5 have been demonstrated in the eye, where HSPB5 aggregates are associated with cateractogenesis[6], and in the nervous system[7], where it transduces signals from the dopamine receptor to modulate responsivity to immune stimuli[8], and where loss of HSPB5 leads to worsening of experimental encephalomyelitis[7].

Interestingly, despite the animal model links to the immune system and neurological function, human mutations in *HSPB5* are associated with the development of skeletal muscle and cardiac myopathies[9,10], as well as with congenital cataract formation. Expression of human HSPB5 mutant proteins in mice leads to similar myopathies downstream of alterations in the cellular redox balance[11], suggesting that these are, at least in part, gain-of-function phenotypes.

Generation of *hspb5b* mutant zebrafish lines

In order to investigate the extent to which *hspb5b* is able to compensate for loss of *hspb7*, I am using CRISPR technology to generate *hspb5b* mutant zebrafish lines. As for *hspb7* TALENs, the sgRNA selected targets the 5' end of the gene (Appendix Figure A-2A), in order to generate early mutations that render the resultant protein completely inactive.

Embryos from F0 adults injected with the CRISPR targeting *hspb5b* were screened by T7E1 assay for transmission of mutant alleles (Appendix Figure A-2B) and clutches of embryos carrying mutations are being raised. Intriguingly, injection of this CRISPR leads to enhanced rates of embryonic cardiomyopathy in the *hspb7* mutant background, compared to injection in wildtype embryos (Appendix Figure A-2C). This strengthens the hypothesis of a compensatory role for Hspb5b, which allows the embryos to tolerate *hspb7* mutations, and facilitates our ability to evaluate Hspb7 function in adult fish.

I have recovered several mutant alleles of *hspb5b*, including a 26 base pair mutation that leads to a frameshift and subsequent premature stop codon (Appendix Figure A-2D). Mouse models of HSPB5 loss-of-function survive

embryogenesis and heterozygotes are fertile[7], leading me to hypothesize that I should be able to recover zebrafish homozygous for *hspb5b* mutation.

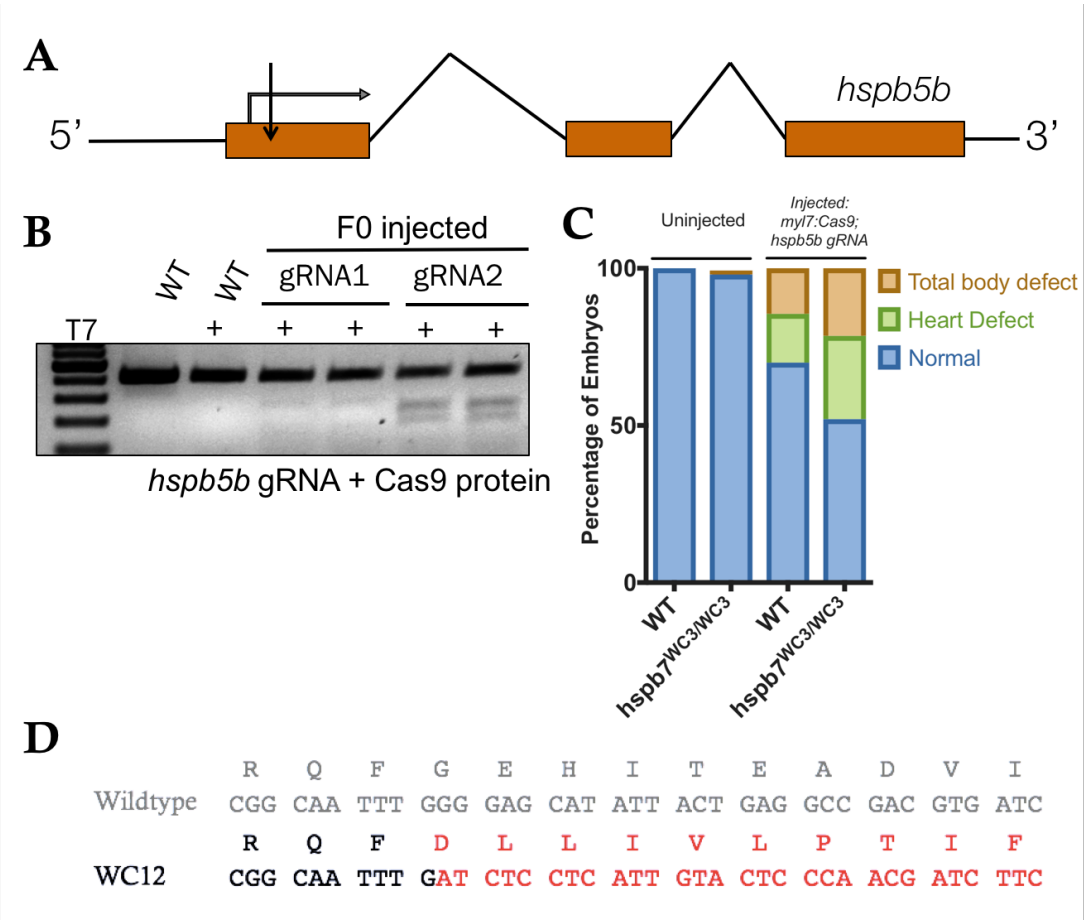

Appendix Figure A-2: Generation of* hspb5b *mutant zebrafish lines.
(A) Schematic showing structure of zebrafish hspb5b gene with arrow indicating locus targeted by the CRISPR. (B) T7E1 assay showing successful generation of mutations in pools of 10 embryos injected with CRISPR-Cas9 complexes targeting hspb5b. (C) Quantification of phenotypes observed in F0 injected embryos of wildtype or hspb7 mutant genotype, showing an increase in both total body defects and heat defects in hspb7 null embryos when compared with wildtype controls. (D) Sequence of wildtype hspb5b *and a frameshift mutation that leads to a premature stop codon and is predicted to lead to a loss of normal protein function.*

Generation of cardiomyocyte-specific *hspb5b* mutations in zebrafish

Due to the multi-system roles of HSPB5, I also wanted to make a cardiomyocyte-specific loss-of-function model. I adapted a tissue-specific zebrafish CRISPR system designed by the Zon labarotory[12] by cloning the cardiomyocyte specific *myl7* promoter into a Tol2 vector to drive expression of Cas9 and GFP (Plasmid EM02, Appendix Figure A-3A). Injection of this construct at the one cell stage, in combination with *tol2* mRNA led to mosaic expression of GFP in embryonic zebrafish hearts, indicating successful integration of the transgene.

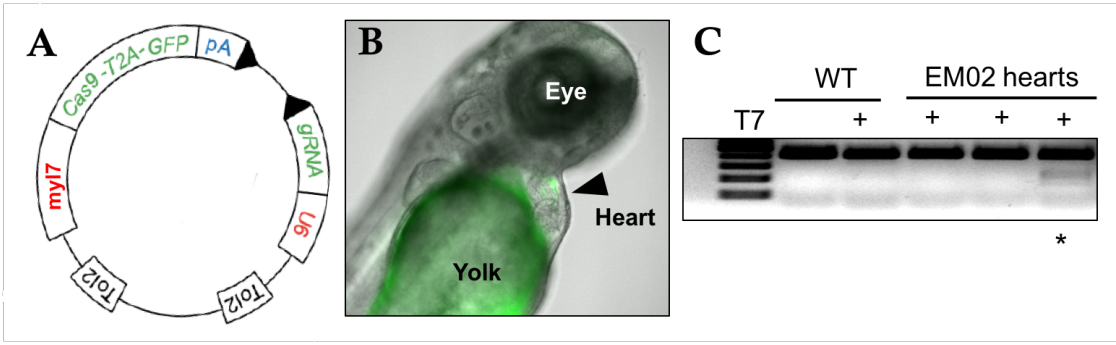

Appendix Figure A-3: Generation of zebrafish with cardiomyocyte-specific mutation of hspb5b.
(A) EM02 Vector map showing myl7 promoter driving expression of Cas9 protein and GFP. An hspb5b *specific guide RNA is cloned under the U6 promoter. (B) Mosaic expression of GFP in the heart of 72hpf embryos injected with EM02 vector and Tol2 mRNA, indicating successful DNA integration and subsequent protein expression. (C) T7 assay of gDNA extracted from hearts of adult wildtype or EM02 F0 zebrafish showing generation of mutations in EM02-injected animals. The star indicates successful generation. The first two EM02 hearts are from animals that did not transmit the EM02 vector to their progeny, suggesting low mosaicism. Animal 3 (annotated with a star) transmitted GFP expression to around 10% of embryos.*

I isolated gDNA from the hearts of adult zebrafish injected with EM02 construct. Hearts were taken from animals that did, and did not, transmit GFP positive hearts to their progeny. T7E1 assay indicated the presence of mutations in *hspb5b* only in the hearts of zebrafish that successfully transmitted the *myl7::Cas9-T2A-GFP*

transgene. An important caveat in the use of these lines for future studies is that the nature of the mutations in the heart of a given animal will be technically challenging to ascertain given the high likelihood of mosaicism.

Generation of *HSPB5* mutant hESC lines.

As a complimentary model system in which to study the role of *HSPB5* in *HSPB7* mutant cardiomyocytes, I generated *HSPB5* null hESCs using the iCRISPR system[13]. Given the propensity of *HSPB5* mutations to themselves cause protein aggregation[9,10], I targeted the gRNA to the start codon of *HSPB5 (*Appendix Figure A-4*)*.

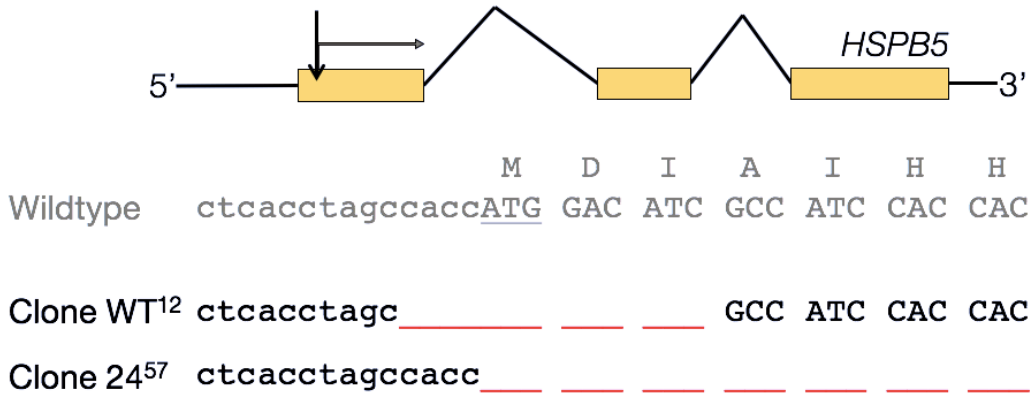

Appendix Figure A-4: Generation of* HSPB5 *mutant cardiomyocytes
Schematic of the structure and partial sequence of the human HSPB5 *gene. Straight arrow indicates CRISPR targeted location. Clone 12 and Clone 57 sequences have complete loss of start codon (underlined in wildtype). Sequences from resultant* HSPB5 *mutant clones derived from wildtype (WT) or* HSPB7 *mutant (Clone 24) hESCs are detailed.*

I successfully recovered hESC clones in which the start codon of *HSPB5* was deleted. It is a strong hypothesis that cardiomyocytes derived from hESCs carrying these mutations will be entirely absent of HSPB5 protein.

No large differences in hESC survival or proliferation were observed following mutation of HSPB5, although this has not been confirmed by direct assay. The

normal expression of pluripotency markers in these *HSPB5* mutant clones will need to be confirmed, however previous work performed in *HSPB5* mutant iPSC lines suggests that they are unlikely to be altered[14].

Discussion and Future Directions

Intriguingly, I documented an upregulation in *hspb5b* in the hearts of hspb7$^{WC3/WC}$ embryos, and observed a similar upregulation of *HSPB5* in our HSPB7$^{-/-}$ hESC-CMs. The drosophila homolog of HSPB5 has been shown to act as a chaperone for Cheerio, the drosophila filamin protein[15]. I hypothesize that upregulation of HSPB5 may be at least partially compensating for loss of HSPB7 in our mutant models. In order to address this hypothesis, I have generated zebrafish lines carrying mutations in *hspb5b* and hESC lines with complete loss of *HSPB5.* In addition, I have generated a cardiomyocyte-specific CRISPR system to drive mutation of *hspb5b* in zebrafish in a tissue-specific manner.

In the immediate future, I intend to cross specific *hspb5b* mutations into animals homozygous for *hspb*7^{WC3} or *hspb*7^{WC4}. I hypothesize that compound homozygotes will exhibit an increase in cardiac abnormalities when compared to siblings. Additionally, I hypothesize that *hspb7*$^{WC3/WC3}$*;hspb5b*$^{WC12/WC12}$ animals will be less able to tolerate exercise challenge and will exhibit a worsening of the cardiomyopathies seen in *hspb7* mutant zebrafish, as described in Chapter 4. Additionally, I expect that exposure of compound homozygote embryos to autophagy inhibitors will precipitate defects in cardiomorphogenesis in compound mutants but not *hspb5b* null animals.

I am also working to generate cardiomyocytes from hESCs that have mutations in *HSPB5*. I predict that loss of *HSPB5* in an *HSPB7* mutant background will increase

the propensity of FLNC to aggregate, and will magnify the upregulation of autophagy that I have observed in these cells.

These data will confirm that *HSPB5*/*hspb5b* is compensating for loss of *HSPB7* in the cardiomyocyte.

APPENDIX B: GENERATION OF *GATA5* MUTANT ZEBRAFISH

Introduction

As discussed extensively in this thesis, the GATA factor proteins play important roles in the development and function of various organ systems. GATA5 is a member of the subfamily of GATA factors, alongside GATA4 and GATA6, that are important in the development of mesendoderm and mesendoderm-derived organs. Our laboratory has previously identified redundancy between *gata5* and *gata6* in zebrafish development[109], and there is evidence for functional redundancy between murine GATA5 and the other GATA factors in the mouse heart[197,198]. To complement the work described in Chapter 7 of this thesis, and to further investigate the unique and redundant roles of *gata5* in zebrafish, we set out to generate *gata5* null zebrafish lines.

Generation of *gata5* mutant fish

Following the same reasoning as discussed in Chapter 7, we designed a CRISPR to target the zinc finger domain of *gata5* (Appendix Figure B-1A,B). Successful generation of mutant alleles was confirmed by T7E1 assay performed on pools of embryos injected with CRISPR constructs at the single cell stage. F0 fish were screened for transmission of mutant alleles. From F1 fish we recovered a variety of *gata5* mutant alleles, summarized in Appendix Figure B-1. Of particular interest to us were a 10 base pair deletion that leads to a frame shift and a predicted truncation of Gata5 with complete loss of both zinc fingers and the entire C terminal of the protein ($gata5^{WC8}$), and an 18bp deletion that lead to disturbance exclusively of the C-X-X-C motif ($gata5^{WC9}$).

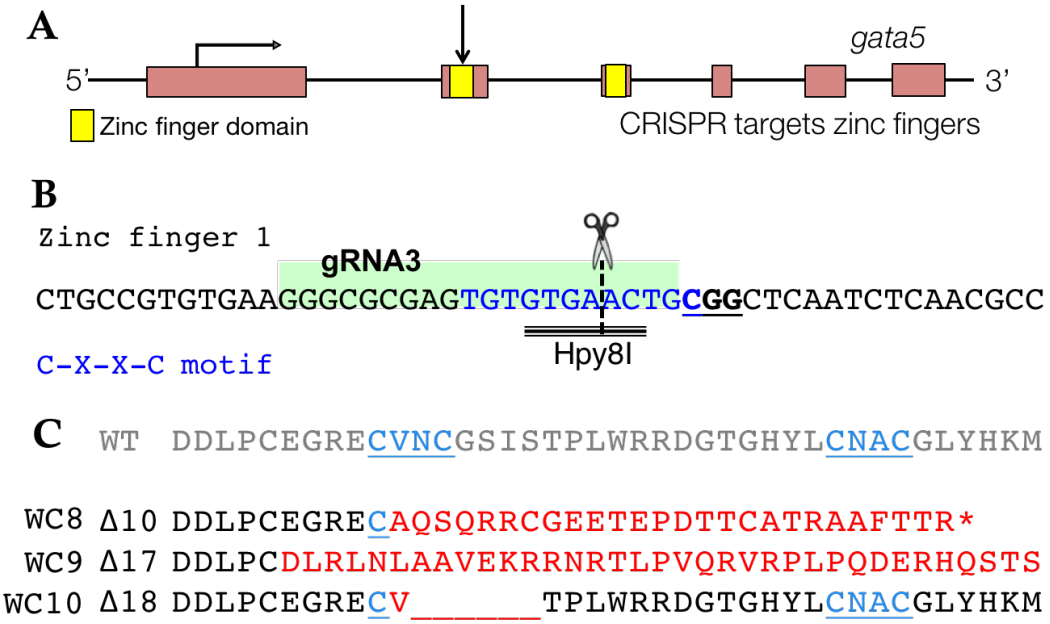

Appendix Figure B-1: Generation and identification of mutant gata5 alleles. *(A) Structure of* gata5 *gene showing the locations of the zinc finger domains and CRISPR target zone. (B) Partial nucleotide sequence detail of the N-terminal zinc finger of* gata5*, showing targeting region of CRISPR. (C) Partial amino acid sequence of Gata5 protein detailing alleles recovered from F1 fish following CRISPR targeting.*

Homozygous mutation of *gata5* recapitulates the Faust mutant phenotype

We crossed two F1 animals that were heterozygous for the *gata5*^{WC9} allele and observed the phenotypes of the resultant pool of embryos. Around 25% of embryos had noticeable defects in cardiac development by 24hpf, at which time they did not have visible heart tubes. By 48hpf, this subset of embryos had developed bilateral edema (Appendix Figure B-2B). In some embryos beating patches of cardiomyocytes could be observed bilaterally, whereas in others no cardiac tissue could be determined by brightfield microscopy. Genotyping of embryos following initial phenotyping revealed that all homozygous *gata5*

mutants displayed the characteristic bilateral edematous patches with concomitant lack of fully formed heart tube (Appendix Figure B-2C).

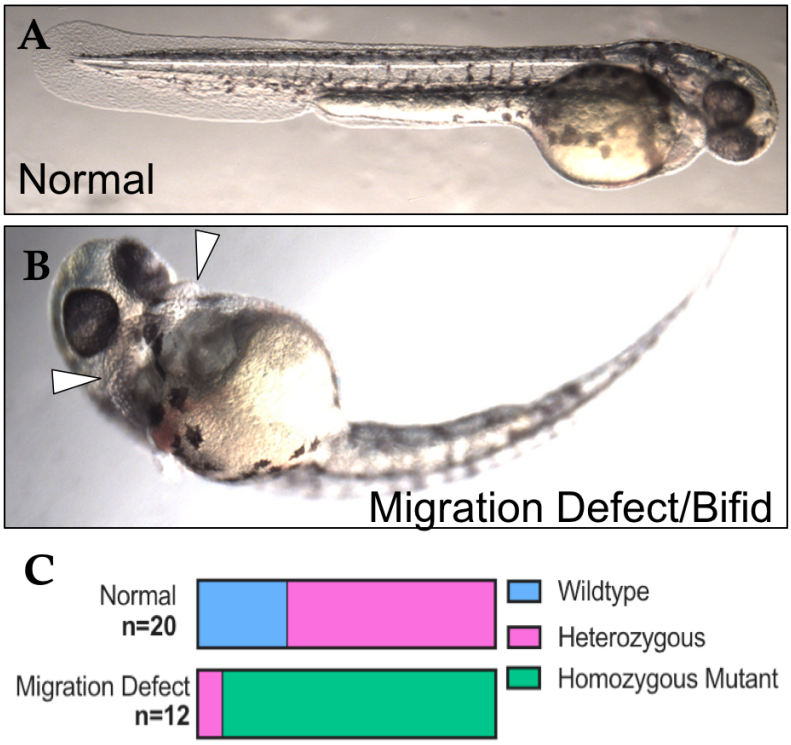

Appendix Figure B-2: Gata5 mutant embryos have severe defects in cardiac development.
Brightfield images of (A) normal embryos and (B) embryos with defects in cardiac migration at 48hpf. White arrowheads point to edematous swellings. (C) Quantification of genotypes for normal or migration defect embryos determined that the phenotype of abnormal cardiogenesis was found in embryos null for gata5.

The previously characterized *gata5* mutant allele, *faust*, displays a range of defects in the migration of cardiac progenitors[199]. We hypothesize that the same migration defects lead to the bilateral edema and occasional bifid hearts we observe in *gata5* mutant embryos.

Future Directions

In the immediate future, we are working to characterize the gata5 homozygous mutant phenotype. The *faust* allele is a well characterized mutant of *gata5* with

defects in the development of the heart and in endoderm-derived organs, including the gut. We will initially confirm that these abnormalities are also seen in our novel *gata5* mutant zebrafish, through WISH and qPCR analysis.

In addition, we are interested in the phenotypes of embryos carrying various combinations of *gata4, gata5* and *gata6* mutant alleles. Our preliminary observations indicate that triple heterozygous ($gata4^{WC6/+};gata5^{WC8/+};gata6^{WC7/+}$) animals are recovered in expected ratios and develop normally. Excitingly we observe that triple heterozygotes are viable to at least larval day 28, suggesting that we may be able to recover triple heterozygous adults and perform crosses that will provide us with a full gamut of *gata* genotypes.

BIBLIOGRAPHY

1. Mozaffarian D, Benjamin EJ, Go AS, Arnett DK, Blaha MJ, Cushman M, et al. Heart Disease and Stroke Statistics - 2016 Update: A Report From the American Heart Association. Circulation. 2015. 1-324 p.

2. Townsend N, Bhatnagar P, Wilkins E, Wickramasinghe K, Rayner M. Cardiovascular Disease Statistics 2015. 2015. 1-144 p.

3. Benjamin EJ, Blaha MJ, Chiuve SE, Cushman M, Das SR, Deo R, et al. Heart Disease and Stroke Statistics—2017 Update: A Report From the American Heart Association. Circulation. 2017 Jan 25;131(6):e29–39.

4. Barry SP, Townsend P a. What causes a broken heart--molecular insights into heart failure. Int Rev Cell Mol Biol. 2010 Jan;284(10):113–79.

5. Richard P, Charron P, Carrier L, Ledeuil C, Cheav T, Pichereau C, et al. Hypertrophic cardiomyopathy: Distribution of disease genes, spectrum of mutations, and implications for a molecular diagnosis strategy. Circulation. 2003;107(17):2227–32.

6. Sun N, Yazawa M, Liu J, Han L, Sanchez-Freire V, Abilez OJ, et al. Patient-specific induced pluripotent stem cells as a model for familial dilated cardiomyopathy. Sci Transl Med. 2012 Apr 18;4(130):130ra47.

7. Valdés-Mas R, Gutiérrez-Fernández A, Gómez J, Coto E, Astudillo A, Puente D a, et al. Mutations in filamin C cause a new form of familial hypertrophic cardiomyopathy. Nat Commun. 2014 Jan;5:5326.

8. Fürst DO, Goldfarb LG, Kley RA, Vorgerd M, Olivé M, Van Der Ven PFM. Filamin C-related myopathies: Pathology and mechanisms. Acta Neuropathol. 2013;125(1):33–46.

9. Epstein FH. Cardiovascular Disease Epidemiology - A journey from the past into the future. Circulation. 1996;93(1755–1764).

10. Kimmel CBCB, Ballard WW, Kimmel SR, Ullmann B, Schilling TF. Stages of embryonic development of the zebrafish. Dev …. 1995 Jul;10(3):253–310.

11. Bakkers J. Zebrafish as a model to study cardiac development and human cardiac disease. Cardiovasc Res. 2011;

12. Alexander J, Rothenberg M, Henry GL, Stainier DY. Casanova plays an early and essential role in endoderm formation in zebrafish. Dev Biol. 1999;215:343–57.

13. Kikuchi Y, Trinh LA, Reiter JF, Alexander J, Yelon D, Stainier DYR. The zebrafish bonnie and clyde gene encodes a Mix family homeodomain protein that regulates the generation of endodermal precursors. Genes Dev. 2000;14(10):1279–89.

14. Kupperman E, An S, Osborne N, Waldron S, Stainier DY. A sphingosine-1-phosphate receptor regulates cell migration during vertebrate heart

development. Nature. 2000 Jul 13;406(6792):192–5.

15. Buckingham M, Meilhac S, Zaffran S. Building the mammalian heart from two sources of myocardial cells. Nat Rev Genet. 2005 Nov;6(11):826–35.

16. Reischauer S, Arnaout R, Ramadass R, Stainier DYR. Actin Binding GFP Allows 4D In Vivo Imaging of Myofilament Dynamics in the Zebrafish Heart and the Identification of Erbb2 Signaling as a Remodeling Factor of Myofibril Architecture. Circ Res. 2014 Sep 16;115:845–56.

17. Berdougo E, Coleman H, Lee DH, Stainier DYR, Yelon D. Mutation of weak atrium/atrial myosin heavy chain disrupts atrial function and influences ventricular morphogenesis in zebrafish. Development. 2003 Dec;130(24):6121–9.

18. Auman HJ, Coleman H, Riley HE, Olale F, Tsai HJ, Yelon D. Functional modulation of cardiac form through regionally confined cell shape changes. PLoS Biol. 2007;5(3):0604–15.

19. Staudt D, Stainier D. Uncovering the molecular and cellular mechanisms of heart development using the zebrafish. Annu Rev Genet. 2012;46:397–418.

20. Sylva M, Van den Hoff MJB, Moorman AFM. Development of the human heart. Am J Med Genet Part A. 2014;164(6):1347–71.

21. Beis D, Bartman T, Jin S-W, Scott IC, D'Amico L a, Ober E a, et al. Genetic and cellular analyses of zebrafish atrioventricular cushion and valve development. Development. 2005 Sep;132(18):4193–204.

22. George V, Colombo S, Targoff KL. An early requirement for nkx2.5 Ensures first and Second heart field ventricular identity and cardiac function into adulthood. Dev Biol. 2014 Dec 20;400(1):10–22.

23. Junker JP, No??l ES, Guryev V, Peterson KA, Shah G, Huisken J, et al. Genome-wide RNA Tomography in the Zebrafish Embryo. Cell. 2014;159(3):662–75.

24. Singh AR, Sivadas A, Sabharwal A, Vellarikal SK, Jayarajan R, Verma A, et al. Chamber specific gene expression landscape of the zebrafish heart. PLoS One. 2016;11(1).

25. Wu CC, Kruse F, Vasudevarao MD, Junker JP, Zebrowski DC, Fischer K, et al. Spatially Resolved Genome-wide Transcriptional Profiling Identifies BMP Signaling as Essential Regulator of Zebrafish Cardiomyocyte Regeneration. Dev Cell. 2016;36(1):36–49.

26. Choi W-Y, Gemberling M, Wang J, Holdway JE, Shen M-C, Karlstrom RO, et al. In vivo monitoring of cardiomyocyte proliferation to identify chemical modifiers of heart regeneration. Development. 2013 Mar;140(3):660–6.

27. Cripps R, Olson E. Control of cardiac development by an evolutionarily conserved transcriptional network. Dev Biol. 2002;246:14–28.

28. Schlesinger J, Schueler M, Grunert M, Fischer JJ, Zhang Q, Krueger T, et al. The cardiac transcription network modulated by Gata4, Mef2a, Nkx2.5, Srf, histone modifications, and microRNAs. PLoS Genet. 2011

Feb;7(2):e1001313.

29. Hami D, Grimes AC, Tsai H-J, Kirby ML. Zebrafish cardiac development requires a conserved secondary heart field. Development. 2011 Jun;138(11):2389–98.

30. McCulley DJ, Black BL. Transcription factor pathways and congenital heart disease. Vol. 100, Current topics in developmental biology. Elsevier Inc.; 2012. 253-77 p.

31. Hwang PM, Sykes BD. Targeting the sarcomere to correct muscle function. Nat Rev Drug Discov. 2015 May;14(5):313–28.

32. Huang W, Zhang R, Xu X. Myofibrillogenesis in the developing zebrafish heart: A functional study of tnnt2. Dev Biol. 2009 Jul 15;331(2):237–49.

33. Skwarek-Maruszewska A, Hotulainen P, Mattila PK, Lappalainen P. Contractility-dependent actin dynamics in cardiomyocyte sarcomeres. J Cell Sci. 2009 Jun 15;122(Pt 12):2119–26.

34. da Silva Lopes K, Pietas A, Radke MH, Gotthardt M. Titin visualization in real time reveals an unexpected level of mobility within and between sarcomeres. J Cell Biol. 2011;193(4):785–98.

35. Leber Y, Ruparelia AA, Kirfel G, Ven PFM Van Der. Filamin C is a highly dynamic protein associated with fast repair of myofibrillar microdamage. Hum Mol Genet. 2016;

36. Bergmann O, Bhardwaj RD, Bernard S, Zdunek S, Walsh S, Zupicich J, et al. Evidence for Cardiomyocyte Renewal in Humans. Science (80-). 2009;324(5923):98–102.

37. Porrello ER, Mahmoud AI, Simpson E, Hill J a, Richardson J a, Olson EN, et al. Transient regenerative potential of the neonatal mouse heart. Science. 2011 Feb 25;331(6020):1078–80.

38. Mollova M, Bersell K, Walsh S, Savla J, Das LT, Park S-Y, et al. Cardiomyocyte proliferation contributes to heart growth in young humans. Proc Natl Acad Sci U S A. 2013;110(4):1446–51.

39. Poss KD, Wilson LG, Keating MT. Heart regeneration in zebrafish. Science. 2002 Dec 13;298(5601):2188–90.

40. Naqvi N, Li M, Calvert JW, Tejada T, Lambert JP, Wu J, et al. A proliferative burst during preadolescence establishes the final cardiomyocyte number. Cell. 2014 May 8;157(4):795–807.

41. Gupta V, Poss K. Clonally dominant cardiomyocytes direct heart morphogenesis. Nature. 2012;484(7395):479–84.

42. Maiuri MC, Zalckvar E, Kimchi A, Kroemer G. Self-eating and self-killing: crosstalk between autophagy and apoptosis. Nat Rev Mol Cell Biol. 2007 Sep;8(9):741–52.

43. Li WW, Li J, Bao JK. Microautophagy: Lesser-known self-eating. Cell Mol Life

Sci. 2012;69(7):1125–36.

44. Chiang HL, Terlecky SR, Plant CP, Dice JF. A role for a 70-kilodalton heat shock protein in lysosomal degradation of intracellular proteins. Science (80-). 1989;246(August):382–5.

45. Thompson LM, Aiken CT, Kaltenbach LS, Agrawal N, Illes K, Khoshnan A, et al. IKK phosphorylates Huntingtin and targets it for degradation by the proteasome and lysosome. J Cell Biol. 2009;187(7):1083–99.

46. Arndt V, Dick N, Tawo R, Dreiseidler M, Wenzel D, Hesse M, et al. Chaperone-assisted selective autophagy is essential for muscle maintenance. Curr Biol. 2010 Jan 26;20(2):143–8.

47. Ulbricht A, Gehlert S, Leciejewski B, Schiffer T, Bloch W, Höhfeld J, et al. Induction and adaptation of chaperone-assisted selective autophagy CASA in response to resistance exercise in human skeletal muscle Induction and adaptation of chaperone-assisted selective autophagy CASA in response to resistance exercise in human skeleta. 2015;8627(September).

48. Ulbricht A, Eppler FJ, Tapia VE, van der Ven PFM, Hampe N, Hersch N, et al. Cellular mechanotransduction relies on tension-induced and chaperone-assisted autophagy. Curr Biol. 2013 Mar 4;23(5):430–5.

49. Rubinsztein DC, Codogno P, Levine B. Autophagy modulation as a potential therapeutic target for diverse diseases. Nat Rev Drug Discov. 2012 Sep;11(9):709–30.

50. Mizushima N, Levine B, Cuervo AM, Klionsky DJ. Autophagy fights disease through cellular self-digestion. Nature. 2008 Feb 28;451(7182):1069–75.

51. Green DR, Levine B. To be or not to be? How selective autophagy and cell death govern cell fate. Cell. 2014;157(1):65–75.

52. Nakai A, Yamaguchi O, Takeda T. The role of autophagy in cardiomyocytes in the basal state and in response to hemodynamic stress. Nat Med. 2007;13:619–24.

53. Sybers H, Ingwall J, DeLuca M. Autophagy in cardiac myocytes. Recent Adv Stud Card Struct Metab. 1976;12:453–63.

54. Nishida K, Kyoi S, Yamaguchi O, Sadoshima J, Otsu K. The role of autophagy in the heart. Cell Death Differ. 2009 Jan;16(1):31–8.

55. Tannous P, Zhu H, Johnstone JL, Shelton JM, Rajasekaran NS, Benjamin IJ, et al. Autophagy is an adaptive response in desmin-related cardiomyopathy. Proc Natl Acad Sci. 2008 Jul 15;105(28):9745–50.

56. Ding Y, Sun X, Huang W, Hoage T, Redfield M, Kushwaha S, et al. Haploinsufficiency of target of rapamycin attenuates cardiomyopathies in adult zebrafish. Circ Res. 2011 Sep 2;109(6):658–69.

57. Kawaguchi T, Takemura G, Kanamori H, Takeyama T, Watanabe T, Morishita K, et al. Prior starvation mitigates acute doxorubicin cardiotoxicity through restoration of autophagy in affected cardiomyocytes. Cardiovasc Res. 2012

Dec 1;96(3):456–65.

58. Portbury AL, Willis MS, Patterson C. Tearin' up my heart: proteolysis in the cardiac sarcomere. J Biol Chem. 2011 Mar 25;286(12):9929–34.

59. White RM, Sessa A, Burke C, Bowman T, LeBlanc J, Ceol C, et al. Transparent adult zebrafish as a tool for in vivo transplantation analysis. Cell Stem Cell. 2008 Feb 7;2(2):183–9.

60. Hwang WY, Fu Y, Reyon D, Maeder ML, Tsai SQ, Sander JD, et al. Efficient genome editing in zebrafish using a CRISPR-Cas system. Nat Biotechnol. 2013;31(3):227–9.

61. Dahlem TJ, Hoshijima K, Jurynec MJ, Gunther D, Starker CG, Locke AS, et al. Simple methods for generating and detecting locus-specific mutations induced with TALENs in the zebrafish genome. PLoS Genet. 2012 Jan;8(8):e1002861.

62. Bedell VVM, Wang Y, Campbell JMJ, Poshusta TLT, Starker CCG, Krug RGR, et al. In vivo genome editing using a high-efficiency TALEN system. Nature. 2012 Nov 1;491(7422):114–8.

63. Bongso A, Fong CY, Ng SC, Ratnam S. Isolation and culture of inner cell mass cells from human blastocysts. Hum Reprod. 1994 Nov;9(11):2110–7.

64. Takahashi K, Yamanaka S. Induction of pluripotent stem cells from mouse embryonic and adult fibroblast cultures by defined factors. Cell. 2006 Aug;126(4):663–76.

65. Kehat I, Kenyagin-Karsenti D. Human embryonic stem cells can differentiate into myocytes with structural and functional properties of cardiomyocytes. J Clin Invest. 2001;108(3):407–14.

66. Barbuti A, Benzoni P, Campostrini G, Dell'Era P. Human derived cardiomyocytes: A decade of knowledge after the discovery of induced pluripotent stem cells. Dev Dyn. 2016;245(12):1145–58.

67. Yang X, Pabon L, Murry CE. Engineering adolescence: Maturation of human pluripotent stem cell-derived cardiomyocytes. Circ Res. 2014;114(3):511–23.

68. Claycomb WC, Lanson N a, Stallworth BS, Egeland DB, Delcarpio JB, Bahinski A, et al. HL-1 cells: a cardiac muscle cell line that contracts and retains phenotypic characteristics of the adult cardiomyocyte. Proc Natl Acad Sci U S A. 1998 Mar 17;95(6):2979–84.

69. Gunther A, Baumann A, Guenther A, Baumann A. Distinct expression patterns of HCN channels in HL-1 cardiomyocytes. BMC Cell Biol. 2015;16:18.

70. Evans T, Reitman M, Felsenfeld G. An erythrocyte-specific DNA-binding factor recognizes a regulatory sequence common to all chicken globin genes. Proc Natl Acad Sci. 1988;85(16):5976–80.

71. Yang HY, Evans T. Distinct roles for the two cGATA-1 finger domains. Mol

Cell Biol. 1992;12(10):4562–70.

72. Lentjes MH, Niessen HE, Akiyama Y, de Bruïne AP, Melotte V, van Engeland M. The emerging role of GATA transcription factors in development and disease. Expert Rev Mol Med. 2016;18:e3.

73. Chlon TM, Crispino JD. Combinatorial regulation of tissue specification by GATA and FOG factors. Development. 2012;139(21):3905–16.

74. Kuo CT, Morrisey EE, Anandappa R, Sigrist K, Lu MM, Parmacek MS, et al. GATA4 transcription factor is required for ventral morphogenesis and heart tube formation. Genes Dev. 1997;11(8):1048–60.

75. Molkentin JD, Lin Q, Duncan SA, Olson EN. Requirement of the transcription factor GATA4 for heart tube formation and ventral morphogenesis. Genes Dev. 1997;11(8):1061–72.

76. Lepage D, Bélanger É, Jones C, Tremblay S, Allaire JM, Bruneau J, et al. Gata4 is critical to maintain gut barrier function and mucosal integrity following epithelial injury. Sci Rep. 2016;6(October):36776.

77. Beuling E, Kerkhof IM, Nicksa GA, Giuffrida MJ, Haywood J, aan de Kerk DJ, et al. Conditional Gata4 deletion in mice induces bile acid absorption in the proximal small intestine. Gut. 2010;59(7):888–95.

78. Güemes M, Garcia AJ, Rigueur D, Runke S, Wang W, Zhao G, et al. GATA4 is essential for bone mineralization via ER?? and TGF??/BMP pathways. J Bone Miner Res. 2014;29(12):2676–87.

79. Delgado I, Carrasco M, Cano E, Carmona R, García-Carbonero R, Marín-Gómez LM, et al. GATA4 loss in the septum transversum mesenchyme promotes liver fibrosis in mice. Hepatology. 2014;59(6):2358–70.

80. Chen S, Tang J, Cheng J, Li J, Jin C, Li X. Loss of Gata4 in Sertoli cells impairs the spermatogonial stem cell niche and causes germ cell exhaustion by attenuating chemokine signaling. 2015;6(35).

81. Hu YC, Okumura LM, Page DC. Gata4 Is Required for Formation of the Genital Ridge in Mice. PLoS Genet. 2013;9(7).

82. Holtzinger A, Evans T. Gata4 regulates the formation of multiple organs. Development. 2005;4005–14.

83. Online Mendelian Inheritance in Man, OMIM®. Johns Hopkins University, Baltimore, MD. MIM Number: 600576 [Internet]. [cited 2017 Jan 29]. Available from: https://omim.org/600576

84. Watt AJ, Battle M a, Li J, Duncan SA. GATA4 is essential for formation of the proepicardium and regulates cardiogenesis. Proc Natl Acad Sci U S A. 2004 Aug 24;101(34):12573–8.

85. Zeisberg E, Ma Q, Juraszek A, Moses K, Schwartz R, Izumo S, et al. Morphogenesis of the right ventricle requires myocardial expression of Gata4. J Clin Invest. 2005;115:1522–31.

86. Rajagopal SK, Ma Q, Obler D, Shen J, Manichaikul A, Tomita-Mitchell A, et al. Spectrum of heart disease associated with murine and human GATA4 mutation. J Mol Cell Cardiol. 2007;43(6):677–85.

87. Gupta V, Gemberling M, Karra R, Rosenfeld GEE, Evans T, Poss KDD. An Injury-Responsive Gata4 Program Shapes the Zebrafish Cardiac Ventricle. Curr Biol. 2013 Jun 8;23(13):1–7.

88. Oka T, Maillet M, Watt AJ, Schwartz RJ, Aronow BJ, Duncan S a, et al. Cardiac-specific deletion of Gata4 reveals its requirement for hypertrophy, compensation, and myocyte viability. Circ Res. 2006 Mar 31;98(6):837–45.

89. Olson EN, Molkentin JD. Prevention of Cardiac Hypertrophy by Calcineurin Inhibition : Hope or Hype? Circ Res. 1999 Apr 2;84(6):623–32.

90. Lowes BD, Minobe W, Abraham WT, Rizeq MN, Bohlmeyer TJ, Quaife RA, et al. Changes in Gene Expression in the Intact Human Heart. J Clin Invest. 1997;100:2315–24.

91. Perrino C, Rockman H a. GATA4 and the two sides of gene expression reprogramming. Circ Res. 2006 Mar 31;98(6):715–6.

92. Bisping E, Ikeda S, Won Kong S, Tarnavski O, Bodyak N, McMullen J, et al. Gata4 is required for maintenance of postnatal cardiac function and protection from pressure overload-induced heart failure. Proc Natl Acad Sci. 2006;103(39):14471–6.

93. Kobayashi S, Mao K, Zheng H, Wang X, Patterson C, O'Connell TD, et al. Diminished GATA4 protein levels contribute to hyperglycemia-induced cardiomyocyte injury. J Biol Chem. 2007 Jul 27;282(30):21945–52.

94. Aries A, Paradis P, Lefebvre C, Schwartz RJ, Nemer M. Essential role of GATA-4 in cell survival and drug-induced cardiotoxicity. Proc Natl Acad Sci. 2004 May 4;101(18):6975–80.

95. Kobayashi S, Volden P, Timm D, Mao K. Transcription factor GATA4 inhibits doxorubicin-induced autophagy and cardiomyocyte death. J Biol …. 2010;

96. Suzuki Y, Nagase H, Day R, Das D. GATA-4 regulation of myocardial survival in the preconditioned heart. J Mol Cell …. 2004;37:1195–203.

97. Kobayashi S, Lackey T, Huang Y, Bisping E, Pu WT, Boxer LM, et al. Transcription factor gata4 regulates cardiac BCL2 gene expression in vitro and in vivo. FASEB J. 2006 Apr;20(6):800–2.

98. Chen B, Zhong L, Roush SF, Pentassuglia L, Peng X, Samaras S, et al. Disruption of a GATA4/Ankrd1 signaling axis in cardiomyocytes leads to sarcomere disarray: implications for anthracycline cardiomyopathy. PLoS One. 2012 Jan;7(4):e35743.

99. Rajasekaran NS, Connell P, Christians ES, Yan L-J, Taylor RP, Orosz A, et al. Human alpha B-crystallin mutation causes oxido-reductive stress and protein aggregation cardiomyopathy in mice. Cell. 2007 Aug 10;130(3):427–39.

100. Bienengraeber M, Olson TM, Selivanov V a, Kathmann EC, O'Cochlain F, Gao F, et al. ABCC9 mutations identified in human dilated cardiomyopathy disrupt catalytic KATP channel gating. Nat Genet. 2004 Apr;36(4):382–7.

101. Duboscq-Bidot L, Charron P, Ruppert V, Fauchier L, Richter A, Tavazzi L, et al. Mutations in the ANKRD1 gene encoding CARP are responsible for human dilated cardiomyopathy. Eur Heart J. 2009 Sep;30(17):2128–36.

102. He A, Kong SW, Ma Q, Pu WT. Co-occupancy by multiple cardiac transcription factors identifies transcriptional enhancers active in heart. Proc Natl Acad Sci. 2011 Apr 5;108(14):5632–7.

103. Schrode N, Saiz N, Di Talia S, Hadjantonakis AK. GATA6 levels modulate primitive endoderm cell fate choice and timing in the mouse blastocyst. Dev Cell. 2014;29(4):454–67.

104. Zhao R, Watt AJ, Li J, Luebke-wheeler J, Morrisey EE, Duncan SA. GATA6 Is Essential for Embryonic Development of the Liver but Dispensable for Early Heart Formation. 2005;25(7):2622–31.

105. Lepore JJ, Mericko PA, Cheng L, Lu MM, Morrisey EE, Parmacek MS. GATA-6 regulates semaphorin 3C and is required in cardiac neural crest for cardiovascular morphogenesis. J Clin Invest. 2006;116(4):929–39.

106. Endothelial GATA-6 Deficiency Promotes Pulmonary Arterial Hypertension.

107. Online Mendelian Inheritance in Man, OMIM®. Johns Hopkins University, Baltimore, MD. MIM Number: 601656 [Internet]. [cited 2017 Jan 1]. Available from: https://omim.org/601656

108. Xin M, Davis CA, Molkentin JD, Lien C-L, Duncan SA, Richardson JA, et al. A threshold of GATA4 and GATA6 expression is required for cardiovascular development. Proc Natl Acad Sci. 2006;103(30):11189–94.

109. Holtzinger A, Evans T. Gata5 and Gata6 are functionally redundant in zebrafish for specification of cardiomyocytes. Dev Biol. 2007;312(2):613–22.

110. Singh MK, Li Y, Li S, Cobb RM, Zhou D, Lu MM, et al. Gata4 and Gata5 cooperatively regulate cardiac myocyte proliferation in mice. J Biol Chem. 2010;285(3):1765–72.

111. Carrasco M, Delgado I, Soria B, Martín F, Rojas A. GATA4 and GATA6 control mouse pancreas organogenesis. 2012;122(10).

112. Borok MJ, Papaioannou VE, Sussel L. Unique functions of Gata4 in mouse liver induction and heart development. Dev Biol. 2016;410(2):213–22.

113. Svensson EC, Huggins GS, Lin H, Clendenin C, Jiang F, Tufts R, et al. A syndrome of tricuspid atresia in mice with a targeted mutation of the gene encoding Fog-2. Nat Genet. 2000;25(3):353–6.

114. Bagu ET, Layoun A, Calvé A, Santos MM. Friend of GATA and GATA-6 modulate the transcriptional up-regulation of hepcidin in hepatocytes during inflammation. BioMetals. 2013;26(6):1051–65.

115. Beuling E, Bosse T, aan de Kerk DJ, Piaseckyj CM, Fujiwara Y, Katz SG, et al. GATA4 mediates gene repression in the mature mouse small intestine through interactions with friend of GATA (FOG) cofactors. Dev Biol. 2008;322(1):179–89.

116. Ang Y, Rivas RN, Ribeiro AJS, Pruitt BL, Snyder MP, Srivastava D, et al. Disease Model of GATA4 Mutation Reveals Transcription Factor Cooperativity in Human Article Disease Model of GATA4 Mutation Reveals Transcription Factor Cooperativity in Human Cardiogenesis. Cell. 2016;167(7):1734–1737.e22.

117. Ma Y, Wang J, Yu Y, Schwartz RJ. PKG-1?? mediates GATA4 transcriptional activity. Cell Signal. 2016;28(6):585–94.

118. Suzuki H, Katanasaka Y, Sunagawa Y, Miyazaki Y, Funamoto M, Wada H, et al. Tyrosine phosphorylation of RACK1 triggers cardiomyocyte hypertrophy by regulating the interaction between p300 and GATA4. Biochim Biophys Acta - Mol Basis Dis. 2016;1862(9):1544–57.

119. Charron F, Tsimiklis G, Arcand M, Robitaille L, Liang Q, Molkentin JD, et al. Tissue-specific GATA factors are transcriptional effectors of the small GTPase RhoA. Genes Dev. 2001 Oct 15;15(20):2702–19.

120. Rosenfeld GE, Mercer EJ, Mason CE, Evans T. Small heat shock proteins Hspb7 and Hspb12 regulate early steps of cardiac morphogenesis. Dev Biol. 2013 Jul 11;15(2):1–12.

121. Wojtowicz I, Jabłońska J, Zmojdzian M, Taghli-lamallem O, Renaud Y, Junion G, et al. Drosophila small heat shock protein CryAB ensures structural integrity of developing muscles, and proper muscle and heart performance. Development. 2015;142(5):994–1005.

122. Garrido C, Paul C, Seigneuric R, Kampinga HH. The small heat shock proteins family: the long forgotten chaperones. Int J Biochem Cell Biol. 2012 Oct;44(10):1588–92.

123. Marvin M, O'Rourke D. Developmental expression patterns of the zebrafish small heat shock proteins. Dev …. 2008;(December 2007):454–63.

124. Elicker KS, Hutson LD. Genome-wide analysis and expression profiling of the small heat shock proteins in zebrafish. Gene. 2007 Nov 15;403(1–2):60–9.

125. Kappé G, Franck E, Verschuure P, Boelens WC, Leunissen J a M, de Jong WW. The human genome encodes 10 alpha-crystallin-related small heat shock proteins: HspB1-10. Cell Stress Chaperones. 2003 Jan;8(1):53–61.

126. Ke L, Meijering R a M, Hoogstra-Berends F, Mackovicova K, Vos MJ, Van Gelder IC, et al. HSPB1, HSPB6, HSPB7 and HSPB8 protect against RhoA GTPase-induced remodeling in tachypaced atrial myocytes. PLoS One. 2011 Jan;6(6):e20395.

127. Vos MJ, Zijlstra MP, Kanon B, van Waarde-Verhagen M a WH, Brunt ERP, Oosterveld-Hut HMJ, et al. HSPB7 is the most potent polyQ aggregation suppressor within the HSPB family of molecular chaperones. Hum Mol

Genet. 2010 Dec 1;19(23):4677–93.

128. Morrow G, Tanguay RM. Small heat shock protein expression and functions during development. Int J Biochem Cell Biol. 2012 Oct;44(10):1613–21.

129. Vicart P, Caron a, Guicheney P, Li Z, Prévost MC, Faure a, et al. A missense mutation in the alphaB-crystallin chaperone gene causes a desmin-related myopathy. Nat Genet. 1998 Sep;20(1):92–5.

130. Huang L, Min JN, Masters S, Mivechi NF, Moskophidis D. Insights into function and regulation of small heat shock protein 25 (HSPB1) in a mouse model with targeted gene disruption. Genesis. 2007;45(8):487–501.

131. Christians ES, Ishiwata T, Benjamin IJ. Small heat shock proteins in redox metabolism: implications for cardiovascular diseases. Int J Biochem Cell Biol. 2012 Oct;44(10):1632–45.

132. Krief S, Faivre JJ-F, Robert P, Le Douarin B, Brument-larignon N, Lefrere I, et al. Identification and Characterization of cvHsp. J Biol Chem. 1999;274(51):36592–600.

133. Gehler S, Baldassarre M, Lad Y, Leight JL, Wozniak MA, Riching KM, et al. Filamin A – 1 Integrin Complex Tunes Epithelial Cell Response to Matrix Tension. 2009;20:3224–38.

134. Ehrlicher a J, Nakamura F, Hartwig JH, Weitz D a, Stossel TP. Mechanical strain in actin networks regulates FilGAP and integrin binding to filamin A. Nature. 2011 Oct 13;478(7368):260–3.

135. Eenjes E, Dragich JM, Kampinga HH, Yamamoto A. Distinguishing aggregate formation and aggregate clearance using cell based assays. J Cell Sci. 2016;129(6):1260–70.

136. Juo L-Y, Liao W-C, Shih Y-L, Yang B-Y, Liu A-B, Yan Y-T. HSPB7 interacts with dimerized FLNC and its absence results in progressive myopathy in skeletal muscles. J Cell Sci. 2016;1661–70.

137. Westerfield M. The Zebrafish Book; a laboratory guide for the use of zebrafish (Brachydanio rerio). University of Oregon; 1993.

138. Korzh S, Pan X, Garcia-Lecea M, Winata CL, Pan X, Wohland T, et al. Requirement of vasculogenesis and blood circulation in late stages of liver growth in zebrafish. BMC Dev Biol. 2008;8:84.

139. Meijering E, Dzyubachyk O, Smal I. Methods for cell and particle tracking. Methods Enzymol. 2012;504(February):183–200.

140. Yang J, Xu X. Immunostaining of Dissected Zebrafish Embryonic Heart . 2012;(59):e3510.

141. Arnaout R, Ferrer T, Huisken J, Spitzer K, Stainier DYR, Tristani-firouzi M, et al. Zebrafish model for human long QT syndrome. 2007;104(27).

142. Doyle E, Booher N. TAL Effector-Nucleotide Targeter (TALE-NT) 2.0: tools for TAL effector design and target prediction. Nucleic Acids ....

2012;40(W117-22).

143. Cermak T, Doyle EL, Christian M, Wang L, Zhang Y, Schmidt C, et al. Efficient design and assembly of custom TALEN and other TAL effector-based constructs for DNA targeting. Nucleic Acids Res. 2011 Jul;39(12):e82.

144. Montague TG, Cruz JM, Gagnon JA, Church GM, Valen E. CHOPCHOP: A CRISPR/Cas9 and TALEN web tool for genome editing. Nucleic Acids Res. 2014;42(W1):401–7.

145. Zhu Z, González F, Huangfu D. The iCRISPR Platform for Rapid Genome Editing in Human Pluripotent Stem Cells. Vol. 546, Methods in enzymology. 2014. 215-50 p.

146. Wilkinson RN, Elworthy S, Ingham PW, van Eeden FJM. A method for high-throughput PCR-based genotyping of larval zebrafish tail biopsies. Biotechniques. 2013;55(6):314–6.

147. Ablain J, Durand EM, Yang S, Zhou Y, Zon LI. A CRISPR/Cas9 Vector System for Tissue-Specific Gene Disruption in Zebrafish. Dev Cell. 2015;32(6):756–64.

148. González F, Zhu Z, Shi Z-DD, Lelli K, Verma N, Li Q V., et al. An iCRISPR platform for rapid, multiplexable, and inducible genome editing in human pluripotent stem cells. Cell Stem Cell. 2014 Jun 11;15:215–26.

149. Lian X, Hsiao C, Wilson G, Zhu K, Hazeltine LB, Azarin SM, et al. Robust cardiomyocyte differentiation from human pluripotent stem cells via temporal modulation of canonical Wnt signaling. Proc Natl Acad Sci. 2012;109(27):E1848–57.

150. Burridge PW, Holmström A, Wu JC. Chemically Defined Culture and Cardiomyocyte Differentiation of Human Pluripotent Stem Cells. Curr Protoc Hum Genet. 2015;(October):21.3.1-21.3.15.

151. Arnaout R, Reischauer S, Stainier DYR. Recovery of Adult Zebrafish Hearts for High-throughput Applications Video Link. J Vis Exp. 2014;(94).

152. de Bruijn WC. Glycogen, its chemistry and morphologic appearance in the electron microscope. I. A modified OsO4 fixative which selectively contrasts glycogen. J Ultrasructure Res. 1973;42(1–2):29–50.

153. Dagda RK, Zhu J, Kulich SM, Chu CT. Mitochondrially localized ERK2 regulates mitophagy and autophagic cell stress. Autophagy. 2008;4(6):70–782.

154. Holtzinger A, Rosenfeld GE, Evans T. Gata4 directs development of cardiac-inducing endoderm from ES cells. Dev Biol. 2010 Jan 1;337(1):63–73.

155. Nuriel T, Whitehouse J, Ma Y, Mercer EJ, Brown N, Gross SS. ANSID: A Solid-Phase Proteomic Approach for Identification and Relative Quantification of Aromatic Nitration Sites. Front Chem. 2015;3(January):70.

156. Holtzinger a. Gata4 regulates the formation of multiple organs. Development. 2006 Jan 1;133(1):181–181.

157. Cappola TP, Li M, He J, Ky B, Gilmore J, Qu L, et al. Common variants in HSPB7 and FRMD4B associated with advanced heart failure. Circ Cardiovasc Genet. 2010;3(2):147–54.

158. Stark K, Esslinger UB, Reinhard W, Petrov G, Winkler T, Komajda M, et al. Genetic association study identifies HSPB7 as a risk gene for idiopathic dilated cardiomyopathy. PLoS Genet. 2010 Oct;6(10):e1001167.

159. Villard E, Perret C, Gary F, Proust C, Dilanian G, Hengstenberg C, et al. A genome-wide association study identifies two loci associated with heart failure due to dilated cardiomyopathy. Eur Heart J. 2011 May;32(9):1065–76.

160. Garnier S, Hengstenberg C, Lamblin N, Dubourg O, De Groote P, Fauchier L, et al. Involvement of BAG3 and HSPB7 loci in various etiologies of systolic heart failure: Results of a European collaboration assembling more than 2000 patients. Int J Cardiol. 2015;189:105–7.

161. French B, Lumley T, Cappola TP, Mitra N. Non-iterative, regression-based estimation of haplotype associations with censored survival outcomes. Stat Appl Genet Mol Biol. 2012 Jan;11(3):Article 4.

162. Lahvic JL, Ji Y, Marin P, Zuflacht JP, Springel MW, Wosen JE, et al. Small heat shock proteins are necessary for heart migration and laterality determination in zebrafish. Dev Biol. 2013 Oct 17;384(2):1–15.

163. Miura GI, Yelon D. A guide to analysis of cardiac phenotypes in the zebrafish embryo. Third Edit. Vol. 101, Methods in cell biology. Elsevier Ltd; 2011. 161-80 p.

164. Afzelius BA, Mossberg B, Bergström SE. Immotile Cilia Syndrome (Primary Ciliary Dyskinesia), Including Kartagener Syndrome. In: Beaudet AL, Vogelstein B, Kinzler KW, Antonarakis SE, Ballabio A, Gibson KM, et al., editors. The Online Metabolic and Molecular Bases of Inherited Disease. New York, NY: The McGraw-Hill Companies, Inc.; 2014.

165. Wettstein G, Bellaye PS, Micheau O, Bonniaud P. Small heat shock proteins and the cytoskeleton: an essential interplay for cell integrity? Int J Biochem Cell Biol. 2012 Oct;44(10):1680–6.

166. Kok FO, Shin M, Ni CW, Gupta A, Grosse AS, vanImpel A, et al. Reverse genetic screening reveals poor correlation between morpholino-induced and mutant phenotypes in zebrafish. Dev Cell. 2015;32(1):97–108.

167. Ata H, Clark KJ, Ekker SC. The zebrafish genome editing toolkit. 2016;135:149–70.

168. Palstra AP, Tudorache C, Rovira M, Brittijn SA, Burgerhout E, van den Thillart GEEJM, et al. Establishing zebrafish as a novel exercise model: Swimming economy, swimming-enhanced growth and muscle growth marker gene expression. PLoS One. 2010;5(12):1–9.

169. Giallourakis CC, Rosenberg PM, Friedman LS. The liver in heart failure. Clin Liver Dis. 2002;6(4):947–67, viii–ix.

170. Louie CY, Pham MX, Daugherty TJ, Kambham N, Higgins JP. The liver in heart failure: a biopsy and explant series of the histopathologic and laboratory findings with a particular focus on pre-cardiac transplant evaluation. ModPathol. 2015;28:932–43.

171. Jean MJM, Deverteuil P, Lopez NH, Tapia JD, Schoffstall B. Adult Zebrafish Hearts Efficiently Compensate for Excessive Forced Overload Cardiac Stress with Hyperplastic Cardiomegaly. BioResearch Open …. 2012;1(2):88–91.

172. Khan R, Sheppard R. Fibrosis in heart disease: Understanding the role of transforming growth factor-??1 in cardiomyopathy, valvular disease and arrhythmia. Vol. 118, Immunology. 2006. p. 10–24.

173. Jonsson MKB, Hartman RJG, Ackers-Johnson M, Tan WLW, Lim B, van Veen TAB, et al. A Transcriptomic and Epigenomic Comparison of Fetal and Adult Human Cardiac Fibroblasts Reveals Novel Key Transcription Factors in Adult Cardiac Fibroblasts [Internet]. Vol. 1, JACC: Basic to Translational Science. 2016. p. 590–602. Available from: http://linkinghub.elsevier.com/retrieve/pii/S2452302X16301140

174. Vos MJ, Kanon B, Kampinga HH. HSPB7 is a SC35 speckle resident small heat shock protein. Biochim Biophys Acta. 2009 Aug;1793(8):1343–53.

175. White SM, Constantin PE, Claycomb WC. Cardiac physiology at the cellular level: use of cultured HL-1 cardiomyocytes for studies of cardiac muscle cell structure and function. Am J Physiol Heart Circ Physiol. 2004 Mar;286(3):H823-9.

176. Lewinter MM, Granzier HL. Titin is a major human disease gene. Circulation. 2013;127(8):938–44.

177. van der Ven PF, Bartsch JW, Gautel M, Jockusch H, Fürst DO. A functional knock-out of titin results in defective myofibril assembly. J Cell Sci. 2000;113 (Pt 8:1405–14.

178. Dalkilic I, Schienda J, Thompson TG, Kunkel LM. Loss of FilaminC (FLNc) results in severe defects in myogenesis and myotube structure. Mol Cell Biol. 2006 Sep;26(17):6522–34.

179. Fujita M, Mitsuhashi H, Isogai S, Nakata T, Kawakami A, Nonaka I, et al. Filamin C plays an essential role in the maintenance of the structural integrity of cardiac and skeletal muscles, revealed by the medaka mutant zacro. Dev Biol. 2012;361(1):79–89.

180. Brodehl A, Ferrier RA, Hamilton SJ, Greenway SC, Brundler MA, Yu W, et al. Mutations in FLNC are Associated with Familial Restrictive Cardiomyopathy. Hum Mutat. 2016;37(3):269–79.

181. Chevessier F, Schuld J, Orfanos Z, Plank A-C, Wolf L, Maerkens A, et al. Myofibrillar instability exacerbated by acute exercise in filaminopathy. Hum Mol Genet. 2015;(October):ddv421.

182. Van Der Ven PFM, Obermann WMJ, Lemke B, Gautel M, Weber K, Fürst DO. Characterization of muscle filamin isoforms suggests a possible role of γ-

Filamin/ABP-L in sarcomeric Z-disc formation. Cell Motil Cytoskeleton. 2000;45(2):149–62.

183. Vorgerd M, van der Ven PFM, Bruchertseifer V, Löwe T, Kley R a, Schröder R, et al. A mutation in the dimerization domain of filamin c causes a novel type of autosomal dominant myofibrillar myopathy. Am J Hum Genet. 2005;77(2):297–304.

184. Lee E, Koo Y, Ng A, Wei Y, Luby-Phelps K, Juraszek A, et al. Autophagy is essential for cardiac morphogenesis during vertebrate development. Autophagy. 2014;10(4):572–87.

185. Levine B, Klionsky DJ. Development by Self-DigestionMolecular Mechanisms and Biological Functions of Autophagy. Dev Cell. 2004;6(4):463–77.

186. Maejima Y, Chen Y, Isobe M, Gustafsson AB, Kitsis RN, Sadoshima J. Recent Progress in Research on Molecular Mechanisms of Autophagy in the Heart. Am J Physiol Heart Circ Physiol. 2014 Nov 14;308(4):H259-68.

187. Peterkin T, Gibson A, Loose M, Patient R. The roles of GATA-4, -5 and -6 in vertebrate heart development. Semin Cell Dev Biol. 2005 Feb;16(1):83–94.

188. Webster LC, Zhang K, Chance B, Ayene I, Culp JS, Huang WJ, et al. Conversion of the E1A Cys4 zinc finger to a nonfunctional His2,Cys2 zinc finger by a single point mutation. Proc Natl Acad Sci U S A. 1991;88(22):9989–93.

189. Xuan S, Sussel L. GATA4 and GATA6 regulate pancreatic endoderm identity through inhibition of hedgehog signaling. 2016;780–6.

190. Rossi A, Kontarakis Z, Gerri C, Nolte H, Hölper S, Krüger M, et al. Genetic compensation induced by deleterious mutations but not gene knockdowns. Nature. 2015;Aug 13(524):230–3.

191. Bielinska M, Seehra A, Toppari J, Heikinheimo M, Wilson DB. GATA-4 Is Required for Sex Steroidogenic Cell Development in the Fetal Mouse. 2007;(November 2006):203–13.

192. Kyrönlahti A, Euler R, Bielinska M, Schoeller EL, Moley KH, Toppari J, et al. Molecular and Cellular Endocrinology GATA4 regulates Sertoli cell function and fertility in adult male mice ♂. 2011;333:85–95.

193. Siddiqui M, Sheikh H, Tran C, Bruce AEE. The Tight Junction Component Claudin E is Required for Zebrafish Epiboly. 2010;(December 2009):715–22.

194. Gene T, Mix H, Bruce AEE, Howley C, Fox MD, Ho RK. NIH Public Access. 2010;233(1):105–14.

195. Ogura T. Tbx5 Specifies the Left/Right Ventricles and Ventricular Septum Position During Cardiogenesis. In: Cardiovascular Development and Congenital Malformations: Molecular & Genetic Mechanisms. 2007. p. 75–7.

196. Hirayama-Yamada K, Kamisago M, Akimoto K, Aotsuka H, Nakamura Y, Tomita H, et al. Phenotypes with GATA4 or NKX2.5 mutations in familial atrial septal defect. Am J Med Genet. 2005;135 A(1):47–52.

197. Laforest B, Nemer M. GATA5 interacts with GATA4 and GATA6 in outflow tract development. Dev Biol. 2011;358(2):368–78.

198. Wang J, Panáková D, Kikuchi K, Holdway JE, Gemberling M, Burris JS, et al. The regenerative capacity of zebrafish reverses cardiac failure caused by genetic cardiomyocyte depletion. Development. 2011 Aug;138(16):3421–30.

199. Reiter JF, Alexander J, Rodaway A, Yelon D, Patient R, Holder N, et al. Gata5 is required for the development of the heart and endoderm in zebrafish. 1999;2983–95.

200. Du S, Draper BW, Mione M, Moens CB, Bruce A. Differential regulation of epiboly initiation and progression by zebrafish Eomesodermin A. Dev Biol. 2012;362(1):11–23.